Modelling verticality estimation during locomotion

Ildar Farkhatdinov

THÈSE

PRESENTÉE À

L'UNIVERSITÉ PIERRE ET MARIE CURIE

ÉCOLE DOCTORALE: SCIENCES MECANIQUE, ACOUSTIQUE, ELECTRONIQUE ET ROBOTIQUE

par Ildar FARKHATDINOV

POUR OBTENIR LE GRADE DE

DOCTEUR

SPÉCIALITÉ: Robotique

MODELING VERTICALITY ESTIMATION DURING LOCOMOTION

Directeur de recherche: Vincent HAYWARD
Co-directeur de recherche: Hannah MICHALSKA

Soutenue le 5 Juin 2013

Devant la commission d'examen formée de:

M.	Jean-Paul LAUMOND	Directeur de recherche, LAAS CNRS	Rapporteur
M.	Etienne BURDET	Professor, Imperial College of London	Rapporteur
M.	Faiz BEN AMAR	Professeur, Université Pierre et Marie Curie	Examinateur
Mme.	Hannah MICHALSKA	Associate Professor, McGill University	Examinateur
M.	Vincent HAYWARD	Professeur, Université Pierre et Marie Curie	Examinateur
	INVITÉ:		
M.	Alain BERTHOZ	Professeur, Collège de France	Examinateur
M.	Michel FLIESS	Professeur, École Polytechnique	Examinateur

Abstract

In this thesis, a nonlinear model of the vestibular system is proposed, with special reference to humans and other locomoting animals. The vestibular system is essential for stable locomotion since it provides idiothetic measurements of spatial orientation that are needed for postural control. The model was constructed from general considerations regarding the Newton-Euler dynamics governing the three-dimensional movements of bodies constrained to oscillate in non-inertial frames, such as the otoliths, which were modeled as spherical damped pendula. Two configurations were considered. The medial model considered only one inner ear located in the center of a head. The lateral model considered two inner ears located laterally with respect to the center of rotation of the head. The differences between these two models were analyzed and the importance of having two vestibular organs discussed. To this end, a nonlinear algebraic observability test was used to verify whether the reconstruction of the head orientation with respect to the gravitational vertical was possible from otoliths measurements only. It could be shown that in order for the head vertical orientation to be observable, the head had to be stabilized during locomotion. Moreover, it was shown that the gravito-inertial ambiguity inherent to inertial idiothetic sensing could be resolved if the head was horizontally stabilized. These results were applied to solve the head vertical orientation estimation problem in the linearized case (Luenberger observer, Kalman filter) as well as in the nonlinear case (Extended Kalman filter, Newton method based observation). These observers were designed and tested in simulations. The simulations indicated that the estimation errors were smaller and the observers converged faster when head was stabilized during locomotion, leading to a nonlinear, combined observation-control system that could be stabilized with respect to the gravitational vertical based on no other information than the prior knowledge of the Newton-Euler dynamics. The results were further tested with a specifically designed experimental setup that comprised an actuated gimbal mechanism to represent the head-neck articulation and a liquid-based inclinometer that represented the otoliths organs. The findings derived from this research would be helpful for analyzing spatial perception in humans and animals, and for improving the perceptual capabilities of robotic systems, such as humanoid robots, rough terrain vehicles, or free-moving drones.

Keywords: vestibular system, head-neck system, nonlinear system, observation, estimation, verticality, spatial perception, locomotion, humanoid robot.

Résumé

Dans cette thèse, nous proposons un modèle non-linéaire du système vestibulaire, en particulier chez l'humain et autres animaux mobiles. Le système vestibulaire est essentiel pour une locomotion stable dans la mesure où il fournit des mesures idiothétiques d'orientation spatiale nécessaires à la stabilité posturale. Le développement du modèle est basé sur les principes généraux de la dynamique de Newton-Euler, régissant le mouvement des corps contraints à osciller en trois dimensions dans un référentiel non-Galiléen. Les otolithes du système vestibulaire constituent un exemple d'un tel système et ont été modèlisés comme des pendules sphériques amortis. Deux types de modèles ont été proposés. Le modèle medial est constitué d'une seule oreille interne se trouvant au centre de la tête. Le modèle latéral est constitué de deux oreilles internes situées latéralement par rapport au centre de la tête. Les différences entre ces deux modèles sont analysées et l'hypothèse de l'utilité de posséder deux d'organes vestibulaires est discutée. Un test algébrique d'observabilité des modèles non-linéaires a permis de montrer que la tête doit être stabilisée pendant la locomotion pour que l'orientation de la tête soit une quantité observable. Nous montrons que le problème de l'ambiguïté gravito-inertielle peut être résolu si la tête est stabilisée horizontalement. Ces résultats ont été appliqués pour estimer la verticalité gravitationnelle lors de la locomotion dans le cas linéarisé et dans le cas non-linéaire. Ces observateurs ont été conçus et testés avec des simulations numériques. Les résultats des simulations ont montré que quand la tête est stabilisée les erreurs d'estimation sont significativement plus faibles et que les observateurs convergent plus rapidement et de façon plus robuste. Cela conduit à un système non-linéaire où observation et la commande sont combinés, qui peut être stabilisé par rapport à la verticale gravitationnelle sans aucune information autre que la connaissance de la dynamique de Newton-Euler. Les résultats sont ensuite testés avec un système expérimental spécialement conçu pour représenter le système tête-cou et les organes vestibulaires. Un inclinomètre utilisant un liquide a été mis en œuvre pour représenter la fonction des otolithes. Les résultats présentés dans cette thèse sont utiles à l'analyse de la perception spatiale chez les humains et autres animaux mobiles et pour l'amélioration des capacités sensorielles des systèmes robotiques tels que robots humanoïdes, véhicules tout terrain, ou drones.

Mots clé: système vestibulaire, système tête-cou, système non-linéaire, observation, estimation, verticalité, perception spatiale, locomotion, robot humanoïde.

Acknowledgements

I would like to express my heartfelt gratitude to Prof. Vincent Hayward for patient guidance during this research work. Thanks to wise and inspiring leading of Prof. Vincent Hayward, I could obtain a broader view on robotic systems and their potential applications in modeling the behavior of living creatures. This research could not happen without his encouragement, optimism and enthusiasm.

I am in debt to Prof. Hannah Michalska from McGill University whose advice was extremely helpful in selecting proper control theory algorithms and their verification methods. I am grateful to Prof. Alain Berthoz from Collège de France whose competence in neuroscience and biology was exceptionally beneficial.

A lot of professional support came from my research group colleagues at UPMC ISIR. In particular, I would like to mention Sheng Chao Wong who helped a lot with electronics integration; Amir Berrezag, Rafal Pijewski from UPMC ISIR and Yves Dupraz from Collège de France for their advice on experimental system manufacturing; Dr. Alexander Terekhov, Dr. Yon Visell, Dr. Nizar Ouarti, Dr. Jonathan Platkiewicz, Dr. Stephen Sinclair, Dr. Abdenbi Mohand Ousaid and Bernard Javot for their valuable critics.

Special thanks for the thesis reviewing committee - Prof. Jean-Paul Laumond from LAAS CNRS, Prof. Etienne Burdet from Imperial College of London and Prof. Faiz Ben Amar from UPMC - for their agreement to read and comment on the present work.

This thesis and related research work were supported by the fellowship from École Doctorale, Sciences Mécaniques, Acoustique, Electronique et Robotique de Paris of Université Pierre et Marie Curie, and additional funding was provided by the European Research Council.

Contents

Chapter 1

Introduction

Contents

1.1 Scope

This thesis develops and investigates a general model of the vestibular otolith organ, a core component of a complete vestibular system, and the potential application of this model to robotics. In the biological world, vestibular organs are, in great part, responsible for spatial perception. In many animals, sensory outputs from the vestibular system play a dominant role in posture control during locomotion because they provide central neural system (CNS) with important information about the motion and orientation of the self. In engineering systems such as mobile robots, drones, humanoid robots, robot fishes, robot submersibles, as well as any other free moving vehicles such as aeroplanes, submarines, rovers, torpedoes, rockets, and so-on, inertial sensors play the role of the vestibular system. Inertial measurements can provide acceleration, velocity and displacement estimates which can be used as feedback

information for control systems. Control objectives can be, for instance, balancing during locomotion for humanoid robots or localization and mapping for mobile robots. Many other functions can be achieved from inertial sensing such as resisting perturbations, tracking desired trajectories, or anticipating the occurrence of dangerous configurations. Previous contributions from neuroscience and recent developments in control engineering were the motivation behind the present research, at the intersection of biological and engineering sciences. The objectives of this work are:

- to develop a mathematical model of the vestibular system which is based on the fundamental principles of mechanics;
- to analyze the proposed model with the methods used in control theory and robotics;
- to apply the result of this analysis to clarify hypotheses regarding the role of head stabilization, a behavior observed in numerous species;
- to perform computational experiments to investigate the putative role of head stabilization;
- to design and implement a hardware model of a head that is stabilized solely from inertial, that is, idiothetic measurements, and experiment with this model.

1.2 Summary of contributions

- We developed a pendulum-based nonlinear model of otoliths. Two models were proposed: the medial model and the lateral model. Medial model considers a spherical pendulum located in the center of the head. Lateral model consists of two pendula located aside from the center of the head.
- Nonlinear observability study of the medial and the lateral models was carried out. We checked whether the head's angular orientation with respect to the gravitational verticality was observable depending on the head stabilization control. Observability study showed that spatial orientation of the head was observable only when the head was stabilized for the medial model. Interestingly, the head's spatial orientation was observable independently from the stabilization control for the lateral model. This may suggest an explanation for having two sets of vestibular organs in order to provide the neural system with an estimate of the spatial orientation of the head.
- Several observation methods for estimating spatial orientation of the head with respect to verticality were designed. A Newton method based observer and Extended Kalman Filter were used in the nonlinear case. A Kalman filter and a Luenberger observer were used in the linearized case. Computational experiments showed that estimation errors were smaller and the observers were more robust to model uncertainties when the head was stabilized.

- Relation between head stabilization and linearization was discussed. We showed that the head up-right stabilization and model linearization around this equilibrium enables the application of the separation principle of control theory. It was shown with numerical tests that independently designed stable linear head controller and linear verticality observer were able to function properly for controlling and estimating the spatial orientation of the head which is a nonlinear system.

- Up-right stabilization of the head during locomotion facilitates estimation of the verticality by providing the observer a way to distinguish between otoliths response to tilt and translational motions. Assumption of having the head stabilized in up-right orientation empowers with an option to consider otoliths measurements as translational accelerations.

1.3 Thesis overview

In the present introductory chapter, we first describe briefly the vestibular system in humans, its anatomy, physiology and its role in vision, postural balance, and locomotion. Special attention is given to recent mathematical models and their experimental evaluations to investigate hypothesis about the basic operational principles of the vestibular system. We then look into some engineering issues, particularly for robotic systems. We provide a short survey on inertial sensing applications in machines, hardware and software methods used to improve the quality of inertial measurements. The application of inertial measurement units (IMUs) to humanoid robots is studied more particularly. We also illuminate the potential advantages of locating the robotic vestibular system such as IMU in stabilized robot heads in a way that is observed in living creatures.

In chapter 2, we present the model of the vestibular system which was derived with the help of the fundamental Newton-Euler dynamics. Two basic models are presented. A model for a centric vestibular system (medial model) and a model for a vestibular system having two symmetrically located organs (lateral model). For both models the nonlinear and the linearized, three-dimensional and planar equations are given. Head stabilization control is also described. The model correctness is verified via computational experiments.

In chapter 3, the observability analysis of the head orientation in space is presented taking advantage of a nonlinear algebraic test. It could be shown that head self-stabilization renders the orientation of the gravitational vertical with respect to the head observable. The problem of ambiguity in gravitoinertial measurements performed by vestibular organs is also addressed. It is suggested that stabilization of the head in an upright position with respect to gravitational field may also help to resolve the gravitoinertial ambiguity.

In chapter 4, the Kalman filter and a nonlinear Newton-method-based observer are designed to perform the estimation of the head vertical orientation. Special attention is given to head stabilization control seen as a way to linearize the overall vestibular-orientation control system. Such stabilization implies the applicability of the separation principle in observer and controller design. The performance of linear and nonlinear observers for horizontally stabilized and non-stabilized head motions is tested and compared by computer simulations.

In chapter 5, a robotic hardware model of the vestibular system and head is presented. Experimental evaluations of linear and non-linear observers are described. The results show that the stabilization of the robotic head facilitated the observation process. The linearized model of the system could be used and more accurate estimates were obtained when the head was stabilized in horizontal orientation.

In the conclusion, the results of this thesis are summarized. Its implications in biology and robotics are discussed.

1.4 The sense of motion in humans and animals

Humans and animals have complex multi sensory system which provides their central nervous systems (CNS) with information about the external world and about their own state. For us, like for other living creatures, it is important to estimate the spatial orientation and localization of our body with respect to the objects of the external world. Most of our sensory systems contribute to this task, including, vision, audition, touch, proprioception, olfaction, and vestibular inputs. Changes in the visual flow on the retina indicate changes in relationship between the body and the environment, unless these changes can be entirely attributed to changes in the environment. Similarly changes in the acoustic pressure impinging on the eardrums can be attributed to movement of the self as well as to changes in the acoustic environment. Tactile and proprioceptive inputs result from change of our body position and configuration during mechanical interaction with the environment. Independent sensory information of one modality is rarely sufficient for proper motion perception. For instance, a change of visual flow can be caused by the movements of the eyes, the movement of a sound source can be confounded with head rotations, and so on. Generally speaking, this problem is solved through multi sensory integration [56, 98]. The central nervous system is highly adept at processing multisensory information to provide the brain with a proper sensation of motion. Interestingly, visual, auditory, tactile, proprioceptive or olfactory sensory inputs can be easily put out of action or uninformative under a great many types of circumstances that are easy to imagine, but the vestibular inputs are always available, even in the absence of gravity! In the latter case, the vestibular organs still respond to linear accelerations and angular velocities. That is why it comes naturally that vestibular system plays a key role in perceiving self motion. It is quite a curious thing that so little attention has been paid to inertial sensing in robotics when, in fact, it takes so little resources to take advantage of it compared to all other sensing modalities. In the next subsections, we describe the principles that govern the function of vestibular organs and their roles for posture control.

1.4.1 Vestibular system

The vestibular system detects motion of the head in space, and, in turn, generates reflexes that are crucial for our daily activities, such as stabilizing the visual axis (gaze) and maintaining head and body posture. In addition, the vestibular system provides us with a subjective sense of movement and orien-

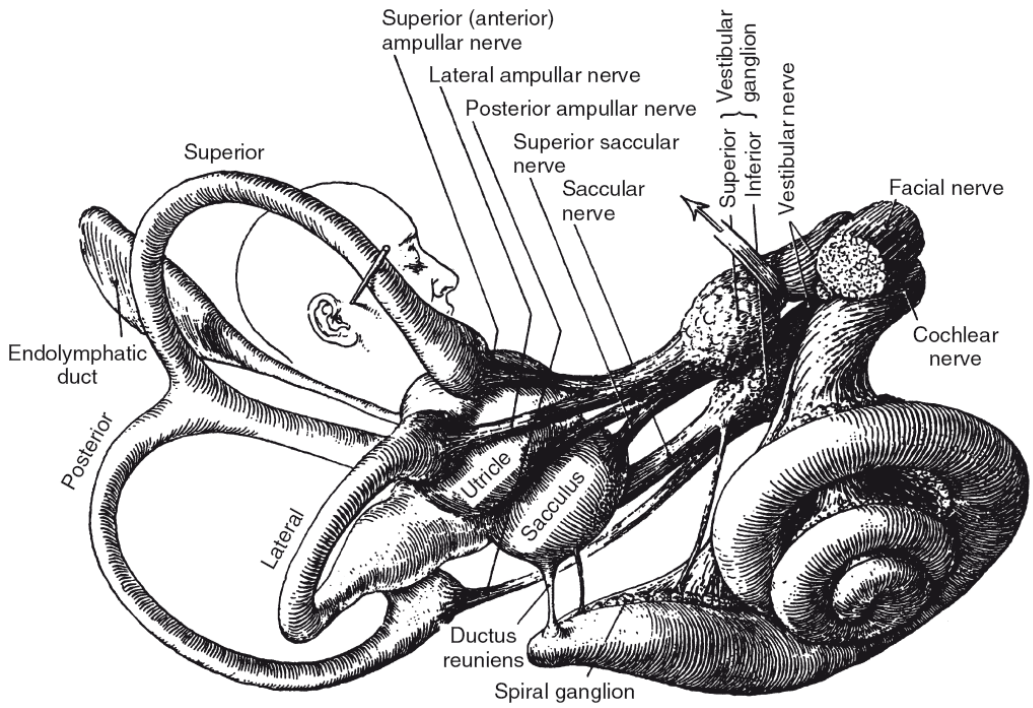

Figure 1.1: The vestibular organs located in each inner ear. The main organs are three almost orthogonal semicircular canals (superior, posterior and lateral) and two otolith organs (utricle and sccaulus). Semicircular calanals are sensitive to the angular velocity of the head. Otolith organs are sensitive to the linear gravitoinertial acceleration. The drawing is adapted from [25].

tation in space. The vestibular sensory organs are located in close proximity to the cochlea. The vestibular system comprises two types of organs: two otolith organs and three semicircular canals. Two otolith organs (the saccule and utricle) sense linear acceleration which includes gravitational and translational components. Semicircular canals sense angular velocities in three planes. The generated receptor signals are conveyed by the vestibular nerve fibers to the neural structures that are responsible for eye movements, posture and balance control. As a result, the vestibular organs participate to our sixth sense - the sense of motion that allows us to perceive and control bodily movements [16]. Vestibular processing is highly multimodal, for instance, visual/vestibular and proprioceptive/vestibular sensory inputs are dominant for gaze and postural control, but at the same time vestibular system itself plays an important role in our everyday activities and contributes to various range of functions [5, 45].

Otolith organs

The otolith organ comprises the utricle and the saccule. The utricle and the saccule are sensitive to linear acceleration. They respond to both head's linear motion and static tilt in vertical plane. The utricle and the saccule are arranged to respond to motion in all three dimensions. When the head is upright, the saccule is vertical and it responds to linear accelerations in the sagittal plane, specifically up and down movements. The utricle is horizontally oriented and responds to accelerations in the interaural transverse (horizontal) plane (anterio-posterior and medio-lateral accelerations) [93]. Both, the utricle and

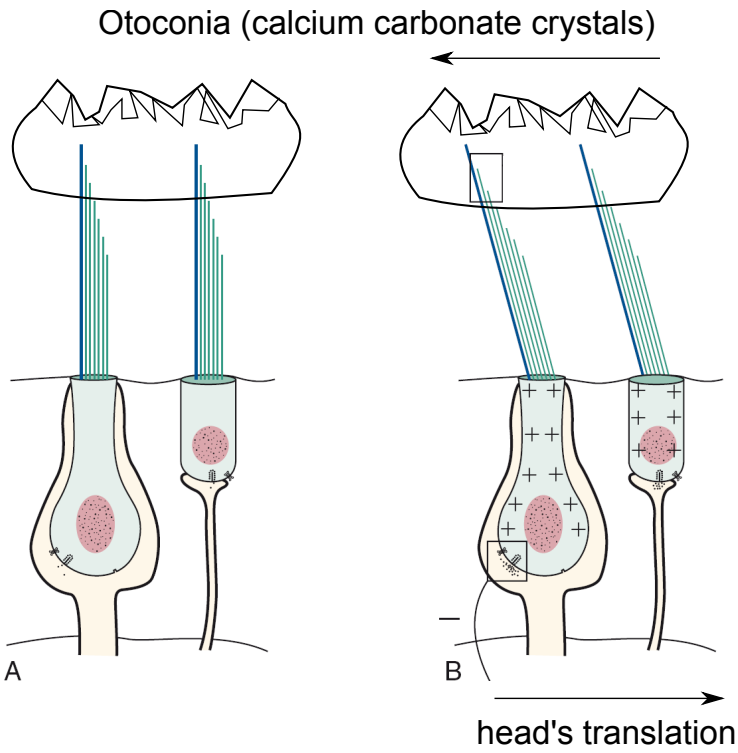

Figure 1.2: Vestibular hair cells in otolith organs. Head is not accelerated (A). Head is accelerated to the right (B). Adapted from [32]

the saccule, contain sheets of hair cells a sensory epithelium (macula). An otolithic membrane (otoconia) composed of calcium carbonate crystals sits atop of hair cells. Fig. 1.2 shows simplified view of otolithic hair cells during still (A) and accelerated motions (B). In response to linear acceleration, the crystals are deflected due to their inertia. Linear acceleration of the head causes otoconia's accelerated motion which in turn causes shear forces acting on the hair cells. Complex molecular level mechano-electro-chemical mechanism of interaction between hair cells results in generation of electrical signals which are sent to neural structures for further processing [32].

Semicircular canals

Each inner ear has three semicircular canals approximately arrayed at right angles to each other. Semicircular canals are sensitive to angular accelerations [167]. Each canal is comprised of a circular path of fluid continuity, interrupted at the ampulla by a water tight, elastic membrane called the cupula [5]. Fig. 1.3 shows a schematic view of one semicircular canal. Each canal is filled with a fluid called endolymph. When the head rotates in the plane of a semicircular canal, inertial forces causes the endolymph in the canal to lag behind the motion of the head [32]. Motion of the endolymph causes pressure applied to the membrane of the cupula and its deflection causes the shearing stress in the hair cells [32]. Then, the corresponding electrical signals are generated and transmitted through neurons in a way similar to the way it is done in the otoliths. Although, the semicircular canals respond to angular acceleration, the neural output from the sensory cells represents the velocity of rotation. This suggests that the operation of mathematical integration of the input signal occurs owing to the mechanics of the canals, mainly the significant viscous

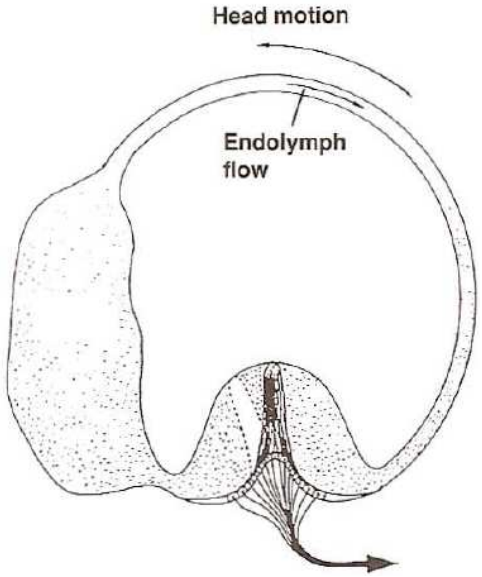

Figure 1.3: Semicircular canal. When head is rotated counter clockwise, the endolymoph flow will rotate clockwise and apply pressure on the ampulla. Adapted from [93]

properties of the fluid due to the small size of the canal [46, 102]. Having measurements of three angular velocities CNS can create a three-dimensional representation of the head's angular velocity vector.

1.4.2 Roles of vestibular system

Humans rely on the multiplicity of sensory inputs and sophisticated anticipatory mechanisms to solve the control problems subserving standing, walking, running, jumping, dancing, and so on. Vestibular inputs play a central role in all these tasks, which are achieved through a combination of postural movements and forces and torques exerted against the environment. We briefly describe some of the roles of vestibular system, which have or may have an important potential application in robotic systems.

Vision. In humans, the head-located vestibular system is known to participate in a number of functions that include gaze stabilization through the vestibulo-ocular reflex [18, 17, 134, 51]. The vestibulo-ocular reflex stabilizes the gaze to ensure clear and stabilized vision. It is a reflex of eye-movement that stabilizes the image projected on the retina during head movements. The eye movements are produced in the direction opposite to head movements. The reflex has both rotational and translational aspects which are driven by semicircular canals and otoliths inputs, respectively.

Self-motion perception. The vestibular system is a key sensory organ for the perception of body motion [19]. Human are always aware of body movements even if other senses such as vision, audition are absent. The vestibular system also provides us with the ability to distinguish between self-generated motion and external ones. It has been shown that vestibular only information is sufficient for us to reconstruct our body's location and time history of its displacements when our body is moved passively [104, 105].

Balance. The vestibular system plays a dominant role in the coordination of postural reflexes, such as vestibulo-collic reflex. Vestibulo-collic reflex is responsible for maintaining head and body posture. This reflex stabilizes the head with respect to inertial space. It produces commands that move the head in the direction opposite to the direction of the actual velocity of the head [58, 10]. Another important role of the vestibular system is the vestibulo-spinal reflex which coordinates head and neck movement with respect to the trunk of the body. The goal of the reflex is to maintain the head in an upright position [3]. Together, the vestibulo-collic and the vestibulo-spinal reflexes are responsible for self-balancing control [205, 206, 174, 2, 131].

Perception of verticality. All of us are subjected to permanent gravitational forces. The vestibular system is the principal sensory system which is able to estimate these forces. When our body is still, otoliths respond to the gravitational acceleration vector only, and its components provide us with a sense of absolute verticality [20, 210]. Knowledge of gravitational verticality is essential for balancing and posture control as well, since it enables the disambiguition of 'up' and 'down' for spatial orientation [34].

Frame of reference. Vestibular systems, like embodied inertial sensors, provides the CNS with a head-centered frame of reference. It may be suggested that low-level balance and posture control is realized in this frame of reference. Spatial transformations from head-fixed and world inertial frame can be performed based on vestibular system measurements. Therefore, this embodied frame of reference is directly related to the world inertial frame, and enables the neural system to perform stable posture control independently from other sensory inputs, such as tactile or proprioception information stimulated by ground inclination. In this way, ground-independent posture and balance control can be implemented.

1.4.3 Mathematical models of vestibular system

There has been a lot of research work about the quantification of the vestibular system dynamic behavior and the creation of the sensory models of spatial orientation perception. In this thesis we refer only to a selected set of research publications which describe the basic dynamic behavior of the vestibular sensors. For more detailed reviews on vestibular organs mathematical modeling an interested reader can further refer to various survey papers and reports, such as [133, 213, 100, 5, 85, 44]. In this subsection we first look into the dynamics of the otoliths and semicircular channels, and then, we briefly describe most frequently used models of vestibular signal processing. Our primary interest in the dynamic model of the vestibular organs is its mechanical component, which defines the relation between motion of the head's and sensory organs response.

Dynamics of otoliths. The displacement of the large saccular otolith of the medium-sized wading birds (ruff) was measured in [49]. The results suggested that the mechanics of the otolith could be described by a critically damped second-order system with a resonant frequency of 50 Hz.

In [63, 64, 65], series of experimental studies of the otolith organs of the squirrel monkey were presented. It was concluded that the mechanical response of the otolith to tilt and translational acceleration can be modeled in terms of linear transfer function with characteristic time $T_{\rm m}$:

$$W_{\rm oto}(s) = \frac{1}{1 + T_{\rm m} s}, \tag{1.1}$$

where s is the Laplace variable. The input for this transfer function is acceleration of the head which includes translation of the head and gravitational acceleration. The output of the transfer function characterizes the deflection or displacement of the sensory organ (otoconia) with respect to its neutral position. The value of characteristic time, $T_{\rm m}$, was estimated based on the experimental measurements. It was found to be in the range of 9 to 67 ms, depending on the experimental conditions. Nonlinear distortion of the measurements was reported, as well, but it did not exceed 10-20%. The latter model suggested that the response of the otolith organs is more heavily damped than was reported in [49].

In some other reports, in addition to second order dynamics of otolith receptors, the mechanical threshold (approx. 0.005 G) and dynamics lead terms was added to represent some neural processing [132, 213].

Dynamics of semicircular canals. Significantly more research was done on the dynamics modeling for the semicircular canals. Most of research use the dynamics of the system deduced from hydrodynamic principles and suggest the torsion-pendulum model [189, 188]. In [189], the equation that defines the angular deviation of the endolymph in the canal was:

$$\Theta\ddot{\xi} + \Pi\dot{\xi} + \Delta\xi = 0, \tag{1.2}$$

where ξ is the deviation of the endolymph, Θ is moment of inertia of the endolymph, Π is moment of friction at unit angular velocity, Δ - directional momentum at unit angle caused by the cupula. Based on experimental observations and system identification procedures it was concluded that the dynamics can be described by the differential equation

$$\ddot{\xi} + 10\dot{\xi} + \xi = 0. \tag{1.3}$$

More advanced experimental studies with human subjects supported the torsion-pendulum representation of the canal dynamics [101, 91, 149]. In [188], it was suggested to model semicircular canals with heavily-damped second-order system which behaved as an angular-velocity meter.

In [73], the frequency-response analysis of central vestibular unit activity to rotational stimulation of the semicircular canals in cats was carried out. It was found that the relation between neural response of the canals and mechanical stimulation was dominated by a single time constant of about 4 seconds. Two response regions were defined, above and below a stimulus frequency of about 0.4 Hz. Above this frequency, the canals response corresponded to the angular velocity of the stimulus, and below that frequency, measurements tended towards the angular acceleration of the stimulus.

More rigorous experimental study with monkeys proposed a more compli-

cated dynamics model of the canals [62]. The latter model considered the difference for low and high frequencies rotation. At low frequencies the phase lag was smaller than predicted by the torsion-pendulum model, which was a consequence of sensory adaptation. There was a gain enhancement at high frequencies which was modeled by additional high-frequency component. The nonlinear distortion was reported to be relatively low, averaging about 13%.

Sensory data integration and processing. Sensory outputs from otoliths and semicircular canals are processed in neural systems at different levels. Some information is processed in low level neural networks, while some are projected to CNS where integration with other sensory modalities takes place. In this part of the chapter we give a brief review of some existing theories on how the vestibular information is processed at the neural level. Most of these models are based on system theory approaches, which are more relevant for our robotics-oriented study. Research on modeling the vestibular signal processing aimed at developing theories of human spatial orientation perception, and was applied mainly to aerospace physiological studies.

L. R. Young and his group proposed an optimal estimator model in [22]. He introduced the concept of internal model which comprised the dynamic model information about the sensory organs and head-neck system. Internal model was considered to be known to the CNS. L. R. Young used the concept of optimal estimator (Kalman filter) to model the human's orientation estimation based on the outputs from visual, vestibular, proprioceptive and tactile sensory systems. Assumptions about sensor dynamics and noise statistics of the internal model were used to correct the estimated states which represented spatial orientation. Estimated states, called perceptions in [22], contained angular orientation of the head, its angular velocity, inertial translation and inertial velocity. Some nonlinear elements were added to the model in order to reproduce the delay of the onset of visually induced motion. In a recent paper by L. R. Young and colleagues [214], an overview of their optimal filter based approaches for spatial orientation estimation in humans is given.

D. M. Merfeld and colleagues developed an observer-based model for spatial orientation estimation based only on vestibular sensory inputs. Their approach was based on the concept of an internal model, as well, but special attention was given to the neural processing of gravito-inertial cues [139]. In [215, 141] experiments were performed to analyze the vestibulo-ocular response during tilt and rotation of the head and of the body. The presented experimental findings were consistent with the hypothesis that the nervous system resolves the ambiguous measurements of gravitoinertial forces into neural estimates of gravity and linear acceleration. In [140], a human model for this vestibular signals processing was presented. The graphical representation of the model is shown in Fig. 1.4. Originally, the model was developped as a result of experimental studies with monkeys [137, 136]. The model consists of semicircular canals and graviceptors (otoliths), their internal models, and four feedback correction channels for the state estimation. A linear system was used to model the semicircular canals' dynamics, and a simple unity gain (identity matrix) was used to model the otoliths. The state of the model includes three vectors in $\mathbb{R}^3$: angular velocity of the head, $\boldsymbol{\omega}$, the translational acceleration of the head, $\boldsymbol{a}$, and the gravitational acceleration vector $\boldsymbol{g}$. The angular velocity of the head, $\boldsymbol{\omega}$, and its translational acceleration define the trajectory of the

head in the space. The angular velocity is measured by the semicircular canals which generate the output signal $\boldsymbol{\alpha}_{\text{scc}}$. The gravitational acceleration vector, $\boldsymbol{g}$, is expressed in the head-fixed frame of reference, and, therefore, contains information on the head's angular orientation with respect to gravitational vertical. The otoliths respond to the vector sum of vectors: $\boldsymbol{f} = \boldsymbol{g} - \boldsymbol{a}$, where $\boldsymbol{f}$ is defined as the gravitoinertial force. As a result, the output of the otoliths, $\boldsymbol{\alpha}_{\text{oto}}$, provides the neural system with information related to the head's static tilt and its linear translation. The actual head's translational acceleration, $\boldsymbol{a}$, and its angular orientation with respect to the gravitational acceleration, $\boldsymbol{g}$, are unknown to the neural system. Merfeld et al. proposed the model in which four types of errors between the measurements and their estimates (observations). It was suggested that the neural system is able to perform the operation of gravitational vector transformation (rotation) from the world frame to the head's frame,

$$\hat{\boldsymbol{g}} = \int -\hat{\boldsymbol{\omega}} \times \hat{\boldsymbol{g}} \, \mathrm{d}t, \tag{1.4}$$

where $\hat{\mathbf{g}}$ is an estimate of gravitational acceleration vector expressed in head's frame and $\hat{\boldsymbol{\omega}}$ is an estimate of angular velocity of the head. This nonlinear integration equation is used by neural system to estimate the relative orientation of gravity with the help of rotational cues. The types of error calculations and feedback channels define the inputs to the internal model. They are used to convert the feedback errors into estimates of motion and orientation. The angular velocity feedback parameters, k_ω, converts the difference between estimated and actual output of semicircular canals to a neural representation of angular velocity. The translational acceleration feedback gain, k_a, converts the acceleration error to a neural representation of translational acceleration. The other two feedback errors were used to feed back the cross product error and were chosen by trial and error to yield responses that matched the experimental data [136]. This structure makes it difficult to interpret this model in accordance with physical and mechanical principles.

More recently, J. Laurens and J. Droulez constructed a Bayesian processing model of self-motion perception in [121]. It was proposed that the brain processes these signals in a statically optimal fashion, reproducing the rules of Bayesian inference. It was also proposed that this Bayesian based processing uses the statistics of natural head movements. The outputs of semicircular canals and head's angular velocity were assumed to be subjected to Gaussian noise. Using particle filtering, the three-dimensional model of vestibular signal processing was developed based on optimal estimation. The model was successfully tested by computational experiments. It was proved to be efficient in modeling the vestibulo-ocular reflex.

Among the vestibular information processing models mentioned above, the concepts of internal model and estimator or observer are crucial. The models which use the Kalman filter, linear observer and particle filtering to model vestibular system were reviewed briefly. Relatively complete reviews of existing vestibular information processing models can be found in [129, 173].

In robotic systems, the concept of observer has been known for decades, since the early works of E. Kalman in linear filtering [111] and D. Luenberger in state estimation for linear systems [128]. In the present work we develop an observer based model of vestibular information processing in which we pay

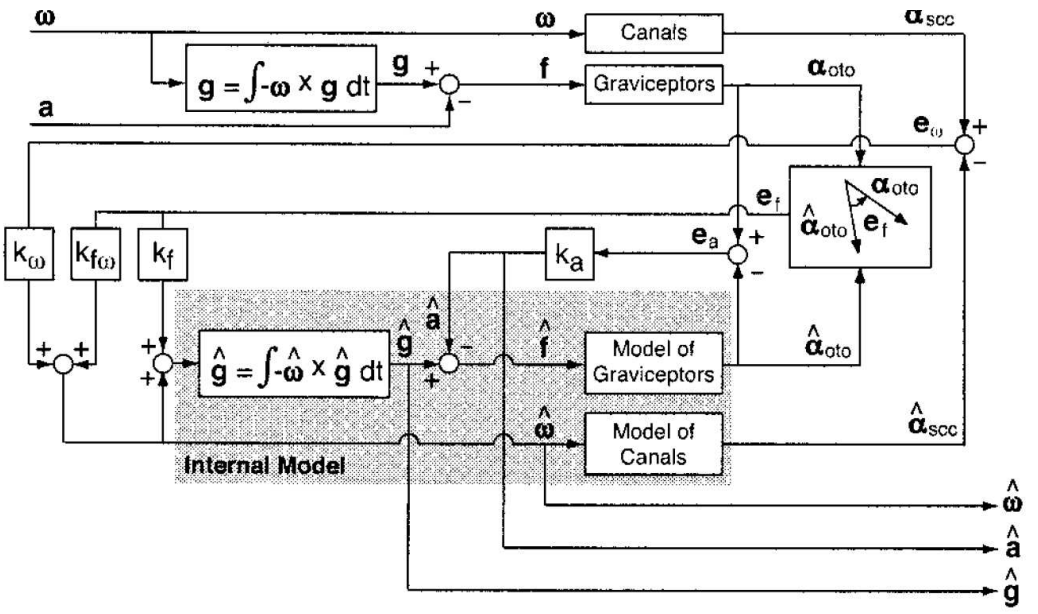

Figure 1.4: A diagram view of vestibular information processing proposed by Merfeld et al. The system is based on the concept of internal model and realized as observer with four feedback channels for estimation correction. Diagram is adapted from [140]

specific attention to the head's stabilization control based on the estimated spatial orientation.

1.4.4 Head stabilization

Various human motion experimental studies showed that humans stabilize their heads while performing different locomoting, balancing or other postural tasks. It has been proposed by T. Pozzo and A. Berthoz that humans stabilize their heads in rotation for different locomotor tasks, such as free walking, walking in place, running in place and hopping [158]. In experiments with ten healthy subjects it was shown that humans stabilized their heads and that the maximum angular amplitude of Frankfort's plane (plane of horizontal semicircular canals) did not exceed 20 degrees. This stabilization probably uses cooperation between both the measurement of head rotations by the semi-circular canals and the measure of translations by the utriculus and sacculus (otolith organs). The plane of stabilization is determined by the task; it can vary and may be controlled by the gaze. Further experiments showed that total darkness did not significantly influence the stabilization of the head, which demonstrated the importance of this behavior in the coordination of the multiple degrees of freedom of the body during gait. Fig. 1.5 shows body links orientation measured during experimental studies [158]. It can be clearly seen that during locomotion the head was stabilized. Similar results were obtained in [182].

Later in [159], it was shown that head stabilization occurred also in the frontal plane during the maintenance of monopodal and bipodal equilibrium on unstable rocking platforms. The head remained stable relatively to the vertical, despite large translations in the frontal plane. Head angular stabilization close to vertical orientation was essential for effective postural control during those complex equilibrium tasks.

Some recent behavioral studies by A. Berthoz and colleagues showed that

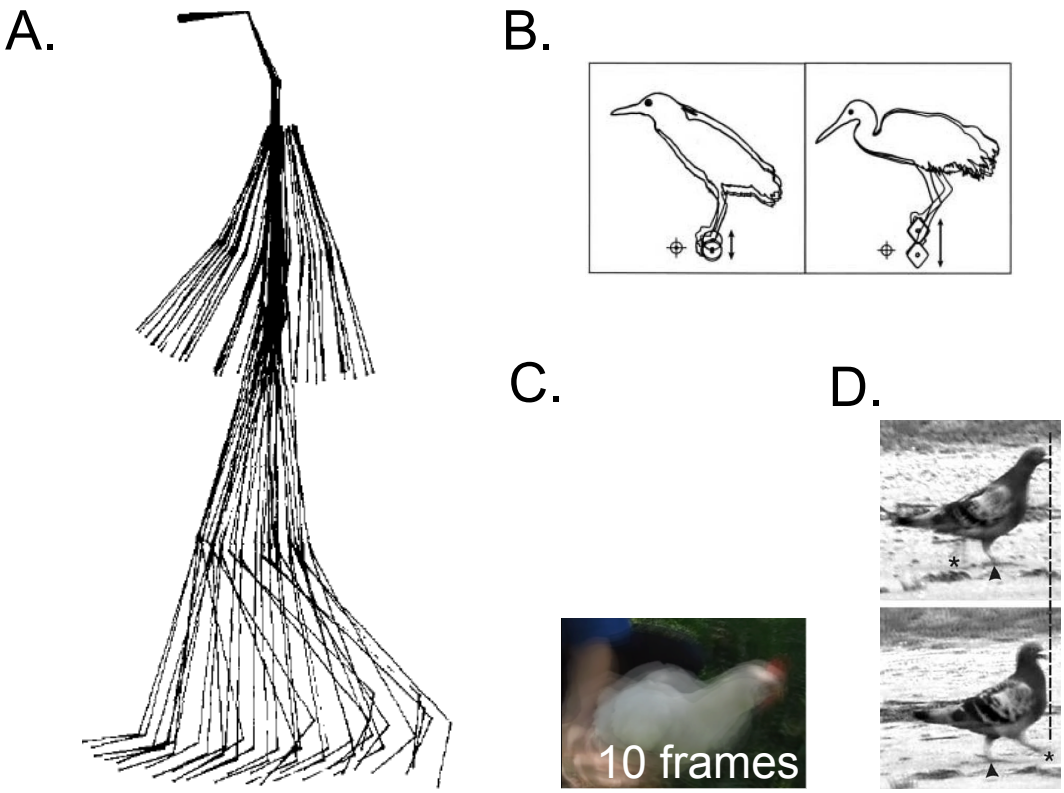

Figure 1.5: Head stabilization during locomotion. Experimental studies have shown that human and some other animals stabilized their heads during locomotion. The drawings are adapted from [158, 113, 147].

head's orientation anticipates during locomotion relatively to the walking direction [84, 160, 96]. This may suggest that the head's orientation and gaze stabilization is important for motion planning during locomotion, and both visual and vestibular cues are processed by the CNS favorably if the head is stabilized and oriented towards the walking direction. Additional studies suggested that the motion of the head, together with gaze control, is closely related to optimal postural control during locomotion [72].

In [114], a control mechanism model for head stabilization was described. Angular velocities of the head and trunk in space were recorded in seated subjects during external perturbations of the trunk. The passive mechanics of the head was changed by adding additional masses in different experimental trials. It was shown that head's stabilization in horizontal plane in yaw orientation did not differ much with respect to changed inertia of the head. For pitch motions, the response of the head-neck stabilization controller was changed when an additional mass was added to the head. However, in all the cases, subjects were stabilizing their heads while their trunk was perturbed.

In [28], balancing on a moving platform with subjects with and without bilateral vestibular loss was studied. Results showed that subjects with vestibular loss were unable to perform this task properly, and that their trunk and head were not stabilized in space, while healthy subjects were stabilizing their heads regardless to the motion of the platform.

Similarly to humans, head stabilization was observed for many other animals. For instance, head stabilization behavior was reported for cats [77]. Similar head stabilization behavior was found in monkeys during locomotion [209]. The head was stabilized and absolute values of pitch and roll head

movements did not exceed 7 degrees. Similar result were obtained for running monkeys [53]. For horses, a weaker head stabilization effect was reported [54].

Head stabilization was observed for birds, as well. In [86], head stabilization behavior in chickens during jumping and walking on surfaces of different slopes was reported. Results suggested that the head was stabilized during locomotion but the angle of stabilization increased with increasing downwards slope of the walking surface and decreased with increasing upwards slope. Head stabilization was reported for other birds such as herons, as well [113]. In most of the cases different types of herons stabilized their heads' spatial orientation and location while their body was disturbed by harmonic oscillations.

Head bobbing during locomotion is a very well known behavior for birds like pigeons, egrets, whooping cranes [70, 48, 43, 71, 185]. Head-bobbing behavior results in stabilization of the head to the surroundings for a part of each locomotion cycle. This bobbing is coupled with the locomotion and is mainly under visual control [70, 147]. In addition, the skeletal geometry of these types of animals can contribute to explain head stabilization and bobbing behavior during locomotion [193]. Some specific skeleton structures for facilitating head stabilization during locomotion were reported in [23].

In the studies just mentioned it was shown that orientation of the head is naturally stabilized during locomotion and balancing. These studies emphasized the importance of head stabilization as a part of the general postural control. In some cases head stabilization may be related to the task performed by a subject. Very often, head stabilization behavior is the result of vestibular-ocular interactions as well [92]. However, in all of these cases vestibular information is important for the head-neck control system, and sometimes it is the only source of information available [26].

One of the key roles of head stabilization is related to the establishment of a stable reference frame in which spatial perception and postural control are realized. Stable frames of reference based on vestibular information provide the brain with a mobile reference frame, which, in cooperation with vision and gaze allows a 'top-down' control of locomotion.

1.5 Perception of self-motion in robots

1.5.1 Inertial sensors

In robotic systems, inertial sensors play a role similar to that of the vestibular system in humans and animals. In this subsection we give a short introduction to inertial sensors and their applications in robotic systems. Inertial sensors are electromechanical transducers which measure mechanical translation and rotation of their bodies. Recent technological developments provided robotics with various types of inertial sensors [12, 203]. The most common types of inertial sensors are accelerometers, gyrometers and inclinometers. Very often they are combined together in what is an called inertial measurement unit (IMU).

Accelerometer

An accelerometer responds to inertial forces and gravitational forces. A schematic drawing of a simple accelerometer is shown in Fig. 1.6. A lumped mass,

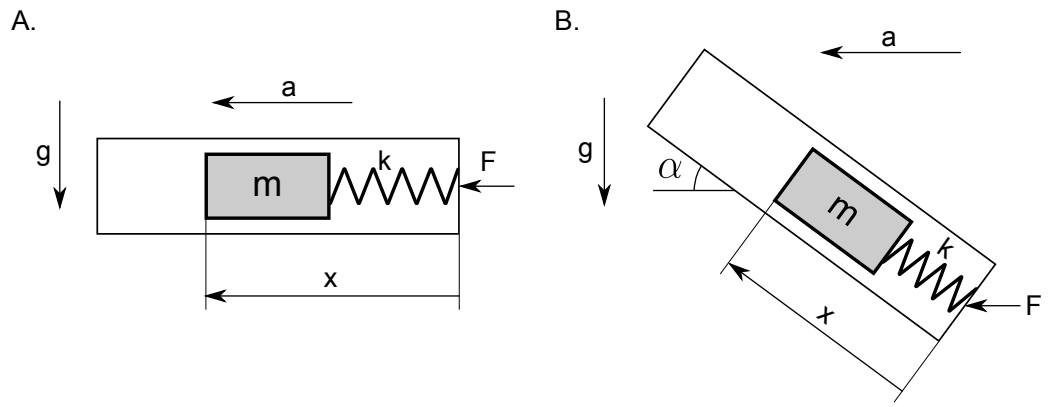

Figure 1.6: Schematic view of a simple accelerometer. Sensor is accelerated to the left (A). Sensor is accelerated to the left and tilted (B).

m, is constrained to undergo linear translation inside the frame of the sensor. The proving mass is connected to the frame by a spring of a known stiffness, k. In Fig. 1.6A, accelerometer is orthogonal to the gravitational acceleration vector, g. When a force, F, is applied to the frame of the sensor, the body moves, and its deflection, x is measured. Knowing the displacement x acceleration of the sensor's frame, a, can be calculated:

$$a = -\frac{kx}{m}. \tag{1.5}$$

Another force which is not discussed here but exists in real systems is damping which prevents infinite oscillations of the moving body.

When the accelerometer is tilted at some angle, α, as presented in Fig. 1.6B, the body's displacement will be the result of the gravitational force mg, which is the weight of the moving body. Acceleration of the sensor frame will be calculated as follows:

$$a = \frac{1}{m}(-mg\sin\alpha - kx). \tag{1.6}$$

In this case accelerometer responds to gravitoinertial acceleration which is a sum of linear and gravitational acceleration. In the situations when the accelerometer is still (no external force is applied) the measurement of accelerometer will provide the information about its frame tilt with respect to gravitational acceleration vector. In this case accelerometer can be used as tiltmeter.

Modern accelerometers are usually implemented in micro-electro-mechanical systems (MEMS) and can have sensitivity in one, two or three axis. Some examples of different technologies used in accelerometer design can be found in [119, 4, 150, 29, 162].

Gyrometer

The gyrometer is a sensor for measuring angular velocity. Modern gyrometers are implemented as MEMS [87, 146]. A common MEMS based gyrometer measures angular velocity by means of Coriolis acceleration [76]. Fig. 1.7 shows a simplified schematic view of a gyrometer. A resonant mass, which is driven in and out, is attached on a rotating disc. When the mass moves

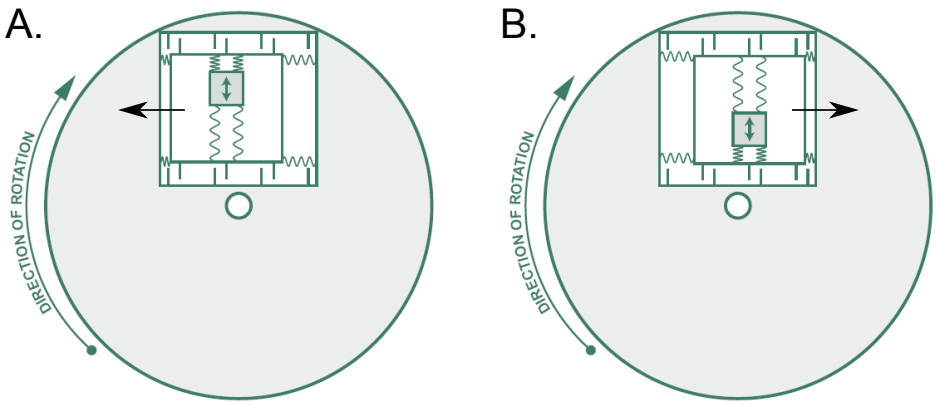

Figure 1.7: Schematic view of a simple gyrometer. A body suspended on a rotating disk is oscillated in radial direction. The tangential Coriolis force will change its direction and amplitude with respect to the angular velocity of the disc. Drawing is adapted from [76]

toward the outer edge of the rotating disk, it is accelerated to the right and exerts on the frame a reaction force to the left. Direction of the reaction force changes to the opposite one when the mass moves towards the center of the disc. The radial motion of the mass is known since it is defined by the sensors controller during the design process. The angular velocity of the rotating disc can be calculated if the tangential displacement of the resonant mass is measured. Usually, capacitive sensing is used to measure this displacement. Accelerometers and gyrometers are often packaged together in one integrated device.

Inclinometer

The inclinometer is a sensor used to measure the absolute angular orientation of a body with respect to gravitational acceleration. A very simple type of inclinometer is shown in Fig. 1.8. It includes a frame and a pendulum with concentrated mass, m, and length, l. When the frame of the sensor is tilted (Fig. 1.8A), the pendulum tends to keep its verticality, and in steady state is aligned with the gravitational acceleration vector. The measurement is an angle, α, between the pendulum and the frame of the sensor. This angle is usually measured by non-contact magnetic, optical or electromechanical means. Pendula in inclinometers are damped in order to achieve steady measurements.

Fig. 1.8B shows the case when the frame of the inclinometer is tilted and accelerated at the same time. In this case, pendulum will be inclined to an angle, β, which is a result of linear and gravitational forces. The measurement from the inclinometer is no longer tilt-related, and the sensor behaves in a same way as the tilted accelerometer in the Fig. 1.6B. Some inclinometers design examples can be found in [142, 130, 124, 212].

1.5.2 Verticality estimation methods

In this subsection we look into some basic methods of verticality estimation methods used in robotic systems. Here we limit our review only to approaches which use inertial measurements. Theoretically, a simple time integration of the gyrometers output will provide us with angular orientation of its body in

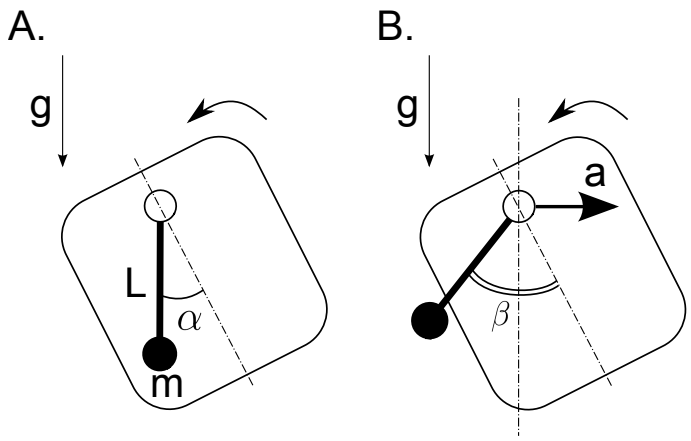

Figure 1.8: Schematic view of a simple inclinometer.

space. However, the initial conditions have to be known, which is not the case for most real life applications. Another problem with rate sensors is bias, which changes with time, temperature and other conditions. An accelerometer can be used as a tilt sensor to measure the vertical orientation of the robot in the cases when linear acceleration of the robot is negligible. But most of robotic systems, such as humanoid robots are continuously moving with varying velocities and are subject to unpredictable mechanical impacts. Generally speaking, inertial sensors are noisy because they pick-up vibrations that become added to the low frequency components of interest of the acceleration and velocity signals. Gyroscopic measurements also suffer from bias and are highly sensitive to dynamic errors. To combat these problems, different approaches to the design state observers and sensor fusion methods have been proposed to improve inertial measurements [13].

In [4], a nonlinear regression model to improve the accuracy of a low-g MEMS accelerometer was proposed. It was assumed that the accelerometer was not translated and its measurements provided the tilt information only. Similarly, in [163] the accelerometer was used as a tilt sensor. Accurate tilt sensing was achieved with a linear kinematic model which included a scale factor, bias and misalignment. It was assumed that the body did not perform any translational motion which makes this approach limited to rotations only. Gyrometer's measurements were used together with acceleration measurements in [89]. A Kalman filter for sensors alignment and calibration errors compensation was designed and implemented. Similarly to previous cases only rotations were considered.

The vertical orientation of a flying robot (autonomous helicopter) was estimated in [9]. The measurement system included an inclinometer and a rate gyro. The data coming from the sensors was fused through a complementary filter, which compensated the slow dynamics of the inclinometer. It was assumed that the robot did not perform fast accelerated motions.

A sensor fusion approach for verticality estimation in mobile robots which are translated and rotated simultaneously was proposed in [187]. The odometry was used to resolve the ambiguity of translational and gravitational components in measurements. Angular measurements from the robots wheels, joints and knowledge of its kinematics were used to provide the estimator with additional information about the robot's orientation.

In [165, 166], drift-free attitude estimation for accelerated rigid bodies was

described. The attitude estimation problem for an accelerated rigid body using gyros and accelerometers was solved with a switching algorithm which included Kalman filters. Switching was performed based on the values of estimated linear acceleration of the body. The main idea of the algorithm was to consider the translational accelerations as disturbances that were partially measured through the accelerometer. When the acceleration of the body was high, the accelerometer measurements were considered completely unreliable to provide verticality measurements and switching algorithm forced the estimator to rely on the rate gyros by setting the accelerometer noise covariance matrix to infinity.

An additional inclination sensor was used in [122]. A state estimation technique was developed for sensing inclination angles using a low-bandwidth tilt sensor along with an inaccurate rate gyro and a low-cost accelerometer. The model of rate gyro included an inherent bias along with sensor noise. The tilt sensor was modeled as a pendulum and was characterized by its own slow dynamics. These sensor dynamics was combined with the gyrometer model to achieve high-bandwidth measurements using an optimal linear state estimator. Acceleration of the system in inertial frame was measured by additional accelerometer and was considered as a known input for the estimator. However, in many robotic systems knowledge of the acceleration vector expressed in world inertial frame is unavailable or requires additional global measurements.

In [57] acceleration of a unmanned aerial vehicle expressed in world frame is estimated by an airflow sensor. This estimation together with the raw measurement from accelerometer is used to calculate the gravitational component of acceleration. But the accuracy of this method is probably not suitable for different types of robotic systems.

A multiple accelerometer based sensory system is used for attitude estimation in [184]. A set of accelerometers was attached to different locations of a rigid body and an optimal linear estimation algorithm was developed for determining pitch and roll angles of the body rotating about a fixed pivot. The estimated tilt angles values were filtered based on additional angular velocity measurements. It was however assumed that the body was supported by a fixed pivot, and therefore, limited to rotations only.

As shown above, the attitude estimation problem for robotic systems is a difficult one and its solution requires complicate, sometimes nonlinear, techniques [42]. One of the key problems of verticality estimation based on inertial sensors is the ambiguity in acceleration and inclinometer measurements. Special methods are required to separate the gravitational component of acceleration from translational component. In many cases extra sensors may facilitate the solution. For example, global positioning system (GPS) was used in [75]; magnetic field sensors were utilized in [143, 68], additional bearing information was required in [11]; landmark measurements were used in [190], Earth horizon sensor was utilized in [83], active vision system was employed in [24]. Like robotic systems, living creatures solve the problem of estimation gravitational verticality using limited set of sensors.

In this thesis we will study the problem of verticality estimation from the robotic and biological points of view, and, as a result, propose a model of human and animal sense of verticality.

1.5.3 Application in humanoid robots

In robotic systems, inertial sensors provide control systems with important information about the actual robot's state such as its acceleration, velocity and orientation. This information is important for maintaining stable motion while performing a target task. Accelerometers are often utilized as tilt sensors and gyroscopes are used to measure the change in the robot's orientation. Here, we provide a short survey on application of inertial sensors in humanoid robots.

Balancing and walking. Ordinary humanoid robot locomotion strategies are based on zero moment point (ZMP) control originally proposed by M. Vukobratovic [196, 195]. In this case, knowledge about the robot kinematic configuration and mass distribution is sufficient for stable locomotion. Modern humanoid robotics requires robots to move faster and perform more complicated tasks. This may require additional sensory information, such as inertial measurements, which can be helpful for balance control of a humanoid body.

For example, in [181] the AAU-BOT1 humanoid robot has an IMU placed in the trunk which was used for balance control during locomotion. The orientation of the robot was measured by accelerometers and gyroscopes. Foot-ground force reactions measured by force sensors were considered to be the dominant information for walking controller.

The tilt and angular velocity measurements of the humanoid's torso was used for balance and walking control in [115]. Tilt was measured by accelerometers attached to the torso of the robot. Direct measurements were used by the torso roll and pitch controllers as well as the predicted motion controller to avoid tilt-over situations.

An inertial measurement unit was used for humanoid balance control in [39, 94]. Three axis accelerometer and gyro were attached close to the center of mass in the trunk of the robot. Angular velocity information was used for the center of mass measurement and calculation of the desired ground interaction force direction in order to maintain a stable posture.

The balance control of humanoid robot was described in [33]. The robot's body was equipped with an IMU for measuring trunk's angular velocity and orientation in space. This information was used for the robot's actual posture calculation together with the measurements from joint sensors.

Biologically inspired postural and reaching control for humanoid robot was presented in [183]. A humanoid robot was equipped with an accelerometer and a gyrometer in the head. Normal and tangential contact forces between the robot and the platform were measured by force sensors. Unlike described in most of the humanoid research literature, in [183], the platform's (ground's) non zero inclination was considered to be unknown. Unknown ground tilt and disturbance forces were estimated based on measurements from accelerometer and gyrometer. Estimation was implemented by Kalman filtering. It was claimed that inertial sensors and their signals processing could be called as artificial vestibular system of the humanoid robot [183].

Gaze and head stabilization. In many recently developed humanoid robots, the vestibular ocular reflex is realized for gaze stabilization. Common human-like robots heads are equipped with two video cameras. Stereo information from these cameras is used for robot's localization and visual perception of

the environment. For instance, it may be very important for planning grasping tasks. This visual flow should be stabilized by implementation a gaze stabilization behavior like it is done in biological systems. In addition, this gaze stabilization behavior made a humanoid robot more natural and realistic, which is important in human-robot interaction scenarios.

One of the first humanoid ocular-motor control system was described in [175, 176]. A biomimetic gaze stabilization based on measurement from three gyros in the head of the robot was implemented. A feedback-error learning algorithm with neural networks was applied to achieve human like vestibulo-ocular and optokinetic reflexes.

In [153], the humanoid robot's head was equipped with an IMU and video cameras. Measurements from the IMU and analysis of visual flow from cameras were used for achieving efficient visual stabilization. Inertial sensors provided short latency measurement of rotation and translation of the robot's head. Visual flow information provided a delayed estimate of the motion across the image plane. A self-tuning neural network was used to learn to integrate visual and inertial information and to generate proper oculomotor control signals.

Similar research was published recently. In [39], three axis gyrometer and accelerometer in the head of the humanoid were used for controlling the gaze and implementing visual attention system. In [127], biomimetic eye-neck coordination control was proposed and used for visual target tracking. Proprioceptive feedback from neck joints and vestibular signals from inertial sensors in the head were processed together. The control system was tested with an iCub humanoid robot.

Vision-only gaze stabilization was presented in [74]. Adaptive frequency oscillators were used to learn the frequency, phase and amplitude of the optical flow from the robot's cameras during locomotion. The developed vision based control was used for gaze stabilization during periodic locomotion and for visual object tracking.

Location of inertial sensors in humanoid robots. In living creatures the vestibular system is located in the head, which is explained by their evolutionary development and the specific roles of vestibular organs. In robotic systems, a common design wisdom is that the inertial sensors are located close to the center of mass of a humanoid robot. A majority of humanoid robots have their IMU located in the main body. Locating an IMU close to the center of mass provides information about motion of the center of mass, of rotations about it, and allows the application of simple models (inverted pendulum) for locomotion and balancing control tasks. In the Table 1.1 we summarized our survey results on location of inertial sensors in humanoid robots used in research.

As we can see from the table, a majority of the robots have their IMU, or, we may call it, artificial vestibular system, in the main body: hip, torso, trunk or pelvis. Only some robots have their IMU located in the head. Fig. 1.9, shows some of these robot's with their locations of inertial sensors. In robots like Cog, [27], and iCub, [186, 154], the IMU is located in their heads. However, the original design of these robots did not include locomotion functionalities, since they were mainly used for interaction and computational neuroscience studies. ARMAR-III robot, [7], has its inertial sensors in the head, but the lower body of the robot is based on a wheeled platform, which makes it very different from

Table 1.1: Location of inertial sensors in humanoid robots

Robot's name	IMU location	Publication reference	Year of publication
Cog	head	[27]	1999
ASIMO	upper body	[169, 99]	1999
ATLAS (DASL-1)	pelvis	[107]	2002
H7	upper body	[109]	2004
KHR-3 HUBO	torso	[156]	2005
FHR-1 FIBO	hip	[207]	2006
KHR-2	torso	[115]	2006
CB	head & torso	[39, 94]	2007
iCub	head	[186, 154]	2007, 2012
MAHRU-R	pelvis	[33]	2008
ARMAR-III	head	[7]	2008
Lola	upper body	[30, 126]	2009
NAO	torso	[82]	2009
AAU-BOT1	trunk	[181]	2009
Sarcos Primus	hip	[178]	2010
KOBIAN	head	[118]	2012
WABIAN	head	[59]	2012

legged biological systems. To our knowledge very few physical humanoid robots use inertial sensors in the head for posture control during locomotion and balancing. CB humanoid, [39, 94], uses two IMUs: one in the head and another one in the torso. Information from both of them is used to coordinate eyes, head and torso movements [180]. In [118] and [59], robotic heads were equipped with IMUs which were used for head stabilization during locomotion. In [118], direct measurements of the head's angular orientation were fed back to linear control of the head. However, the performance of this head stabilization system was quite low, because there were no filtering or estimation methods used for sensory data processing. In [59], a feedback learning algorithm was employed to stabilize the head orientation independently from the trunk motion. A neural network was used to learn the unknown head dynamics.

In the humanoid robotics research discussed above, some of the authors mentioned that inertial sensors can be considered as artificial vestibular systems. However, it is only in some cases that inertial sensors may be viewed as artificial vestibular systems. In this subsection we review some of the literature on biologically-inspired design of inertial sensors and some attempts on artificial vestibular system development.

In [191], one of the first attempts to design artificial vestibular system was presented. It was suggested to integrate bi-axial accelerometer and uni-axial gyrometer in a single inertial sensing unit. Later, in [152] a three axial artificial vestibular system was described. It included a sensing unit with three orthogonal planes. Each plane was equipped with a MEMS-based accelerometer and gyrometer. The design approaches described in [191] and [152] are similar to the one used in classical sensor engineering, when a set of individual inertial sensors are integrated together in a single IMU. An attempt to realize a

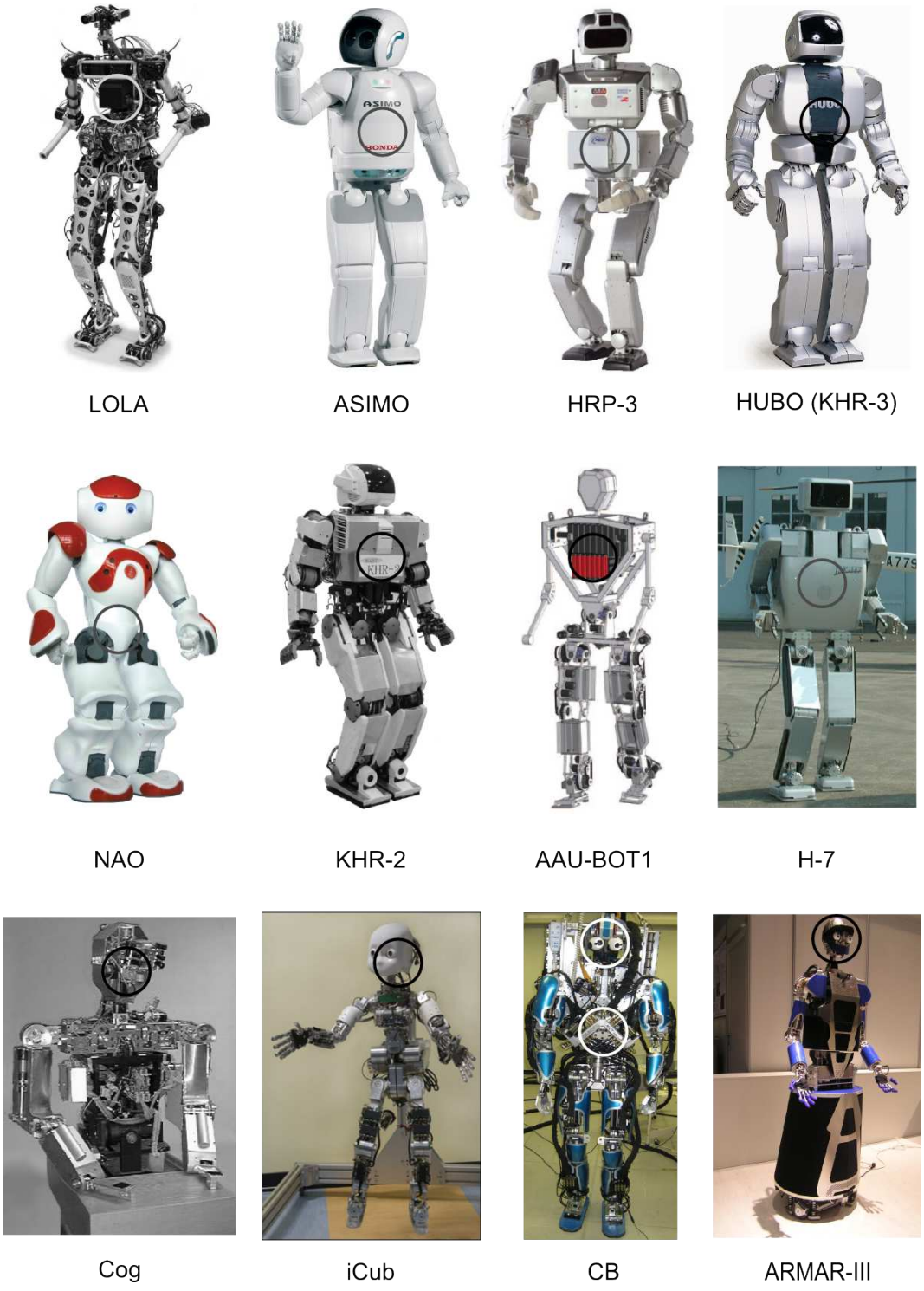

Figure 1.9: Location of inertial sensors in humanoid robots: most of the robots have their IMU located in the main body. All figures are adapted from the relevant research publications.

biomimetic angular rate sensor was presented in [41]. A biomechanical model of the semicircular canals of the human vestibular system was proposed and a first prototype was realized. However, no further experimental results were presented. A more general view of an artificial vestibular system as a part of sensory system of artificial robotic rat is given in [144, 31]. The artificial vestibular system of a rat, which is realized with inertial sensors, was used in robot navigation.

In applied bioengineering and rehabilitation research the artificial vestibular system may be employed as prostheses. This is a relatively new field of rehabilitation engineering research which aims at substituting vestibular information from injured or malfunctioning inner ear organs. Electric signals generated with the help of artificial inertial sensors are used to stimulate the neural system [197, 97]. A gyroscope which measures angular velocity of a human subject was used to replace malfunctioning vestibular system in [50, 138]. The measurements were transmitted to vestibular nerves through implanted electrodes. Initial neural signal decoding and learning was done for proper translation of angular velocity information. This and other research efforts showed that this type of sensory substitution in animals and humans is feasible [40, 123].

1.5.4 Role of head stabilization

Spatial head stabilization in biological systems was discussed at the beginning of this chapter. It was seen that head stabilization is important for vision and it enables the establishement of a stable frame of reference within the body. A stabilized robotic head would presumably benefit from the same advantages as those of natural heads and these observations led us to believe that humanoid robots should also adopt a similar strategy. In this section we describe the advantages of locating an IMU in a the head of a humanoid robot rather than in any other parts of its anatomy.

Among numerous other potential advantages, it is supposed that a robot head that is horizontally stabilized during locomotion facilitates the estimation of the gravitational vertical. Knowledge of the direction of the gravity vector, that is of the gravitational vertical, is essential to achieve stance and locomotion since the gravitational vertical may be poorly estimated from visual cues or from the relationship of the robot to the ground. We suggest that a stabilized robotic head may improve the quality of inertial measurements of the sensors located in this head. First of all, we suppose that a head stabilized independently from the motion of the trunk will be less affected by external forces and disturbances which may occur during locomotion. Second, if a head is stabilized in the upright vertical position, then at least one of the axes of inertial sensors will be aligned with gravitational acceleration. This means that a simpler estimation method can be used to process the measurements from inertial sensors, such as accelerometer. In some situations it may be assumed that an accelerometer located in the upright stabilized head will measure independently gravitational and translational components of acceleration. However, to stabilize a robotic head with respect to gravitational verticality requires knowledge of this verticality, and in our case the only available information related to gravitational verticality can be obtained from inertial sensors, in particular from an accelerometer. This means that the control loop has to be

closed by the feedback of the measured or estimated vertical orientation of the head, leading to an observer based closed loop control system. The task of observer is to estimate the vertical orientation of the head based on inertial sensor measurements without the explicit knowledge of translational acceleration of the head. Hence, our head observation-stabilization system can be considered to be self-sufficient, or, in other words, ideothetic.

Idiothetic sensing, or sensing entirely based on states measured with reference to one's own body, is of course not special to robots. In aerospace engineering, flying and rocketing vehicles also use IMUs. Long ago, it was noticed that rocket guidance was greatly simplified if the inertial sensors were placed on stabilized platforms [55, 116]. In such systems, the application of fundamental mechanical principles and stabilizing control provided engineers with the possibility to establish a gravity referenced Earth's inertial frame without the need of other external references. Ideothetic inertial sensing can be useful to any type of mobile robotic systems [13].

In this thesis, we address the problem of gravitational vertical estimation with consideration of the nonlinear dynamics of inertial sensors, and we show that the horizontal stabilization of a sensing platform yields a dramatic improvement in the estimation of the gravitational vertical in the face of strong perturbations, compared to when the same sensors are rigidly attached to an arbitrary body of a humanoid robot kinematic tree.

Top-down control in locomotion Recent research literature on locomotion proposed the concept of top-down control organization. It was suggested the posture control during locomotion is governed in the head's frame of reference. As the head is stabilized, a stable frame of reference is achieved. Inertial measurements from vestibular system are expressed in this frame of reference and are used for gaze control. Gaze direction anticipates on head orientation which in turn anticipates on the body segments during locomotion [108, 120, 15].

Following this concept, a humanoid robot can be controlled in its stabilized head's frame of reference as it was done in [177]. A humanoid robot was teleoperated and its desired walking direction and posture were given to the controller in head's frame. This example of humanoid control with top-down organization is different from classical humanoid locomotion control when posture configuration is defined in the world (ground) reference frame. In most of humanoid walking applications, the ground is assumed to be flat and rigid, and its inclination has to be known. However, the concept of top-down control organization suggests that the only information which is required is joint (proprioceptive) information of the robot's body with respect to a stabilized head's frame of reference.

We believe that this study on modeling verticality estimation presented in the next chapters may clarify some aspects of vestibular system functioning, and results of this study may be helpful to improve future human like robotic systems.

Chapter 2

Model

Contents

In this chapter we introduce a general model for a vestibular system. Since our primary interest is verticality estimation, we model the function of the otoliths. We apply the robotic based dynamics representation for otoliths modeling and present two models: the medial model and the lateral model. The medial model considers a vestibular system located in the center of the head, while the lateral model includes two sets of vestibular organs located aside from the center of the head.

2.1 Models of otoliths

In this section we present mathematical models of the otoliths as principal organs of the vestibular system, which are responsible for verticality measurement. We consider the three-dimensional case when human head can be rotated and translated, as shown in Fig. 2.1. Three planes are defined in Fig. 2.1. The sagittal plane is a vertical plane which divides the head into right and left halves. The coronal plane is a vertical plane which is orthogonal to the sagittal plane. The horizontal plane is orthogonal to the first two vertical planes. We take into account several assumptions. First of all, we consider that the head-neck kinematics can be described with a simple spherical joint. We also assume that the intersection point of the head's three planes coincides with the center of rotation of the head. We assume that the vestibular organs of both inner ears lie in the intersection line of the horizontal and coronal planes. Three head rotations are considered: the sagittal tilt in the sagittal plane, the coronal tilt in the coronal plane, and the yaw rotation in the horizontal plane (Fig. 2.1B). The head can be accelerated in three directions:

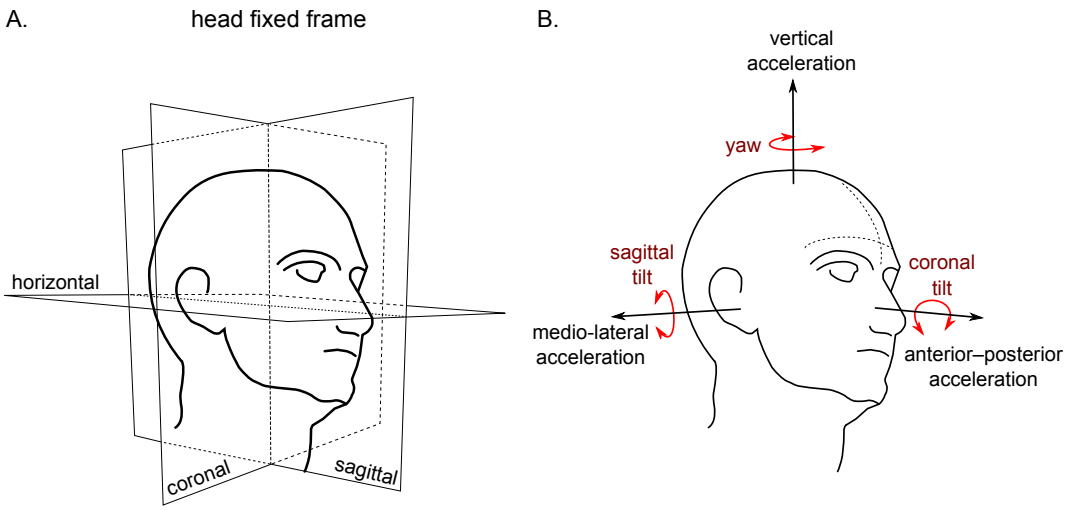

Figure 2.1: Human head and its body fixed frame. A: Three orthogonal planes are defined - sagittal, coronal and horizontal. B: Head can be rotated and translated in three orthogonal directions.

the anterior-posterior direction, the medio-lateral direction and the vertical direction.

In the foregoing discussion, vector and tensor quantities that are sensitive to the frame in which they are expressed receive a left superscript to indicate it. Therefore, a rotation transformation written as ${}_{\mathbb{B}}\mathbf{R}_{\mathbb{A}} \in \mathcal{SO}(3)$ is a rotation matrix that transforms, by left multiplication, vectors expressed in frame $\mathbb{A}$ into vectors expressed in some frame $\mathbb{B}$. Alternatively, it expresses the orientation of $\mathbb{A}$ with respect to $\mathbb{B}$. If $\mathbb{B}$ is a frame moving with respect to $\mathbb{A}$ and ${}^{\mathbb{A}}\boldsymbol{q}$ is a position vector expressed in frame $\mathbb{A}$, then $\mathrm{d}^{\mathbb{B}}\boldsymbol{q}/\mathrm{d}t = \mathrm{d}^{\mathbb{A}}\boldsymbol{q}/\mathrm{d}t + {}^{\mathbb{B}}_{\mathbb{B}}\boldsymbol{\omega}_{\mathbb{A}} \times {}^{\mathbb{A}}\boldsymbol{q}$, where ${}^{\mathbb{B}}_{\mathbb{B}}\boldsymbol{\omega}_{\mathbb{A}}$ is the angular velocity of frame $\mathbb{A}$ relatively to $\mathbb{B}$, expressed in frame $\mathbb{B}$. Given an angular velocity vector ${}^{\mathbb{B}}_{\mathbb{B}}\boldsymbol{\omega}_{\mathbb{A}}$, the symbol ${}^{\mathbb{B}}_{\mathbb{B}}\tilde{\boldsymbol{\omega}}_{\mathbb{A}}$ is used to denote the corresponding skew-symmetric matrix, facilitating differentiation.

The key element of the models proposed in the following sections is three dimensional spherical pendulum. Newton-Euler based formulation of the pendulum dynamics is used. Detailed mathematical analysis of three dimensional pendulum dynamics and related control problems can be found in recently published works by N. H. McClamroch and his colleagues [36, 38, 35, 170].

2.1.1 Medial model

We first present a model for verticality estimation based on one spherical pendulum. Fig. 2.2 shows schematic view of the model with one pendulum attached to the center of the head through a spherical joint. We model human's head as a symmetric rigid body which may freely rotate around its center of mass in three-dimensional space. To formulate the model we define the following coordinate frames: (i) frame $\mathbb{I}$ is the inertial frame with unit vectors, $\left\{{}^{\mathbb{I}}\boldsymbol{i}, {}^{\mathbb{I}}\boldsymbol{j}, {}^{\mathbb{I}}\boldsymbol{k}\right\}$; (ii) frame $\mathbb{H}$ is the body-fixed head frame with unit vectors, $\left\{{}^{\mathbb{H}}\boldsymbol{i}, {}^{\mathbb{H}}\boldsymbol{j}, {}^{\mathbb{H}}\boldsymbol{k}\right\}$ and with origin at the center of mass of the head; (iii) frame $\mathbb{S}$ is the body-fixed pendulum (sensor) coordinate frame with unit vectors, $\left\{{}^{\mathbb{S}}\boldsymbol{i}, {}^{\mathbb{S}}\boldsymbol{j}, {}^{\mathbb{S}}\boldsymbol{k}\right\}$ such that its ${}^{\mathbb{S}}\boldsymbol{k}$ axis is aligned with the arm of the pendulum and such that the pivot coincides with the center of the head. The orientation of the head's frame, $\mathbb{H}$, with respect to inertial world frame, $\mathbb{I}$, is described by a rotation matrix ${}_{\mathbb{I}}\mathbf{R}_{\mathbb{H}} \in \mathcal{SO}(3)$. The center of mass of the head is located

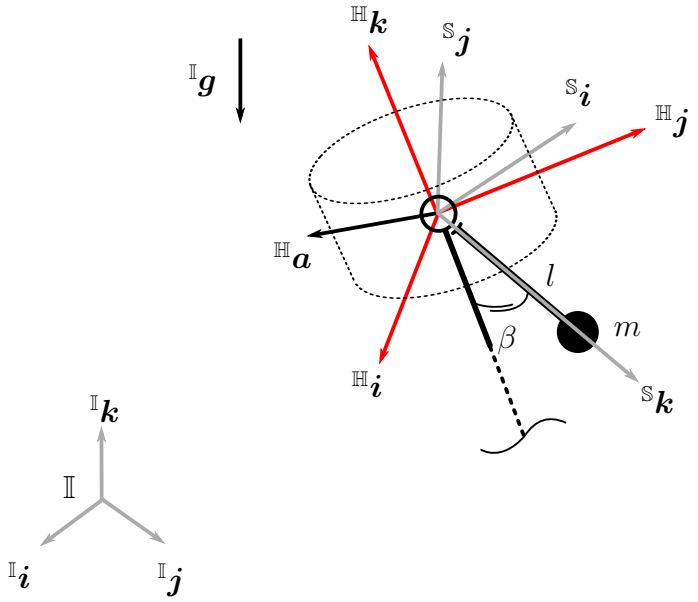

Figure 2.2: Schematic view of the medial model. The medial model comprises a rigid body (head) and a damped spherical pendulum attached to the center of rotation of the body.

at the center of rotation of the head. The head-neck joint is modeled as a spherical joint. The principal moment of inertia of the head expressed in the body-fixed frame $\mathbb{H}$ is defined as ${}^{\mathbb{H}}\mathbf{J}_{\mathrm{H}}$. The head's angular momentum and its derivative are:

$$\boldsymbol{h}_{\mathrm{H}} = {}^{\mathbb{H}}\mathbf{J}_{\mathrm{H}\,\mathbb{I}}^{\mathbb{H}}\boldsymbol{\omega}_{\mathbb{H}}, \tag{2.1}$$

$$\dot{\boldsymbol{h}}_{\mathrm{H}} = \frac{\mathrm{d}}{\mathrm{d}t}\left({}^{\mathbb{H}}\mathbf{J}_{\mathrm{H}\,\mathbb{I}}^{\mathbb{H}}\boldsymbol{\omega}_{\mathbb{H}}\right) = {}^{\mathbb{H}}\mathbf{J}_{\mathrm{H}\,\mathbb{I}}^{\mathbb{H}}\dot{\boldsymbol{\omega}}_{\mathbb{H}} + {}_{\mathbb{I}}^{\mathbb{H}}\boldsymbol{\omega}_{\mathbb{H}} \times {}^{\mathbb{H}}\mathbf{J}_{\mathrm{H}\,\mathbb{I}}^{\mathbb{H}}\boldsymbol{\omega}_{\mathbb{H}}, \tag{2.2}$$

where ${}_{\mathbb{I}}^{\mathbb{H}}\boldsymbol{\omega}_{\mathbb{H}}$ is the angular velocity of the head's frame $\mathbb{H}$ around the inertial world frame $\mathbb{I}$ expressed in $\mathbb{H}$. Then, the dynamics of the head which is driven by torque, ${}^{\mathbb{H}}\boldsymbol{\tau}$, is

$${}^{\mathbb{H}}\mathbf{J}_{\mathrm{H}\,\mathbb{I}}^{\mathbb{H}}\dot{\boldsymbol{\omega}}_{\mathbb{H}} = -{}_{\mathbb{I}}^{\mathbb{H}}\boldsymbol{\omega}_{\mathbb{H}} \times {}^{\mathbb{H}}\mathbf{J}_{\mathrm{H}\,\mathbb{I}}^{\mathbb{H}}\boldsymbol{\omega}_{\mathbb{H}} + {}^{\mathbb{H}}\boldsymbol{\tau}. \tag{2.3}$$

Here, the torque, ${}^{\mathbb{H}}\boldsymbol{\tau}$, represent the efforts of the neck muscles for orienting the head with respect to the torso. The kinematics of the head rotations is described by

$${}_{\mathbb{I}}\dot{\mathbf{R}}_{\mathbb{H}} = {}_{\mathbb{I}}\mathbf{R}_{\mathbb{H}\,\mathbb{I}}^{\mathbb{H}}\tilde{\boldsymbol{\omega}}_{\mathbb{H}}, \tag{2.4}$$

where ${}_{\mathbb{I}}^{\mathbb{H}}\tilde{\boldsymbol{\omega}}_{\mathbb{H}}$ is a skew-symmetric matrix of the angular velocity ${}_{\mathbb{I}}^{\mathbb{H}}\boldsymbol{\omega}_{\mathbb{H}}$.

Next, we model the vestibular system. Consider a damped spherical pendulum attached to the center of the head as shown in Fig. 2.2. The dynamics

and kinematics of this pendulum is described by the following equations:

$$
\begin{aligned}
{}^{\mathbb{S}}\mathbf{J}_{\mathrm{S}}\,{}^{\mathbb{S}}_{\mathbb{I}}\dot{\boldsymbol{\omega}}_{\mathbb{S}} = &- \underbrace{{}^{\mathbb{S}}_{\mathbb{I}}\boldsymbol{\omega}_{\mathbb{S}} \times {}^{\mathbb{S}}\mathbf{J}_{\mathrm{S}}\,{}^{\mathbb{S}}_{\mathbb{I}}\boldsymbol{\omega}_{\mathbb{S}}}_{\text{gyroscopic}} + \underbrace{m\,{}^{\mathbb{S}}\boldsymbol{l} \times {}_{\mathbb{S}}\mathbf{R}_{\mathbb{I}}\,{}^{\mathbb{I}}\boldsymbol{g}}_{\text{gravity}} - \underbrace{\beta({}^{\mathbb{S}}_{\mathbb{I}}\boldsymbol{\omega}_{\mathbb{S}} - {}_{\mathbb{S}}\mathbf{R}_{\mathbb{I}}\,{}_{\mathbb{I}}\mathbf{R}_{\mathbb{H}}\,{}^{\mathbb{H}}_{\mathbb{I}}\boldsymbol{\omega}_{\mathbb{H}})}_{\text{damping}} \\
&- \underbrace{m\,{}^{\mathbb{L}}\boldsymbol{l} \times {}_{\mathbb{S}}\mathbf{R}_{\mathbb{I}}\,{}_{\mathbb{I}}\mathbf{R}_{\mathbb{H}}\,{}^{\mathbb{H}}\boldsymbol{a}}_{\text{acceleration}}, \qquad (2.5) \\
{}_{\mathbb{I}}\dot{\mathbf{R}}_{\mathbb{S}} = &\,{}_{\mathbb{I}}\mathbf{R}_{\mathbb{S}}\,{}^{\mathbb{S}}_{\mathbb{I}}\tilde{\boldsymbol{\omega}}_{\mathbb{S}}, \qquad (2.6)
\end{aligned}
$$

where ${}^{\mathbb{S}}\mathbf{J}_{\mathrm{S}}$ is the pendulum's principal inertia tensor; ${}^{\mathbb{S}}_{\mathbb{I}}\boldsymbol{\omega}_{\mathbb{S}}$ is the angular velocity of the pendulum-fixed frame with respect to the world frame; ${}^{\mathbb{S}}\boldsymbol{l} = \begin{pmatrix} 0 & 0 & l \end{pmatrix}^{\top}$ is the vector from the pivot of the pendulum to the center of its mass; ${}_{\mathbb{S}}\mathbf{R}_{\mathbb{I}} = {}_{\mathbb{I}}\mathbf{R}_{\mathbb{S}}{}^{\top}$ and ${}_{\mathbb{I}}\mathbf{R}_{\mathbb{S}} \in \mathcal{SO}(3)$ is rotation matrix which defines the orientation of the pendulum (sensor) frame, $\mathbb{S}$, with respect to the world frame, $\mathbb{I}$; and ${}^{\mathbb{H}}\boldsymbol{a}$ the linear acceleration of the head's center of mass expressed in the head's frame. In addition to the gyroscopic term as in the head dynamics, here we have a gravitational component with the gravitational acceleration vector ${}^{\mathbb{I}}\boldsymbol{g} = \begin{pmatrix} 0 & 0 & -9.81 \end{pmatrix}^{\top}$, a damping term β and a linear acceleration component. The head's motion influences the pendulum's motion through damping coupling (head rotation) and through acceleration component (head translation). As a result the pendulum moves in a non inertial frame. When the head is in steady state, in the presence of the Earth's gravity field the pendulum will tilt towards the gravitational vertical. For further analysis of the model we employ the following assumptions. The influence of the pendulum on the motion of the head is disregarded, as the mass of the pendulum is considered negligibly small, however, the viscous torque resulting from the difference of the angular velocities of the head and pendulum must be accounted for. The gyroscopic term for the head dynamics is assumed to be negligibly small, as well. As a result, we obtain the following system of coupled equations,

$$
\begin{aligned}
{}^{\mathbb{S}}\mathbf{J}_{\mathrm{S}}\,{}^{\mathbb{S}}_{\mathbb{I}}\dot{\boldsymbol{\omega}}_{\mathbb{S}} &= m\,{}^{\mathbb{S}}\boldsymbol{l} \times {}_{\mathbb{S}}\mathbf{R}_{\mathbb{I}}\,{}^{\mathbb{I}}\boldsymbol{g} - \beta({}^{\mathbb{S}}_{\mathbb{I}}\boldsymbol{\omega}_{\mathbb{S}} - {}_{\mathbb{S}}\mathbf{R}_{\mathbb{I}}\,{}_{\mathbb{I}}\mathbf{R}_{\mathbb{H}}\,{}^{\mathbb{H}}_{\mathbb{I}}\boldsymbol{\omega}_{\mathbb{H}}) - m\,{}^{\mathbb{L}}\boldsymbol{l} \times {}_{\mathbb{S}}\mathbf{R}_{\mathbb{I}}\,{}_{\mathbb{I}}\mathbf{R}_{\mathbb{H}}\,{}^{\mathbb{H}}\boldsymbol{a}, \\
{}^{\mathbb{H}}\mathbf{J}_{\mathrm{H}}\,{}^{\mathbb{H}}_{\mathbb{I}}\dot{\boldsymbol{\omega}}_{\mathbb{H}} &= {}^{\mathbb{H}}\boldsymbol{\tau}, \\
{}_{\mathbb{I}}\dot{\mathbf{R}}_{\mathbb{S}} &= {}_{\mathbb{I}}\mathbf{R}_{\mathbb{S}}\,{}^{\mathbb{S}}_{\mathbb{I}}\tilde{\boldsymbol{\omega}}_{\mathbb{S}}, \\
{}_{\mathbb{I}}\dot{\mathbf{R}}_{\mathbb{H}} &= {}_{\mathbb{I}}\mathbf{R}_{\mathbb{H}}\,{}^{\mathbb{H}}_{\mathbb{I}}\tilde{\boldsymbol{\omega}}_{\mathbb{H}}.
\end{aligned} \qquad (2.7)
$$

In the vestibular system, the otolith organs measure inclination of the head with respect to the gravitational vertical in the sagittal and the coronal planes. In our model the measurements will correspond to the angles between unit vector ${}^{\mathbb{S}}\boldsymbol{k}$ (projected to the sagittal and the coronal planes of frame $\mathbb{H}$) and unit vector ${}^{\mathbb{H}}\boldsymbol{k}$. These projections can be expressed through the elements of rotations and therefore we can easily express the inclination angles of the pendulum in the sagittal and the coronal planes,

$$
\tan\phi_x = \frac{\left[{}_{\mathbb{H}}\mathbf{R}_{\mathbb{S}}\right]_{\{3,2\}}}{\left[{}_{\mathbb{H}}\mathbf{R}_{\mathbb{S}}\right]_{\{3,3\}}}, \qquad (2.8)
$$

$$
\tan\phi_y = \frac{\left[{}_{\mathbb{H}}\mathbf{R}_{\mathbb{S}}\right]_{\{3,1\}}}{\left[{}_{\mathbb{H}}\mathbf{R}_{\mathbb{S}}\right]_{\{3,3\}}}, \qquad (2.9)
$$

where ${}_{\mathbb{H}}\mathbf{R}_{\mathbb{S}} = {}_{\mathbb{I}}\mathbf{R}_{\mathbb{H}}{}^{\top}\,{}_{\mathbb{I}}\mathbf{R}_{\mathbb{S}}$; notation $[\mathbf{M}]_{\{n,m\}}$ is used to define the element of

the matrix $\mathbf{M}$ in the n-th row and m-th column. Angles ϕ_x, ϕ_y are the angles between the projections of ${}^{\mathbb{S}}\boldsymbol{k}$ in the sagittal and coronal head planes and ${}^{\mathbb{H}}\boldsymbol{k}$, respectively. We consider equations (2.8)-(2.9) as outputs for the system (2.7) which correspond to the otolith measurements in the human vestibular system. Outputs of the system are driven by head rotations (torque ${}^{\mathbb{H}}\boldsymbol{\tau}$) and head's translations (linear acceleration ${}^{\mathbb{H}}\boldsymbol{a}$).

To generalize these expressions, we define the state, $\boldsymbol{x}_1 = \left({}^{\mathbb{S}}_{\mathbb{I}}\boldsymbol{\omega}_{\mathbb{S}}, {}^{\mathbb{H}}_{\mathbb{I}}\boldsymbol{\omega}_{\mathbb{H}}, {}_{\mathbb{I}}\mathbf{R}_{\mathbb{S}}, {}_{\mathbb{I}}\mathbf{R}_{\mathbb{H}}\right)^{\top}$, made of the elements of the vectors where the matrices are arranged in a single vector. The system is then conveniently expressed in the form,

$$\dot{\boldsymbol{x}}_1 = f_1(\boldsymbol{x}_1, \boldsymbol{u}) \tag{2.10}$$

where $\boldsymbol{u} = \left({}^{\mathbb{H}}\boldsymbol{\tau}, {}^{\mathbb{H}}\boldsymbol{a}\right)^{\top}$ is an input due to the movement of the robot combined with the torque applied to the head. The output for the system is defined by (2.8)-(2.9).

Planar case

Sometimes, it is practical to only consider the planar case of a model. In this subsection we define the model which is applicable for motions in the sagittal or the coronal planes. The equations of motion (2.7) can be modified for the planar case if the head and pendulum's rotation are restricted to one plane. Then, the rotation matrix of the head is of the form

$${}_{\mathbb{I}}\mathbf{R}_{\mathbb{H}} = \begin{pmatrix} 1 & 0 & 0 \\ 0 & r_{\mathrm{h}[2,2]} & r_{\mathrm{h}[2,3]} \\ 0 & r_{\mathrm{h}[3,2]} & r_{\mathrm{h}[3,3]} \end{pmatrix}$$

where $r_{\mathrm{h}[\cdot,\cdot]}$ is an element of the rotation matrix. Noting that $r_{\mathrm{h}[2,2]} = r_{\mathrm{h}[3,3]}$ and $r_{\mathrm{h}[2,3]} = -r_{\mathrm{h}[3,2]}$ and applying the same modifications to ${}_{\mathbb{I}}\mathbf{R}_{\mathbb{S}}$ in (2.7) we obtain the following equations of motion in plane expressed in scalar form,

$$\begin{aligned}
J\dot{\omega}_{\mathrm{s},x} &= mlgr_{\mathrm{s}[3,2]} - \beta(\omega_{\mathrm{s},x} - \omega_{\mathrm{h},x}) \\
&\quad + ml((r_{\mathrm{s}[3,3]}r_{\mathrm{h}[3,3]} + r_{\mathrm{s}[3,2]}r_{\mathrm{h}[3,2]})a_y + (r_{\mathrm{s}[3,2]}r_{\mathrm{h}[3,3]} - r_{\mathrm{s}[3,3]}r_{\mathrm{h}[3,2]})a_z), \\
\dot{r}_{\mathrm{s}[3,2]} &= r_{\mathrm{s}[3,3]}\omega_{\mathrm{s},x}, \\
\dot{r}_{\mathrm{s}[3,3]} &= -r_{\mathrm{s}[3,2]}\omega_{\mathrm{s},x}, \\
J_{\mathrm{h}}\dot{\omega}_{\mathrm{h},x} &= \tau_x, \\
\dot{r}_{\mathrm{h}[3,2]} &= r_{\mathrm{h}[3,3]}\omega_{\mathrm{h},x}, \\
\dot{r}_{\mathrm{h}[3,3]} &= -r_{\mathrm{h}[3,2]}\omega_{\mathrm{h},x},
\end{aligned}$$

with $\omega_{\mathrm{s},x}$ and $\omega_{\mathrm{h},x}$ angular velocities of the pendulum and the head in the sagittal plane, $r_{\mathrm{s}[\cdot,\cdot]}$ - elements of thependulum's rotation matrix. Equations of motion for the coronal plane can be derived in the same way.

2.1.2 Lateral model

The normal vestibular system comprises two inner ears located laterally from the center of the head. In this subsection we extend our previous model by considering the dynamics of two spherical damped pendulums. We consider that pendulum's dynamic parameters are identical to the model with one pendu-

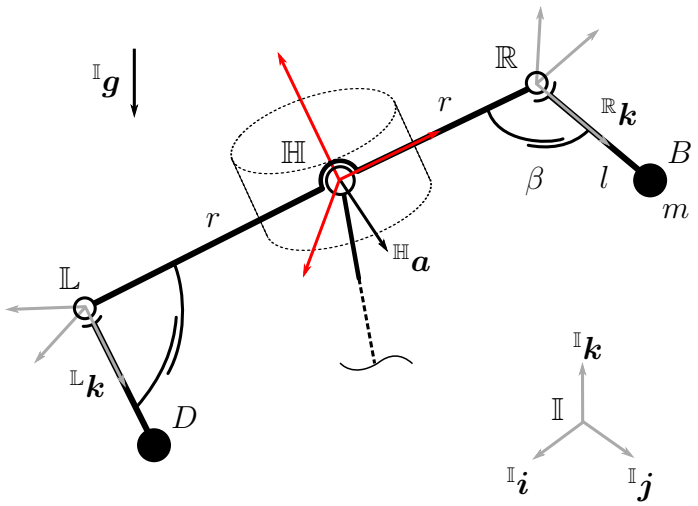

Figure 2.3: Schematic view of the lateral model. The lateral model comprises a rigid body (head) and two damped spherical pendulums attached aside from the center of rotation of the body.

lum. Schematic view of the model is shown in Fig. 2.3. The head's body-fixed frame, $\mathbb{H}$, is attached to the center of the head. Two spherical damped pendula are attached laterally with respect to the center of the head. The orientation of the left and right pendulums is described by body-fixed frames $\mathbb{L}$ and $\mathbb{R}$, respectively. In our model, the left and the right pendula have identical parameters: concentrated mass m, length l, damping β. Dynamics of the head is described by the same equation as for the medial model (2.3). Dynamics of the left pendulum can be expressed by

$$\begin{aligned} {}^{\mathbb{L}}\mathbf{J}_{\mathrm{L}}\,{}^{\mathbb{L}}_{\mathbb{I}}\dot{\boldsymbol{\omega}}_{\mathbb{L}} = &- \underbrace{{}^{\mathbb{L}}_{\mathbb{I}}\boldsymbol{\omega}_{\mathbb{L}} \times {}^{\mathbb{L}}\mathbf{J}_{\mathrm{L}}\,{}^{\mathbb{L}}_{\mathbb{I}}\boldsymbol{\omega}_{\mathbb{L}}}_{\text{gyroscopic}} + \underbrace{m\,{}^{\mathbb{L}}\boldsymbol{l} \times {}_{\mathbb{L}}\mathbf{R}_{\mathbb{I}}\,{}^{\mathbb{I}}\boldsymbol{g}}_{\text{gravity}} \\ &- \underbrace{\beta({}^{\mathbb{L}}_{\mathbb{I}}\boldsymbol{\omega}_{\mathbb{L}} - {}_{\mathbb{L}}\mathbf{R}_{\mathbb{I}}\,{}_{\mathbb{I}}\mathbf{R}_{\mathbb{H}}\,{}^{\mathbb{H}}_{\mathbb{I}}\boldsymbol{\omega}_{\mathbb{H}})}_{\text{damping}} - \underbrace{m\,{}^{\mathbb{L}}\boldsymbol{l} \times {}_{\mathbb{L}}\mathbf{R}_{\mathbb{I}}\,{}_{\mathbb{I}}\mathbf{R}_{\mathbb{H}}\,{}^{\mathbb{H}}\boldsymbol{a}}_{\text{acceleration}} \\ &+ \underbrace{m\,{}^{\mathbb{L}}\boldsymbol{l} \times {}_{\mathbb{L}}\mathbf{R}_{\mathbb{I}}\,{}_{\mathbb{I}}\mathbf{R}_{\mathbb{H}}\left[{}^{\mathbb{H}}_{\mathbb{I}}\dot{\boldsymbol{\omega}}_{\mathbb{H}} \times {}^{\mathbb{H}}\boldsymbol{r} + {}^{\mathbb{H}}_{\mathbb{I}}\boldsymbol{\omega}_{\mathbb{H}} \times ({}^{\mathbb{H}}_{\mathbb{I}}\boldsymbol{\omega}_{\mathbb{H}} \times {}^{\mathbb{H}}\boldsymbol{r})\right]}_{\text{Euler and centrifugal accelerations}}, \end{aligned} \tag{2.11}$$

where ${}^{\mathbb{L}}\mathbf{J}_{\mathrm{L}}$ is the pendulum's principal inertia tensor, ${}^{\mathbb{L}}_{\mathbb{I}}\boldsymbol{\omega}_{\mathbb{L}}$ is angular velocity of the pendulum-fixed frame with respect to the world frame; ${}^{\mathbb{L}}\boldsymbol{l} = \begin{pmatrix} 0 & 0 & l \end{pmatrix}^{\top}$ is the vector from the pivot of the pendulum to the center of its mass; ${}_{\mathbb{L}}\mathbf{R}_{\mathbb{I}} = {}_{\mathbb{I}}\mathbf{R}_{\mathbb{L}}{}^{\top}$; and ${}_{\mathbb{I}}\mathbf{R}_{\mathbb{L}}$ is a rotation matrix which defines orientation of the pendulum frame, $\mathbb{L}$, with respect to the world frame, $\mathbb{I}$; ${}^{\mathbb{H}}\boldsymbol{r} = \begin{pmatrix} 0 & 0 & r \end{pmatrix}^{\top}$ is a vector expressed in frame $\mathbb{H}$ with r the distance from the center of the head to the pivot of the pendulum. Compare to (2.6) in (2.11) two new acceleration terms appeared which are Euler and centrifugal accelerations. In this model, the head's motion effects the pendulum's motion through damping components (head's rotation) and through the acceleration component (head's rotation and translation). The dynamics of the right pendulum will be expressed in an analog way with the exception of the Euler and centrifugal terms that should be taken with the negative sign (vector ${}^{\mathbb{H}}\boldsymbol{r}$ has an opposite direction).

After the model verification and analysis we neglected some of the dynamics of the model. We consider the influence of gyroscopic and Euler terms to be

negligibly small. After arranging head's and pendula dynamic and kinematic equations we obtain the following system of coupled equations,

$$\begin{aligned}
{}^{\mathbb{L}}\mathbf{J}_{\mathrm{L}}\,{}^{\mathbb{L}}_{\mathbb{I}}\dot{\boldsymbol{\omega}}_{\mathbb{L}} =& m\,{}^{\mathbb{L}}\boldsymbol{l} \times {}_{\mathbb{L}}\mathbf{R}_{\mathbb{I}}\,{}^{\mathbb{I}}\boldsymbol{g} - \beta({}^{\mathbb{L}}_{\mathbb{I}}\boldsymbol{\omega}_{\mathbb{L}} - {}_{\mathbb{L}}\mathbf{R}_{\mathbb{I}}\,{}_{\mathbb{I}}\mathbf{R}_{\mathbb{H}}\,{}^{\mathbb{H}}_{\mathbb{I}}\boldsymbol{\omega}_{\mathbb{H}}) \\
& - m\,{}^{\mathbb{L}}\boldsymbol{l} \times {}_{\mathbb{L}}\mathbf{R}_{\mathbb{I}}\,{}_{\mathbb{I}}\mathbf{R}_{\mathbb{H}}\,{}^{\mathbb{H}}\boldsymbol{a} - m\,{}^{\mathbb{L}}\boldsymbol{l} \times {}_{\mathbb{L}}\mathbf{R}_{\mathbb{I}}\;{}_{\mathbb{I}}\mathbf{R}_{\mathbb{H}}({}^{\mathbb{H}}_{\mathbb{I}}\boldsymbol{\omega}_{\mathbb{H}} \times ({}^{\mathbb{H}}_{\mathbb{I}}\boldsymbol{\omega}_{\mathbb{H}} \times {}^{\mathbb{H}}\boldsymbol{r})), \\
{}^{\mathbb{R}}\mathbf{J}_{\mathrm{R}}\,{}^{\mathbb{R}}_{\mathbb{I}}\dot{\boldsymbol{\omega}}_{\mathbb{R}} =& m\,{}^{\mathbb{L}}\boldsymbol{l} \times {}_{\mathbb{R}}\mathbf{R}_{\mathbb{I}}\,{}^{\mathbb{I}}\boldsymbol{g} - \beta({}^{\mathbb{R}}_{\mathbb{I}}\boldsymbol{\omega}_{\mathbb{R}} - {}_{\mathbb{R}}\mathbf{R}_{\mathbb{I}}\,{}_{\mathbb{I}}\mathbf{R}_{\mathbb{H}}\,{}^{\mathbb{H}}_{\mathbb{I}}\boldsymbol{\omega}_{\mathbb{H}}) \\
& - m\,{}^{\mathbb{R}}\boldsymbol{l} \times {}_{\mathbb{R}}\mathbf{R}_{\mathbb{I}}\,{}_{\mathbb{I}}\mathbf{R}_{\mathbb{H}}\,{}^{\mathbb{H}}\boldsymbol{a} + m\,{}^{\mathbb{R}}\boldsymbol{l} \times {}_{\mathbb{R}}\mathbf{R}_{\mathbb{I}}\;{}_{\mathbb{I}}\mathbf{R}_{\mathbb{H}}({}^{\mathbb{H}}_{\mathbb{I}}\boldsymbol{\omega}_{\mathbb{H}} \times ({}^{\mathbb{H}}_{\mathbb{I}}\boldsymbol{\omega}_{\mathbb{H}} \times {}^{\mathbb{H}}\boldsymbol{r})), \\
{}^{\mathbb{H}}\mathbf{J}_{\mathrm{H}}\,{}^{\mathbb{H}}_{\mathbb{I}}\dot{\boldsymbol{\omega}}_{\mathbb{H}} =& {}^{\mathbb{H}}\boldsymbol{\tau}, \\
{}_{\mathbb{I}}\dot{\mathbf{R}}_{\mathbb{L}} =& {}_{\mathbb{I}}\mathbf{R}_{\mathbb{L}}\,{}^{\mathbb{L}}_{\mathbb{I}}\tilde{\boldsymbol{\omega}}_{\mathbb{L}}, \\
{}_{\mathbb{I}}\dot{\mathbf{R}}_{\mathbb{R}} =& {}_{\mathbb{I}}\mathbf{R}_{\mathbb{R}}\,{}^{\mathbb{R}}_{\mathbb{I}}\tilde{\boldsymbol{\omega}}_{\mathbb{R}}, \\
{}_{\mathbb{I}}\dot{\mathbf{R}}_{\mathbb{H}} =& {}_{\mathbb{I}}\mathbf{R}_{\mathbb{H}}\,{}^{\mathbb{H}}_{\mathbb{I}}\tilde{\boldsymbol{\omega}}_{\mathbb{H}}.
\end{aligned} \tag{2.12}$$

It is important to note here that the centrifugal acceleration terms have different signs for the left and right pendulums. The system (2.12) describes the overall dynamic behavior of the head and pendulums seen as a model of vestibular organs. We define the output equations for the system (2.12) using the same principles as for the system (2.7). The angles between the pendula body-fixed frames ($\mathbb{L}$ and $\mathbb{R}$) and the head body-fixed frame ($\mathbb{H}$) define the orientation of the head with respect to the verticality in steady-state (in the absence of angular and linear accelerations). The otolith organs of each inner ear report the head tilt in the sagittal and the coronal planes. Orientation of the pendula and of the head are described with the help of rotation matrices. The following equations can be used to calculate the angles between the pendulum and the head frames in the sagittal and the coronal planes:

$$\tan\phi_x^L = \frac{\left[{}_{\mathbb{H}}\mathbf{R}_{\mathbb{L}}\right]_{\{3,2\}}}{\left[{}_{\mathbb{H}}\mathbf{R}_{\mathbb{L}}\right]_{\{3,3\}}} \tag{2.13}$$

$$\tan\phi_y^L = \frac{\left[{}_{\mathbb{H}}\mathbf{R}_{\mathbb{L}}\right]_{\{3,1\}}}{\left[{}_{\mathbb{H}}\mathbf{R}_{\mathbb{L}}\right]_{\{3,3\}}} \tag{2.14}$$

$$\tan\phi_x^R = \frac{\left[{}_{\mathbb{H}}\mathbf{R}_{\mathbb{R}}\right]_{\{3,2\}}}{\left[{}_{\mathbb{H}}\mathbf{R}_{\mathbb{R}}\right]_{\{3,3\}}} \tag{2.15}$$

$$\tan\phi_y^R = \frac{\left[{}_{\mathbb{H}}\mathbf{R}_{\mathbb{R}}\right]_{\{3,1\}}}{\left[{}_{\mathbb{H}}\mathbf{R}_{\mathbb{R}}\right]_{\{3,3\}}} \tag{2.16}$$

where ${}_{\mathbb{H}}\mathbf{R}_{\mathbb{L}} = {}_{\mathbb{I}}\mathbf{R}_{\mathbb{H}}{}^{\top}\,{}_{\mathbb{I}}\mathbf{R}_{\mathbb{L}}$ and ${}_{\mathbb{H}}\mathbf{R}_{\mathbb{R}} = {}_{\mathbb{I}}\mathbf{R}_{\mathbb{H}}{}^{\top}\,{}_{\mathbb{I}}\mathbf{R}_{\mathbb{R}}$; angles ϕ_x^L, ϕ_y^L are the angles between the projections of the projections of ${}^{\mathbb{L}}\boldsymbol{k}$ in the sagittal and coronal head planes and ${}^{\mathbb{H}}\boldsymbol{k}$, respectively. Similarly, the angles ϕ_x^R, ϕ_y^R are the angles between the projections of projections of ${}^{\mathbb{R}}\boldsymbol{k}$ in the sagittal and coronal head planes and ${}^{\mathbb{H}}\boldsymbol{k}$, respectively.

To generalize system (2.12) we define the state

$$\boldsymbol{x}_2 = \left({}^{\mathbb{L}}_{\mathbb{I}}\boldsymbol{\omega}_{\mathbb{L}}, {}^{\mathbb{R}}_{\mathbb{I}}\boldsymbol{\omega}_{\mathbb{R}}, {}^{\mathbb{H}}_{\mathbb{I}}\boldsymbol{\omega}_{\mathbb{H}}, {}_{\mathbb{I}}\mathbf{R}_{\mathbb{L}}, {}_{\mathbb{I}}\mathbf{R}_{\mathbb{R}}, {}_{\mathbb{I}}\mathbf{R}_{\mathbb{H}}\right)^{\top}, \tag{2.17}$$

made of the elements of the vectors where the matrices are arranged in a single

vector. Then, the system is expressed in the form,

$$\dot{\boldsymbol{x}}_2 = f_2(\boldsymbol{x}_2, \boldsymbol{u}) \tag{2.18}$$

where $\boldsymbol{u} = \left({}^{\mathbb{H}}\boldsymbol{\tau}, {}^{\mathbb{H}}\boldsymbol{a}\right)^\top$ is an input due to the movement of the robot combined with the torque applied to the head. Output or measurement for the system is defined by (2.13)-(2.16). Both for models with one pendulum and two pendulums control torque ${}^{\mathbb{H}}\boldsymbol{\tau}$ which corresponds to the torque produced by neck muscles with respect to the trunk is considered as control input which orients the head with respect to trunk. Acceleration, ${}^{\mathbb{H}}\boldsymbol{a}$, presented here as control input, from control theory point of view can be seen as a disturbance which effects the motion of the pendulums during accelerated translations. This acceleration cannot be measured by vestibular system separately from gravitational term. It will be shown later, how head stabilization can provide a simple way to use otolith measurements for calculation of ${}^{\mathbb{H}}\boldsymbol{a}$, which can be plugged into the system models (2.7) and (2.12) as a known input.

Planar case

We consider motion of the head in sagittal and coronal planes as we did it for medial model. In case of lateral model dynamics of the system in sagittal and coronal planes will be different. Dynamics in sagittal plane is the same as for the medial model. For the coronal plane dynamics will be expressed as:

$$\begin{aligned}
J\dot{\omega}_{l,y} &= mlgr_{l[3,1]} - \beta(\omega_{l,y} - \omega_{\mathrm{h},y}) \\
&\quad - ml((r_{l[1,1]}r_{\mathrm{h}[1,1]} + r_{l[3,1]}r_{\mathrm{h}[3,1]})(a_x + r\omega_{\mathrm{h},y}^2) \\
&\quad + (r_{l[1,1]}r_{\mathrm{h}[1,3]} - r_{l[3,1]}r_{\mathrm{h}[3,3]})a_z), \\
\dot{r}_{l[3,2]} &= r_{l[3,3]}\omega_{l,y}, \\
\dot{r}_{l[3,3]} &= -r_{l[3,2]}\omega_{l,y}, \\
J\dot{\omega}_{r,y} &= mlgr_{r[3,1]} - \beta(\omega_{r,y} - \omega_{\mathrm{h},y}) \\
&\quad - ml((r_{r[1,1]}r_{\mathrm{h}[1,1]} + r_{r[3,1]}r_{\mathrm{h}[3,1]})(a_x - r\omega_{\mathrm{h},y}^2) \\
&\quad + (r_{r[1,1]}r_{\mathrm{h}[1,3]} - r_{r[3,1]}r_{\mathrm{h}[3,3]})a_z), \\
\dot{r}_{r[3,2]} &= r_{r[3,3]}\omega_{r,y}, \\
\dot{r}_{r[3,3]} &= -r_{r[3,2]}\omega_{r,y}, \\
J_{\mathrm{h}}\dot{\omega}_{\mathrm{h},y} &= \tau_y, \\
\dot{r}_{\mathrm{h}[3,2]} &= r_{\mathrm{h}[3,3]}\omega_{\mathrm{h},y}, \\
\dot{r}_{\mathrm{h}[3,3]} &= -r_{\mathrm{h}[3,2]}\omega_{\mathrm{h},y},
\end{aligned} \tag{2.19}$$

with $r_{l[\cdot,\cdot]}$ and $r_{r[\cdot,\cdot]}$ elements of rotation matrices for the left and right pendulums, respectively. Note the difference for the left and right pendulums' dynamics in the sign of centrifugal acceleration $r\omega_{h,y}^2$.

2.1.3 Head stabilization control

Humans and animals stabilize their heads during locomotion as it was discussed in the Chapter 1. In this subsection we present several types of possible feedback stabilization control commands, which may be realized by neck muscles. For global head stabilization we use the control law presented in [37]. The

controller is given by

$$^{\mathbb{H}}\boldsymbol{\tau} = \mathbf{K_p}\boldsymbol{\Omega} - \mathbf{K_d}\,^{\mathbb{H}}_{\mathbb{I}}\boldsymbol{\omega}_{\mathbb{H}} \equiv {}^{\mathbb{H}}\boldsymbol{\tau}(\boldsymbol{x}), \tag{2.20}$$

where $\mathbf{K_p}$, $\mathbf{K_d} \in R^{3\times 3}$ are positive definite matrices; $\boldsymbol{x}$ denotes the state of the system. The mapping $\boldsymbol{\Omega}$ is defined as follows:

$$\boldsymbol{\Omega} \equiv \sum_{i=1}^{3} e_i \times (\mathbf{I}_{\mathbb{I}}\mathbf{R}_{\mathbb{H}} e_i) \tag{2.21}$$

with $\begin{pmatrix} e_1 & e_2 & e_3 \end{pmatrix}$ the identity matrix. This control aims to stabilize the head orientation horizontally (to identity) from any initial orientation.

2.2 Model verification

We performed numerical tests to verify the model behavior and to evaluate the differences between the medial and the lateral models. The model's parameters were selected such that they represented the critically damped dynamic behavior of otoliths with natural frequency of about 300 Hz [78]; the head's moment of inertia was about 0.0174 kg·m^2 and was taken as an average from human biomechanical studies presented in [211]. In all tests, the head was stabilized to an up-right position from initial non-zero angular orientation. Fig. 2.4 presents the simulation results for the medial and the lateral models when the head was tilted independently in sagittal, coronal and horizontal planes. The left panels (A, B and C) contain the results for the lateral model. The right panels (D, E and F) present the results for the medial model. For each model three independent rotations of the head were simulated: sagittal tilt, lateral tilt and horizontal (yaw) rotation. In each case angular orientation of the head and the pendulums and their angular velocities were recorded. In the case of the medial model, the difference between the angular orientations of the left and right pendulums was computed. The pendula angular orientations with respect to the head body-fixed frame were computed based on output equations (2.8)-(2.9) (for the medial model) and (2.13)-(2.16) (for the lateral model). The head's angular orientation with respect to the vertical was computed based on the head's rotation matrix. In these model verification tests the controller (2.20) stabilized the head based on the actual head's angular orientation.

Both pendulums in the medial model behaved identically in the case of tilting in the sagittal plane Fig. 2.4A. In the case of lateral tilt, the pendulum's inclination in the coronal plane differed when the angular velocity of the head was non-zero Fig. 2.4B. There was a difference in inclinations of the left and right pendulums in the sagittal and coronal planes when the head rotated in the horizontal plane Fig. 2.4C. In general, the behavior of the medial model was almost identical to that of the left and right pendula of the medial model Fig. 2.4D-F.

Fig. 2.5 shows the results for the model verification test when the head was tilted and linearly accelerated at the same time. The head linear acceleration

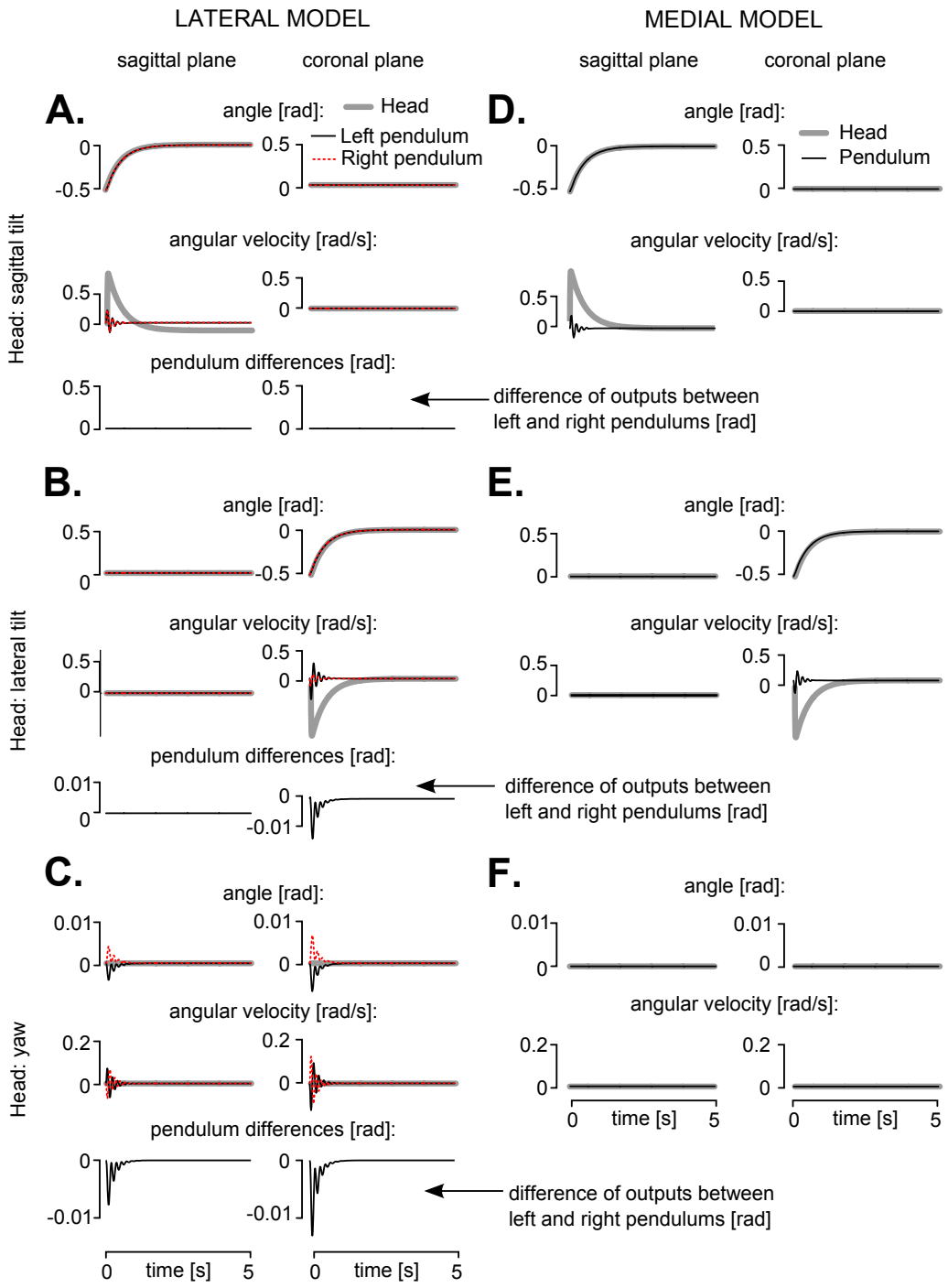

Figure 2.4: Numerical results for model verification during independent rotations of the head for lateral and medial models.

in horizontal plane was calculated as a function of time:

$$a_x = \sin(\pi t), \tag{2.22}$$

$$a_y = \cos(\pi t). \tag{2.23}$$

The head was stabilized to the up-right position from non-zero initial conditions by simultaneous rotation in sagittal and coronal planes. In this test, the behavior of the left and right pendulum differed more than in the previous test due to the more complicated motion of the head. The behavior of the medial model did not differ much from the lateral model.

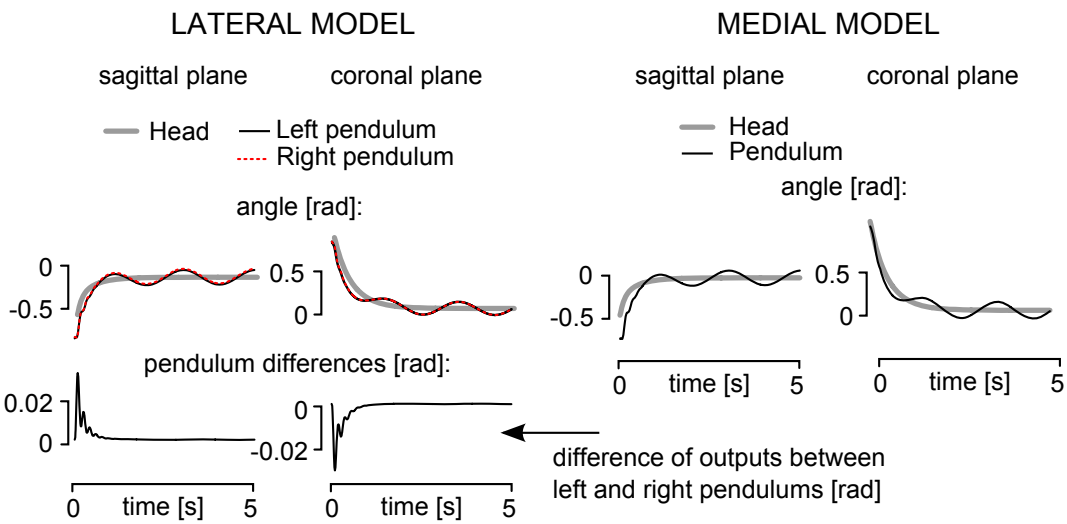

Figure 2.5: Numerical results for model verification during simultaneous rotations and accelerated translations of the head for lateral and medial models.

The numerical model verification tests showed that the models' behavior was reasonable and adequate. In the case of the lateral model, it was shown that the output measurements differ for the left and right pendula. However, these differences are negligibly small if compared to the magnitudes of the pendula motion.

Chapter 3

Observability and ambiguity in otolith measurements

Contents

In this chapter the observability of the vestibular system model is studied. Observability is analyzed for the cases when the head is stabilized and when it is not stabilized, and when linear translation of the head is known and unknown. The ambiguity in otolith measurements is then studied, and contributions of head stabilization in resolving the ambiguity are discussed. Finally, the role of head stabilization and application of the separation principle for observer-based control systems are presented.

3.1 Nonlinear observability

3.1.1 Definitions

Observability. Observability is one of the fundamental properties of systems used in control theory. It was initially introduced by R. Kalman in the early 1960s [110]. Generally speaking, observability is a measure of how well internal states of a system can be inferred from the knowledge of its inputs

and outputs. R. Kalman developed an observability theory for linear stationary systems [110, 112]. Observability of nonlinear systems was studied later by Y. M. Kostyukovskii in 1968 [117], E. W. Griffith et al. in 1971 [90], Y. Inouye in 1977 [103], R. Hermann and A. Krener in 1977 [95], and many other researchers. More recently, M. Fliess has showed that the concept of identifiability is strongly connected with the notion of observability [52, 67].

Identifiability. The definition of identifiability, in some sense, is similar to the definition of observability, but identification of system parameters is considered instead of the estimation of unknown internal state variables. The system model is called identifiable if it is theoretically possible to learn the true values of the model's underlying parameters after obtaining an infinite number of observations [14, 157, 198]. The notion of identifiability is important for system identification and mathematical modeling problems. In [88], a method for linear dynamic system identifiability analysis was presented. E. Walter et al. proposed a group of methods to analyze global identifiability of nonlinear systems in [199, 164, 200] based on symbolic representations from computer algebra. Identifiability analysis of nonlinear systems was successfully applied to different types of biological systems [192, 8, 6].

Mathematical formulation. Next, we give a brief definition of nonlinear observability and identifiability for a general algebraic nonlinear system of the following kind,

$$\dot{X} = F(X, P, U), \tag{3.1}$$

$$\dot{P} = 0, \tag{3.2}$$

$$Y = G(X, P, U), \tag{3.3}$$

with state variables vector $X = (x_1, \ldots, x_n)$, constant parameters variables vector $P = (p_1, \ldots, p_l)$, input variables vector $U = (u_1, \ldots, u_r)$, and output vector Y. System dynamics F and output mapping G can be represented by a vector of rational functions and denoted as $(f_1, \ldots, f_n)$ and $(g_1, \ldots, g_n)$, respectively. Following the notation in [52, 171], we consider the differential field

$$\mathcal{K} := k\langle U \rangle (X, P) \tag{3.4}$$

equipped with the following formal Lie derivation:

$$\mathcal{L} := \frac{\partial}{\partial t} + \sum_{i=1}^{n} f_i \frac{\partial}{\partial x_i} + \sum_{j \in \mathcal{N} \cup \{0\}} \sum_{u \in U} u^{j+1} \frac{\partial}{\partial u^{(j)}} \tag{3.5}$$

A composition of this derivation is denoted as:

$$\mathcal{L}^j := \underbrace{\mathcal{L} \cdot \ldots \cdot \mathcal{L}}_{j\text{-times}}. \tag{3.6}$$

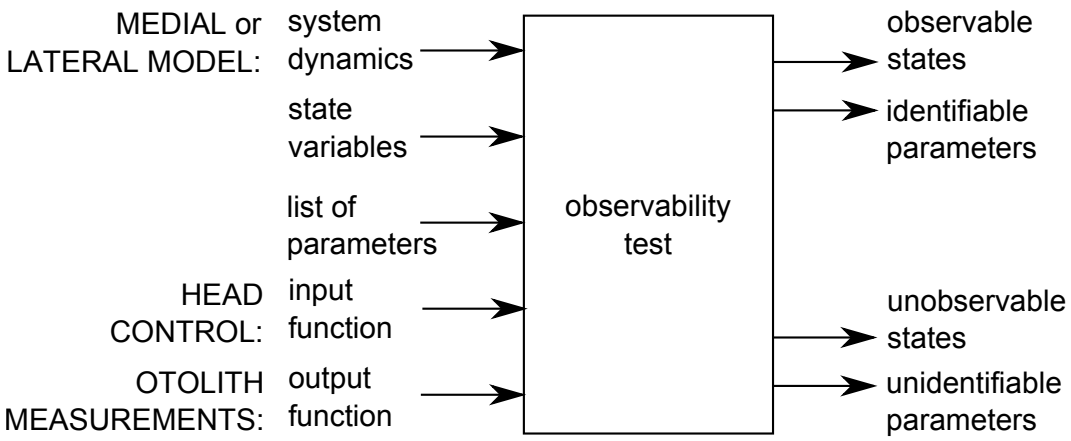

Figure 3.1: Schematic diagram of the observability test inputs and outputs.

Repeated Lie derivation of the output vector Y with recursive state variables substitutions gives us:

$$Y^{(j)} := \mathcal{L}^{(j)} G(X, P, U). \tag{3.7}$$

The following is a definition of a locally algebraically observable system.

Definition. An element z in $\mathcal{K}$ is locally algebraically observable with respect to inputs U and outputs Y if it is algebraic over $k\langle U, Y\rangle$. The system is therefore locally observable if the field extension $k\langle U, Y\rangle \rightarrow \mathcal{K}$ is purely algebraic [52].

Intuitively, a particular state x of the system is observable if this state can be expressed as an algebraic function of the components of U and Y, and a finite number of their derivatives ($Y^{(a)}$ and $U^{(b)}$, where a and b are bounded natural numbers).

3.1.2 Nonlinear algebraic method for observability test

To perform nonlinear observability analysis of the models, we apply an observability test algorithm described in [171, 172] by A. Sedoglavic. The algorithm is implemented in Maple. It has been successfully applied to identifiability in biochemistry and other research fields [69, 106, 125]. The algorithm is based on computational analysis of the algebraic structural connections between the system's inputs and outputs, their derivatives and state variables. The system is said to be observable if its state can be expressed as an algebraic function of the input and output variables and a finite number of their derivatives [52]. This algorithm can also verify the identifiability of the model parameters. However, for the case of our vestibular system model, we assumed that central nervous system has an adequate knowledge of the model parameters, and we can therefore define the parameters of the model to be known with given numerical values.

Observability was analyzed for the cases when the head was rotating only, and when it was rotating and translating simultaneously. In the case of pure rotational motion, the system dynamics was derived with acceleration vector ${}^{\mathbb{H}}\boldsymbol{a} = 0$. For rotational and translational motion, elements of the acceleration vector were defined as symbolic parameters in the observability test. The linear acceleration of the head, ${}^{\mathbb{H}}\boldsymbol{a}$, was defined as an unknown parameter because

the vestibular system does not provide sufficient information to distinguish between the gravitational and translational components during accelerated motion of a body. A simplified schematic diagram of the observability test input and output configuration is shown in figure 3.1.

For each of the motion cases, four types of head control were considered. In the first case, the head was not controlled: torque $\tau_h = 0$. In our model, this means that the neck did not apply any torque on the head. The input set for the observability test was defined to be an empty set. In the later results analysis, we will refer to this case as *zero control*.

In the second case, an unknown torque was applied to the head which we considered to be the state-independent torque. This torque was considered to be unknown for the neural-motor control system which may be the case when the body is disturbed by external forces. To emulate this situation in the nonlinear observability test, we defined the torque's components as parameters, instead of defining them as input variables. The input set was empty. Then, we checked that based on the observability test results, the control torque, τ_h, defined as a parameter remains unidentifiable which means it remains unknown to the system. We will refer to these cases as *unknown control* in the analysis of the results.

For the case when the head's torque was known, but the head was not stabilized, the components of τ_h were defined symbolically as input variables. In the later results analysis, we will refer to this case as *non stabilized* control.

Lastly, we considered the stabilized head. The symbolic definition of torque, τ_h, was replaced by the head stabilization control. It was a state dependent control which stabilized the head in a vertical orientation. The head could be stabilized to any other orientation. The key point was to provide state dependent control which modified the internal structure of the overall system. To emulate this case in the observability test, the dynamics of the system were defined with the head control equations, and the input set was empty. This case is called *stabilized* control in the next sections.

3.1.3 Observability test of the medial model

We analyzed the observability of the models with the help of the nonlinear observability test algorithm. For the model with one ear (2.12) angular orientation of the head with respect to vertical in the sagittal and coronal planes may be calculated from head's rotation matrix, ${}_{\mathbb{I}}\mathbf{R}_{\mathbb{H}}$, as follows,

$$\tan\Theta_x = \frac{\left[{}_{\mathbb{I}}\mathbf{R}_{\mathbb{H}}\right]_{\{3,2\}}}{\left[{}_{\mathbb{I}}\mathbf{R}_{\mathbb{H}}\right]_{\{3,3\}}}, \tag{3.8}$$

$$\tan\Theta_y = \frac{\left[{}_{\mathbb{I}}\mathbf{R}_{\mathbb{H}}\right]_{\{3,1\}}}{\left[{}_{\mathbb{I}}\mathbf{R}_{\mathbb{H}}\right]_{\{3,3\}}}. \tag{3.9}$$

Therefore, it is sufficient to know the last row of the head's rotation matrix, ${}_{\mathbb{I}}\mathbf{R}_{\mathbb{H}}$, for computing the vertical angular orientation of the head. Our interest in the observability analysis is to test whether the corresponding elements of the rotation matrix, ${}_{\mathbb{I}}\mathbf{R}_{\mathbb{H}}$, are observable or not.

First, nonlinear observability of the medial model (2.10) was studied. The results are presented in Table 3.1. The first column defines whether the head

was rotating only or rotating and translating at the same time. The type of control of the head is given in the second column. Last two columns report the results of the observability test. The observability of the head's vertical orientation is given in the third column. The identifiability of the head's linear acceleration vector is presented in the last column.

Table 3.1: Nonlinear algebraic observability results for the medial model. Linear acceleration of the head is unknown.

Motion	Head control	Head orientation is observable	Acceleration is identifiable
Rot.	zero control	No	–
Rot.	unknown control	No	–
Rot.	not stabilized	No	–
Rot.	stabilized	Yes	–
Rot.+Trans.	zero control	No	No
Rot.+Trans.	unknown control	No	No
Rot.+Trans.	not stabilized	No	Yes
Rot.+Trans.	stabilized	Yes	Yes

In the case of rotational motion only, the head's vertical orientation was observable only when the head was stabilized. For all other cases, the algebraic observability test showed that the head orientation was not observable. This means that based on the available measurements and known control inputs it is not possible to reconstruct the head's orientation with respect to the gravitational vertical. The key point is that the head's orientation becomes observable only when the head is stabilized. It is important to have a stabilized head for proper observation of the gravitational verticality. The head's linear acceleration vector was identifiable in the last two cases, when the head control was known to the system.

3.1.4 Observability test of the lateral model

The same observability test and with the same control and movement conditions was applied to the lateral model of the vestibular system (2.18). The results are presented in Table 3.2.

The results for the lateral model are significantly different from the results for the medial model. The head's orientation was observable in all of the cases, independently of the type of head stabilization control and type of motion. The linear acceleration of the head was identifiable in all of the cases, as well. The reason for this is the complex dynamics of the model, which consider extra force terms, such as centrifugal acceleration. It means that having two separate sets of vestibular organs located away from the center of rotation makes the head vertical orientation observable no matter whether the head is stabilized or not.

During normal locomotion, our head's motions are mainly restricted to the sagittal plane and the head's rotation is stabilized in this plane. In this case, dynamic behavior of the left and right pendula in the lateral model will be identical, and therefore, the system's equations of motion will be the same as for the medial model. It is easy to verify this by projecting the two pendulums

Table 3.2: Nonlinear algebraic observability results for the lateral model

Motion	Head control	Head orientation is observable	Acceleration is identifiable
Rot.	zero control	Yes	–
Rot.	unknown control	Yes	–
Rot.	not stabilized	Yes	–
Rot.	stabilized	Yes	–
Rot.+Trans.	zero control	Yes	Yes
Rot.+Trans.	unknown control	Yes	Yes
Rot.+Trans.	not stabilized	Yes	Yes
Rot.+Trans.	stabilized	Yes	Yes

in the lateral model to the sagittal plane while restricting the head's motion to the sagittal plane.

During normal locomotion, the response of vestibular system can therefore be described by the medial model. In this case, head stabilization is required for proper verticality estimation. Theoretical results presented in this and previous subsections are supported by the experimental results on head stabilization and may serve as one of the explanations of head stabilization behavior in humans and some animals [158, 182, 159, 113, 54].

3.2 Role of head up-right stabilization in resolving tilt-acceleration ambiguity

3.2.1 Ambiguity in otolith measurements

In this section we discuss the importance of head stabilization for resolving the ambiguity of acceleration and tilt measurements in otoliths. More specifically, we attempt to explain why the head's up-right stabilization behavior facilitates the processing of vestibular information. We suggest that when the head is stabilized in an up-right orientation with respect to the gravitational vertical, the ambiguity in otolith measurements can be resolved.

In the vestibular system, otoliths respond to the vector sum of gravitational and translational accelerations, which means that otoliths can react in the same way when tilted only or when accelerated only. This is one of the causes for the ambiguity in tilt-acceleration measurements. Our proposed pendulum-based models have the same physical behavior. In both models (2.7) and (2.12), ${}^{\mathbb{H}}\boldsymbol{a}$ is the acceleration of the head which is measured by otoliths and expressed in the head's frame $\mathbb{H}$. This acceleration is caused by the changes in translational motion of the head. However, in a vestibular system it is impossible for otoliths to measure independently the translational and gravitational accelerations, and additional neural processing of sensory information is required. The situation is different when the head is stabilized in the up-right orientation. Next, we show how ambiguity in acceleration measurements can be easily resolved for the case of a horizontally stabilized head.

3.2.2 Head stabilization in up-right position

First, we consider planar motion of the head. During normal locomotion our head is accelerated and tilted in the sagittal plane. Fig. 3.2A shows the case when the head is stabilized in an up-right position and accelerated forward. In this case, the linear acceleration, a_x, causes the pendulum to tilt back to an angle ϕ_x. The system is governed by the following equations of motion in steady state:

$$mla_x \cos\phi_y = mgl \sin\phi_y, \tag{3.10}$$

with m and l mass and length of the pendulum, respectively. When the head is stabilized in an up-right position, the pendulum responds to linear accelerations only, and therefore in this case the pendulum can be seen as accelerometer. The acceleration can be expressed as follows:

$$a_x = g \tan\phi_y. \tag{3.11}$$

For small angles, the acceleration will be linearly related to the tilt:

$$a_x \approx g\phi_y. \tag{3.12}$$

As a result, having the head horizontally stabilized provides the vestibular system with a direct way to know the linear acceleration of the head during locomotion without the necessity of additional computations.

Similarly for the head's motions in the coronal plane (Fig. 3.2B), the linear acceleration of the head, a_y, can be measured directly by otoliths when the head is stabilized in an up-right position,

$$a_y = g \tan\phi_x. \tag{3.13}$$

A more general case of the head being accelerated in all three directions is shown in Fig. 3.2C and 3.2D. The head is stabilized in an up-right position and accelerated forward with acceleration a_x, laterally with acceleration a_y and vertically with acceleration a_z. The accelerations a_x and a_y in steady state can be expressed as follows:

$$a_x = (g - a_z) \tan\phi_y, \tag{3.14}$$

$$a_y = (g - a_z) \tan\phi_x. \tag{3.15}$$

One can easily see that there is no solution for extracting acceleration components from the pendulum's inclination when the head is translated in two and/or three directions at the same time. It is only possible to know the orientation of the acceleration vector, without knowing its length. This can be explained by the limitations of the selected pendulum-based model of the vestibular system. To avoid this limitation we need to assume that the measurement of the vertical acceleration, a_z, is known.

In the vestibular system, vertical accelerations are measured by the saccule. Horizontal accelerations are measured by the utricle. Therefore, we may consider our pendulum-based model as a model of the utricle, while additional information about the vertical component of acceleration, a_z, is available via saccule measurements. Then, assuming that a_z is measured independently,

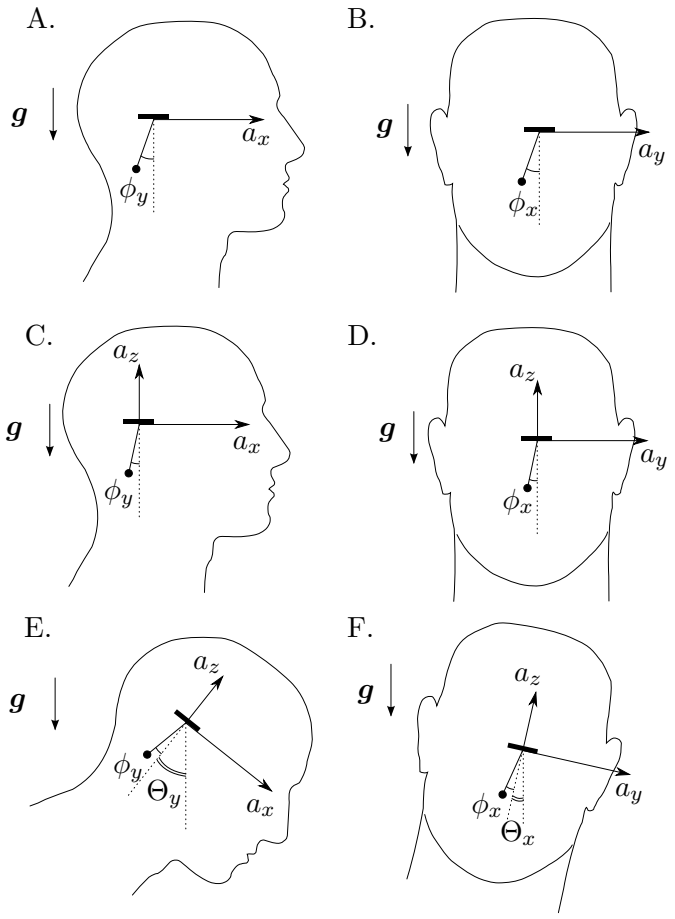

Figure 3.2: Human head horizontal stabilization and linear acceleration

the sagittal and coronal components acceleration, a_x and a_y, can be directly calculated based on the pendulum's tilt as given by equation (3.15).

3.2.3 Non-stabilized head

Next, we consider the case when the head is tilted in the sagittal and/or the coronal planes, while being accelerated during locomotion. In Fig. 3.2E the head is tilted in the sagittal plane to the angle Θ_y and accelerated forward and up. Then, the pendulum's inclination in steady state is

$$a_z \sin \phi_y + a_x \cos \phi_y = g \sin(\phi_y + \Theta_y). \tag{3.16}$$

In the case of small pendulum inclinations we have the following equation for calculating the linear acceleration:

$$a_x = g \sin(\phi_y + \Theta_y) - a_z \phi_y. \tag{3.17}$$

A similar expression can be obtained for the coronal plane (Fig. 3.2F):

$$a_y = g \sin(\phi_x + \Theta_x) - a_z \phi_x. \tag{3.18}$$

To calculate the accelerations, a_x and a_y, in addition to the pendulum's inclination, it is necessary to know the head's actual angular orientation with respect to the gravitational vertical which is represented by the angles Θ_x and Θ_y. Here, like in the previous case, we assume that the vertical component of acceleration, a_z, is measured by the saccule. Actual angular orientation of the head can be known to the neural system based on different sensory inputs, such as visual and proprioceptive inputs, however, the present study is restricted to the vestibular sensory system, and therefore we consider vestibular sensory information as a primary source of head spatial orientation. Neural processing of vestibular measurements may compute the estimate of the head's actual angular orientation based on the measurements from otoliths and semicircular canals, but this estimate may be erroneous and inaccurate. It is a well-known fact that in some situations humans cannot correctly perceive verticality. Most of the time, it is due to the ambiguous measurements of the otoliths when our head is continuously accelerated. For example, an airplane pilot experiences the illusion that the nose of the aircraft is pitching up when the plane suddenly accelerates forward [79, 80]. The pilot's response to this illusion would be to push the yoke or the control stick forward to pitch the nose of the aircraft down. Similarly to accelerated motion, a sudden deceleration causes an erroneous perception of the verticality. The pilot may in contrast experience the illusion that the nose of the aircraft is pitching down. The pilot's response to this illusion would be to pitch the nose of the aircraft up. Incorrect estimation of the head's orientation with respect to the gravitational field directly influences the acceleration estimate based on equations (3.17) and (3.18). In these situations, the otoliths cannot be considered to behave like accelerometers, since their response is a result of both linear accelerated motion and the static tilt of the head. Tilt with respect to the gravitational verticality of the head influences the ability of vestibular system to correctly perceive its spatial orientation and distinguish between linear motion and tilt.

Here, we have used head's motion in the sagittal and coronal planes with

the medial model of the vestibular system for simplicity of explanation. But all the derivations presented above can be directly applied for the head's three-dimensional motion. Additionally, the use of the medial model here does not restrict us from applying the same considerations on head stabilization with the lateral model of the vestibular system.

As a result, we can suggest that the head's up-right stabilization helps the neural system to correctly perceive the gravitational vertical. When the head is stabilized in an up-right position, the otoliths may be considered as accelerometers. Upright orientation of the head when the head's body frame is aligned with gravitational verticality is a natural pose for most standing animals. This suggests that up-right stabilization of the head during locomotion provides the vestibular system with a simple way to measure translational acceleration independently from the gravitational component.

As it was shown and discussed in previous research and in this manuscript, humans stabilize their heads during locomotion. We suppose that this natural stabilization behavior is taken into account by the central neural system and it assumes that in normal conditions head is up-right and its frame is aligned with gravity. This means that, in normal conditions, the human neural system may automatically consider otolith responses as accelerations while assuming that the head is up-right. The cases when the head is not stabilized lead to ambiguities in measurements.

In real life, these ambiguities together with conflicting sensory inputs from other modalities may provoke motion sickness [208, 168, 151]. That is why in an airplane pilot's safety instructions it is recommended to fix the head orientation in an up-right position in the situation when the pilot is experiencing vestibular illusions and/or motion sickness. Various experimental studies for flight ergonomics and sea navigation conditions have shown that motion sickness can be reduced if the head is stabilized [201, 204, 21].

3.3 Discussion

In this chapter, two questions related to the role of head stabilization behavior were considered. First, the nonlinear observability of two vestibular system models was analyzed. With the help of an algebraic observability test, we checked if the head angular orientation was observable based on otolith measurements depending on the type of head stabilization control. It was shown that head stabilization makes the head's spatial orientation observable in the sagittal plane. The head angular orientation with respect to the gravitational verticality was observable only when the head was stabilized by feedback control. Observability was analyzed for the medial and lateral models. It was discovered that having two sets of vestibular organs located laterally with respect to the center of rotation had a significant advantage compared to having only one. In the general case for the lateral model, the head's vertical orientation was observable independently from the head's stabilization control. However, head stabilization control becomes important when motion in the sagittal plane is considered. The lateral model is equivalent to medial model when projected onto the sagittal plane in which normal human locomotion is performed. As a result, the human head should be stabilized in order to enable observation of the head's spatial orientation.

The role of head stabilization in resolving the ambiguity of otolith measurements was discussed in the second part of this chapter. It was shown that when the head is stabilized in an up-right position, otoliths play the role of accelerometers which measure linear translation of the head. In cases when the head is tilted, the otoliths' measurements are influenced by linear acceleration of the head and the inclination with respect to gravitational vertical. This makes the measurement ambiguous and it is not evident for the neural system how to resolve the ambiguity. These dynamics are the source of somatogravic illusions and motion sickness. Upright head stabilization is a simple and efficient method to resolve the gravitoinertial ambiguity and may explain natural head stabilization behavior during locomotion.

Chapter 4

Verticality estimation

Contents

4.1 Observation problem

In this chapter we study the problem of verticality estimation with the help of an observer. The observer can be viewed as an internal model of the vestibular organ which is used by the human neural system to estimate the head's spatial orientation. The simplified diagram of the observation problem is presented in Fig. 4.1. The spatial orientation of the head is controlled by the neck-muscles *controller*. The head's motion influences the vestibular organs and its output is used by the internal model *observer*, together with the control input from the controller, to estimate the actual orientation of the head. This estimated

spatial orientation is compared with the *reference* orientation in the controller which generates the corresponding control input. This observer-based feedback control representation is well-known for robotic systems and may be considered to be a relevant model for our biological system. In the next sections we present several observation techniques, their evaluation and discuss the results.

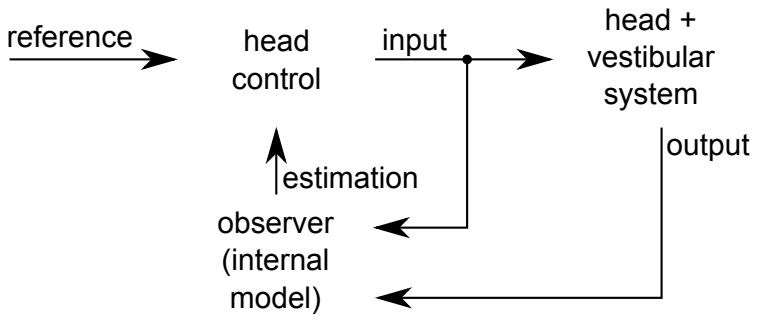

Figure 4.1: Schematic diagram of the observation problem.

4.2 Extended Kalman filter

4.2.1 Filter design

The Kalman filter is a common way to estimate the unknown state of a linear system based on the knowledge of the system model, control inputs and noisy measurements. The extended Kalman filter is a version of the original Kalman filter which is applicable for nonlinear systems, where system linearization is performed at every estimation step. Consider a nonlinear stochastic difference system as follows,

$$\begin{aligned} \boldsymbol{x}_{k+1} &= f(\boldsymbol{x}_k, \boldsymbol{u}_k, \boldsymbol{w}_k), \\ \boldsymbol{y} &= h(\boldsymbol{x}_k, \boldsymbol{\nu}_k), \end{aligned}$$

with state vector of the system $\boldsymbol{x}$; control input vector $\boldsymbol{u}$; output measurements vector $\boldsymbol{y}$; random variables $\boldsymbol{w}_k$ and $\boldsymbol{\nu}_k$ representing process and measurement noise, respectively. The function f relates the state at step $(k-1)$ to the state at time step k. The output function, h, relates the state $\boldsymbol{x}_k$ to the measurement $\boldsymbol{y}_k$. The system process and measurements are subject to noise. A Kalman filter for this system is expressed by

$$\hat{\boldsymbol{x}}_{k+1} = f(\hat{\boldsymbol{x}}_k, \boldsymbol{u}_k, 0) + K_k(\boldsymbol{y}_k - h(\hat{\boldsymbol{x}}_k, 0)),$$

where $\hat{\boldsymbol{x}}$ is the estimation of the state vector; K_k is the matrix of the Kalman gains. For the discretized system, the Kalman gains are calculated at every iteration and the linearization of the system is required. Linearizing around an estimate gives,

$$\begin{aligned} \boldsymbol{x}_k &\approx \tilde{\boldsymbol{x}}_k + A(\boldsymbol{x}_{k-1} - \hat{\boldsymbol{x}}_{k-1}) + W\boldsymbol{w}_{k-1}, \\ \boldsymbol{y}_k &\approx \tilde{\boldsymbol{y}}_k + H(\boldsymbol{x}_{k-1} - \hat{\boldsymbol{x}}_{k-1}) + V\boldsymbol{\nu}_k. \end{aligned}$$

where $\boldsymbol{x}_k$ are the actual state, $\tilde{\boldsymbol{x}}_k$ is its estimate, $\boldsymbol{y}_k$ is the measurement, $\tilde{\boldsymbol{y}}_k$ is an output, $\hat{\boldsymbol{x}}_k$ is the a-posteriori state estimate. The Jacobian matrices are,

$$\begin{aligned} A_k &= \frac{\partial f}{\partial \boldsymbol{x}}(\hat{\boldsymbol{x}}_{k-1}, \boldsymbol{u}_{k-1}, \boldsymbol{0}), \\ W_k &= \frac{\partial f}{\partial \boldsymbol{w}}(\hat{\boldsymbol{x}}_{k-1}, \boldsymbol{u}_{k-1}, \boldsymbol{0}), \\ H_k &= \frac{\partial h}{\partial \boldsymbol{x}}(\tilde{\boldsymbol{x}}_k, \boldsymbol{0}), \\ V_k &= \frac{\partial h}{\partial \nu}(\tilde{\boldsymbol{x}}_k, \boldsymbol{0}). \end{aligned}$$

Computing the covariance matrix P_{k+1}^- is required at every step for obtaining the Kalman gain matrix K_k,

$$\begin{aligned} P_k^- &= A_k P_{k-1} A_k^T + W_k Q_{k-1} W_k^T, \\ K_k &= P_k^- H_k^T (H_k P_k^- H_k^T + V_k R_k V_k^T)^{-1}. \end{aligned}$$

Then, the correction of the state estimation gives:

$$\hat{\boldsymbol{x}}_k = f(\hat{\boldsymbol{x}}_k, \boldsymbol{u}_k, 0) + K_k(\boldsymbol{y}_k - h(\hat{\boldsymbol{x}}_k^-, 0)).$$

Finally, an update of the covariance matrix for the next iteration is required,

$$P_k = (I - K_k H_k) P_k^-.$$

For the case of the medial model, the state space vector is expressed by $\boldsymbol{x}_1 = \left({}^{\mathbb{S}}_{\mathbb{I}}\boldsymbol{\omega}_{\mathbb{S}}, {}^{\mathbb{H}}_{\mathbb{I}}\boldsymbol{\omega}_{\mathbb{H}}, {}_{\mathbb{I}}\mathbf{R}_{\mathbb{S}}, {}_{\mathbb{I}}\mathbf{R}_{\mathbb{H}}\right)^\top$ and the control input as $\boldsymbol{u} = \left({}^{\mathbb{H}}\boldsymbol{\tau}, {}^{\mathbb{H}}\boldsymbol{a}\right)^\top$. Then, the extended Kalman Filter can be easily designed for the medial model (2.10) with the output equations (2.8) and (2.9).

4.2.2 Simulation results

A computational experiment was performed to test the designed extended Kalman filter. The medial model was used in the following simulations. The model parameters were given reasonable values, $m = 50$ g, $l = 0.06$ m, $\mathbf{J} = m\,\mathrm{diag}[l^2, l^2, \frac{1}{20}l^2]$, ${}^{\mathbb{H}}\mathbf{J}_{\mathrm{H}} = \mathrm{diag}[0.125\ 0.125\ 0.125]$ kg·m^2, $\beta = 0.001$ N·m·s. The controller was tuned for a critically damped response, with $k_p = 32$ N·m/rad and $K_d = 5$ N·m·s/rad. The sampling period was 1 ms. The estimation was updated every 20 ms. The initial conditions for the extended Kalman filter differed from that of the system by 0.1 radian. The standard deviation of the process noise, $\boldsymbol{w}_k$, was set to ± 0.001 and that of the measurement noise, $\boldsymbol{v}_k$, to ± 0.02. Moreover, to test the robustness, the model parameters known to the Kalman filter were assumed to differ substantially from the true values, $\tilde{m} = 60$ g, $\tilde{l} = 0.04$ m, $\tilde{\mathbf{J}} = \mathrm{diag}[0.15\ 0.15\ 0.15]$, $\tilde{\beta} = 0.0005$ N·ms.

The computational experiment involved two scenarios. In the first scenario the head underwent an oscillatory movement which resulted in a three-dimensional trajectory. The time history of the head's linear acceleration and its trajectory is shown in the first row of Fig. 4.2. For clarity, the results are presented in Fig. 4.2 with the noise removed, but noise was present during the simulations. We simulated a sudden impact at time 5 s which led to a 30 m/s^2 acceleration spike after which the robot was stopped. Two condi-

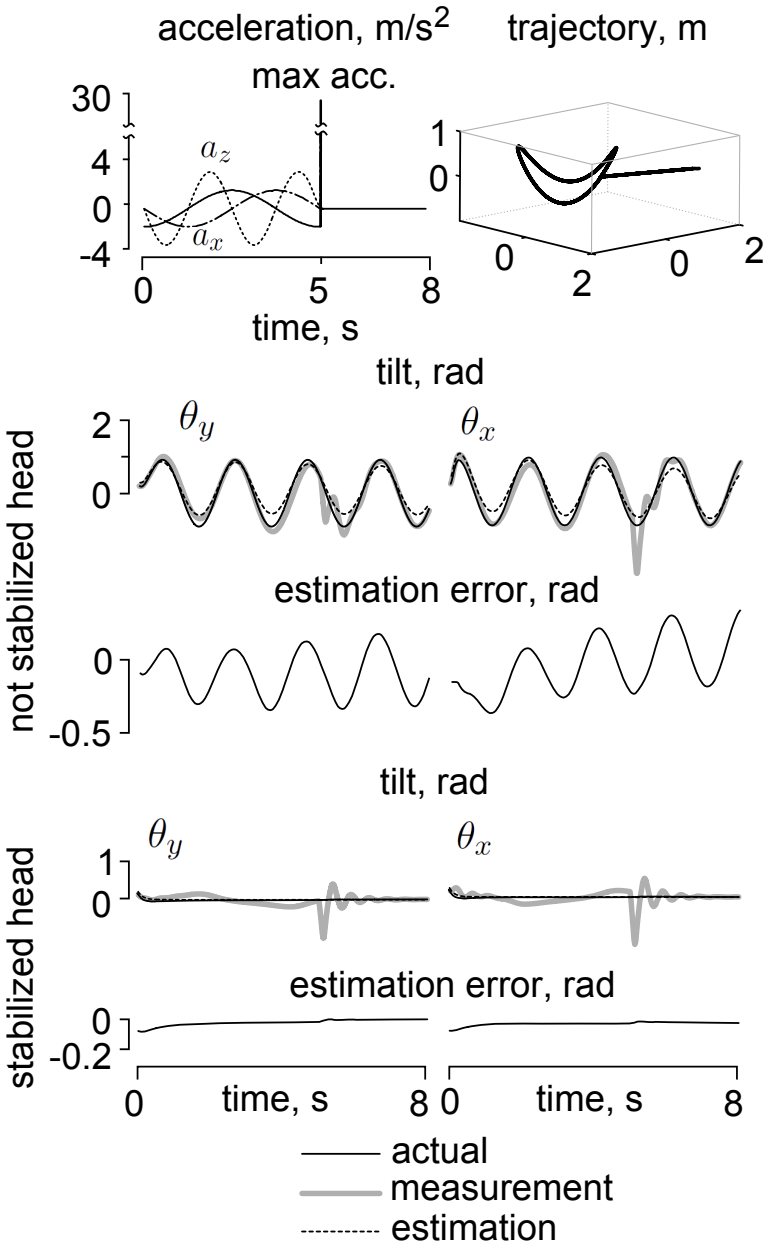

Figure 4.2: Simulation results for verticality estimation with extended Kalman filter during locomotion with sudden impact. The top panel shows the head linear acceleration time history and its trajectory. The middle panel: results for the case of non stabilized head. Bottom panel: results for the stabilized head. Angles θ_x and θ_y denote the head spatial orientation in sagittal and coronal planes with respect to the gravitational vertical.

tions were considered for each scenario. In the first condition, the head was rigidly attached to the trunk, which means that the head was not stabilized with respect to the gravitational verticality and directly followed the motions of the trunk. In the second condition, the head was stabilized in the up-right position using the head stabilization control outlined earlier in Chapter 2. The head stabilization controller used the estimated head's angular orientation and velocity.

Simulation results for the second scenario are presented in Fig. 4.3. In this scenario, the robot jumped in the x-direction. The acceleration history and the

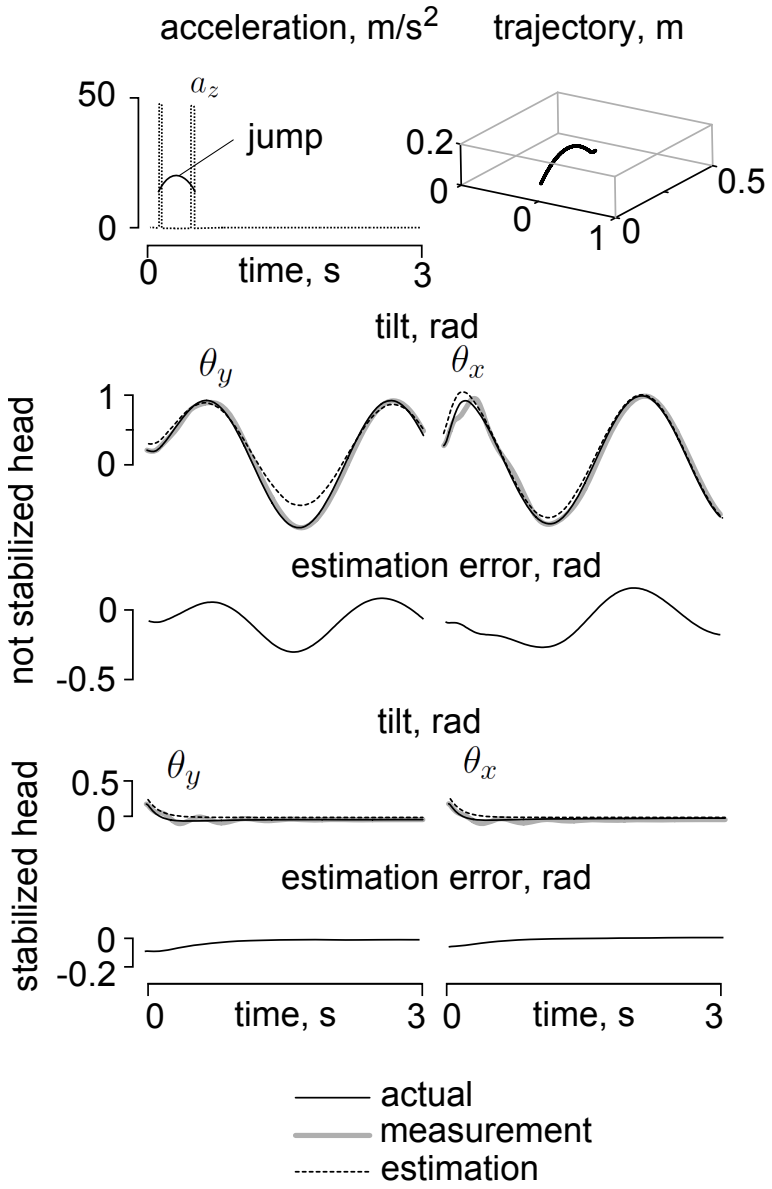

Figure 4.3: Simulation results for verticality estimation with extended Kalman filter during jumping. Top panel shows the head's linear acceleration time history and its trajectory. Middle panel: results for the case of non stabilized head. Bottom panel: results for the stabilized head. The angles θ_x and θ_y denote the head spatial orientation in sagittal and coronal planes with respect to the gravitational vetical.

trajectory are shown in the first row of the Fig. 4.3. At 'lift off' the robot was accelerated in the upward z-direction and at 'landing' the robot experienced an impact from the ground, after which the robot was stopped. The results are presented in Fig. 4.3 with the noise removed, but noise was present during the simulations.

In both simulation scenarios the verticality estimation errors were significantly smaller for the case of the stabilized head. Locating the vestibular system in the stabilized head has a number of combined advantages, including providing a flexible platform that assists seeking and tracking targets with vision and audition. Here, we showed that locating the vestibular system in the head enabled inertial stabilization with the consequence of a reduction of the number states to be estimated, while providing a quasi-inertial refer-

ence frame that can facilitate control. We also found that stabilization was especially helpful in the face of uncertainty in the system model [61].

4.3 Newton method based observer

4.3.1 Observer design

In this section we describe the design of an observer which considers the nonlinear dynamics of the vestibular system model. First we recall the principle of nonlinear observers based on the Newton's method which rely on the numerical solution of the discretized system equations, in a dead-beat fashion, from the knowledge of past inputs and outputs [145]. These observers apply to large classes of smooth nonlinear systems such as our robotic head-vestibular system. A nonlinear system is sampled with period T to give,

$$\boldsymbol{x}_{k+1} = F_T(\boldsymbol{x}_k, \boldsymbol{u}_k), \tag{4.1}$$

$$\boldsymbol{y}_k = h(\boldsymbol{x}_k, \boldsymbol{u}_k), \tag{4.2}$$

where the state vector $\boldsymbol{x} \in \mathbf{R}^n$, input vector $\boldsymbol{u} \in \mathbf{R}^m$, and output (measurements) vector $\boldsymbol{y} \in \mathbf{R}^p$. For the following derivations, it is convenient to define $F_T^u \triangleq F(\boldsymbol{x}, \boldsymbol{u})$ and $h^u(\boldsymbol{x}) \triangleq h(\boldsymbol{x}, \boldsymbol{u})$. Next, we define a set of N consecutive measurements and controls, and denote them as

$$\boldsymbol{Y}_k \triangleq \begin{pmatrix} \boldsymbol{y}_{k-N+1} & \boldsymbol{y}_{k-N+2} & \cdots & \boldsymbol{y}_k \end{pmatrix}^\top,$$
$$\boldsymbol{U}_k \triangleq \begin{pmatrix} \boldsymbol{u}_{k-N+1} & \boldsymbol{u}_{k-N+2} & \cdots & \boldsymbol{u}_k \end{pmatrix}^\top.$$

with a fixed time window N.

Then, we define a matrix of N consecutive computed system measurements,

$$H_T(\boldsymbol{x}_{k-N+1}, \boldsymbol{U}_k) \triangleq \begin{pmatrix} h(\boldsymbol{x}_{k-N+1}) \\ h \circ F_T^{\boldsymbol{u}_{k-N+1}}(\boldsymbol{x}_{k-N+1}) \\ \vdots \\ h \circ F_T^{\boldsymbol{u}_{k-1}} \circ \cdots \circ F_T^{\boldsymbol{u}_{k-N+1}}(\boldsymbol{x}_{k-N+1}) \end{pmatrix}$$

where $\circ$ defines composition. Matrix H_T, is termed the 'observability mapping'. System (4.2) is said to be N-observable ($N \geq 1$) at point $\boldsymbol{x}_k$ [148, 1], if there exists an N-tuple of controls, $\boldsymbol{U}_k$, such that the set of equations

$$\boldsymbol{Y}_k = H_T(\boldsymbol{x}, \boldsymbol{U}_k),$$

has a unique solution for $\boldsymbol{x}$. In the observability matrix, N previous system's outputs are computed based on the knowledge of the state $\boldsymbol{x}_{k-N+1}$, the system dynamics F_T^u and history of control inputs $\boldsymbol{U}_k$. In the ideal case, matrix H_T is equal to the the history of measurements $\boldsymbol{Y}_k$. In the case of the state observation problem, the state vector $\boldsymbol{x}_k$ is unknown while the history of measurements and control inputs are known. Then, the observer problem consists of solving N nonlinear equations,

$$\boldsymbol{Y}_k - H_T(\boldsymbol{x}_{k-N+1}, \boldsymbol{U}_k) = 0, \tag{4.3}$$

something that can be done numerically using Newton's iterative method. The Newton's algorithm for solving (4.3) is expressed by

$$\boldsymbol{\xi}_k^{i+1} = \boldsymbol{\xi}_k^i + \left[\frac{\partial H_T}{\partial \boldsymbol{\xi}}(\boldsymbol{\xi}_k^i, \boldsymbol{U}_k)\right]^{-1} (\boldsymbol{Y}_k - H_T(\xi_k^i, \boldsymbol{U}_k)), \tag{4.4}$$

for $i = 0, \ldots, d-1$ with d selected to give a desired accuracy. Then, going back in time, the estimated state, $\hat{\boldsymbol{x}}_k$, can be reconstructed recursively,

$$\hat{\boldsymbol{x}}_k = F_T^{\boldsymbol{u}_{k-1}} \circ \cdots \circ F_T^{\boldsymbol{u}_{k-N+1}}(\boldsymbol{\xi}_k^d). \tag{4.5}$$

We applied the Newton-method based observer to the medial model of the vestibular system and tested it in computational experiment. In the observer implementation, to program iteration (4.5), it was first necessary to obtain a closed-form expression for the observability mapping, and then to compute its inverse Jacobian matrix for the Newton iterations. However, obtaining a closed-form solution is problematic. Instead, we used a finite difference approximation of the Jacobian matrix by recalculating H_T at each period. The time window for the history of otolith outputs, control torque and the head's linear acceleration was taken to be the same as the number of state variables, $N = 24$. Thus, the observability matrix was square. At time k, the histories of tilt measurements $y_{1,k}$ and control inputs $\boldsymbol{u}_k = (\boldsymbol{a}_k, \boldsymbol{\tau}_k)^T$ are kept in a queue for the last 24 iterations. After d Newton iterations (4.4), the estimate for $\boldsymbol{x}_{k-N+1}$ is projected forward in time by $N-1$ steps to obtain the estimate of the current state $\hat{\boldsymbol{x}}_k$ based on (4.5).

4.3.2 Simulation results

We proceeded with simulations in order to evaluate the performance of our gravitational verticality observer. The simulation and model parameters were similar to those used in the tests with the extended Kalman filter. The sampling period was 1 ms. The head orientation was controlled by a well-tuned PD control. The Newton iterations were executed every 25 ms with $d = 5$.

The simulation involved the trunk and the head of the robot moving through a dynamic planar trajectory,

$$\begin{pmatrix} x(t) \\ z(t) \\ \Theta(t) \end{pmatrix} = \begin{pmatrix} 0.25\sin(0.5\pi t) \\ 0.25\sin(\pi t) \\ 0.25\pi\sin(2\pi t) \end{pmatrix}$$

where $x(t)$ and $z(t)$ are the positions of the head in the coronal plane, $\Theta(t)$ is the angular orientation of the body in the coronal plane with respect to the gravitational vertical, and t is time. The trajectory formed the Lissajous figure represented in Fig. 4.4. The history of the acceleration components are presented in the bottom panel of the figure.

Two situations were considered. In the first case, the head of the robot was fixed to the trunk and followed its motion. In the second case, the head upright stabilization control was applied.

The tests were performed under two conditions. In the first condition, an accurate model of the system dynamics was assumed. In the second condition, the systems parameters given to the observer differed by 10% from the actual value. In addition, noise was added to the output, simulating quantization of

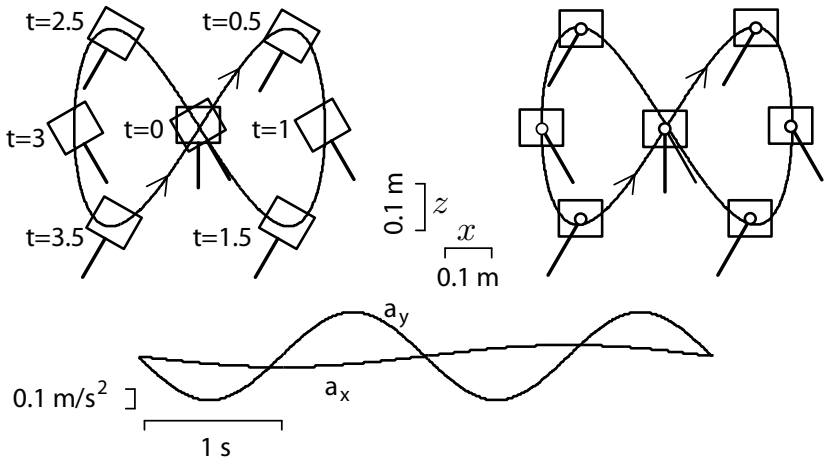

Figure 4.4: Test trajectory used for comparison. In the left panel, the platform oscillates. In the right panel the platform is stabilized despite the movements of the body.

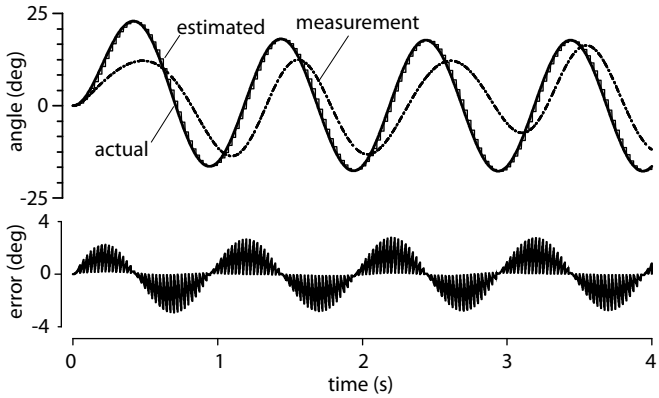

Figure 4.5: Simulation with exact model when the platform (head) is not stabilized.

the sensor signal.

Figure 4.5 shows the simulation results for the fixed-platform system. It can be seen how the platform movements influenced the orientation of the inclinometer, causing the measurement to lag in phase. The observer, however, managed to estimate of the orientation of the platform reasonably well, that is with an error smaller than 3°.

Figure 4.6 shows the results when the inclinometer was on a horizontally stabilized platform for the same trajectory. The platform orientation was almost zero, but the inclinometer oscillated with a magnitude of about 4° due to the residual acceleration. The estimation error with respect to the gravitational vertical was down to less that 0.1°.

Simulations were then performed when the model parameters given to the observer were over estimated by 10%. In addition, white Gaussian noise was added to the tilt measurement which corresponded to a quantization error amplitude of a 16-bit analog-to-digital converter.

The results can be seen in Fig. 4.7 and in Fig. 4.8 for the fixed and actuated systems, respectively. The estimation error reached about 6° for the fixed platform system, but when the horizontally stabilized platform was used, the estimation error never exceeded 0.5°.

An important feature that our system configuration shares with natural

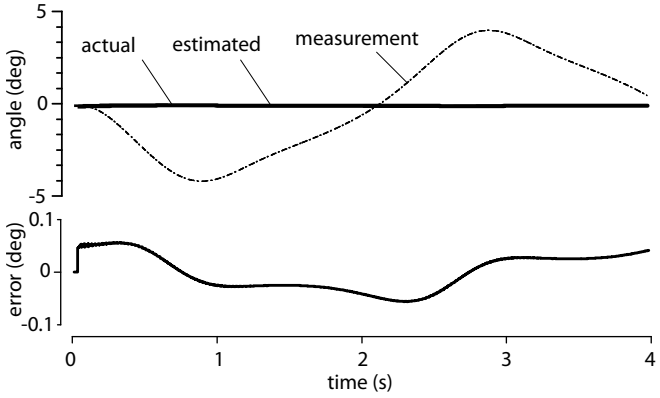

Figure 4.6: Simulation with exact model information and stabilized platform (head).

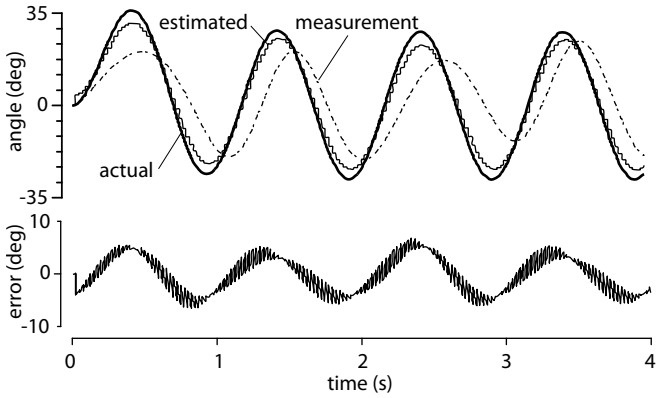

Figure 4.7: Simulation with approximate model and noisy sensors when the platform (head) is not stabilized.

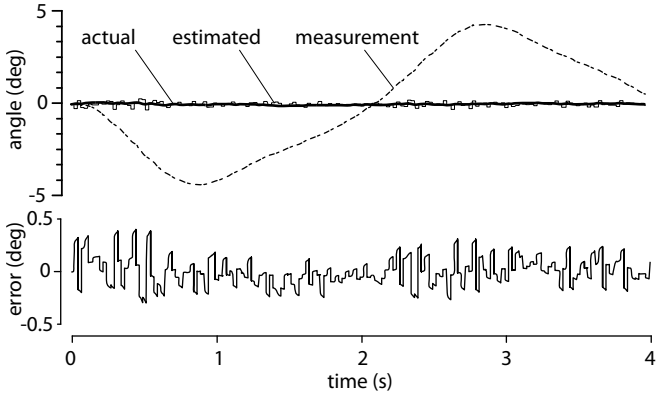

Figure 4.8: Simulation with approximate model and noisy sensors with stabilized platform (head).

vestibular system is to be attached to an actuated, orientable platform able to stabilize the inertial measurement system in the horizontal plane, independently from the movements of the body to which it may be attached. Slaving this platform to the output of the verticality observer could reduce the observer error by more than one order of magnitude under highly dynamic forcing trajectories. This observer may be compared in functionality to the neural machinery associated with natural vestibular systems.

When the "head" of the robot was horizontally stabilized, its angular velocity was zero, ${}^{\mathbb{H}}_{\mathbb{I}}\boldsymbol{\omega}_{\mathbb{H}} = 0$, and the rotation matrix, ${}_{\mathbb{I}}\mathbf{R}_{\mathbb{H}}$, that relates the measurements to the true vertical was close to identity, simplifying the dynamics of the system. In addition, it was shown that head stabilization was useful even if an exact model of the system was not known. It was also found that gains in accuracy were obtained by the same order as when the knowledge of an exact model was assumed.

Further simulations showed that in the case of a stabilized head system, the reference given by the Newton's method based observer gave an absolute error smaller than 3° when the dynamic parameter uncertainties reached up to 50%. Conversely, the observer diverged when the head was not stabilized if the dynamic uncertainties exceeded 15%. This means that the head stabilization strategy considerably enlarges the convergence area of the observer and makes it more robust to model uncertainties [60].

4.4 Head stabilization and the separation principle

4.4.1 Linearization and the separation principle

In this section we show how the separation principle for the observer and the controller design can be applied when the head is stabilized in an up-right position with respect to the gravitational vertical. The application of the separation principle to nonlinear systems is currently an active theoretical research topic and the results are rare and apply to only certain restricted classes of systems [81, 155, 66]. In our case, the separation principle may be considered valid if we carry out the controller and the observer designs for a system linearized around an equilibrium. The price to pay is the possibly small region of controller and estimator convergence.

We may consider that the internal models of the head-neck system and the vestibular organs during normal locomotion can be significantly simplified if the head is stabilized in an up-right orientation. The dynamics linearized around the stabilized head's orientation can be taken into account by the neural system. Then, the local separation principle holds when stabilizing the nonlinear model of the vestibular system by a linear observer and a linear controller designed for the linearized system. Next we will show that it is sufficient to use a simple linear observer and linear controller, which can be designed separately, for verticality estimation.

4.4.2 Linear observer and controller

Linearized PD-regulator. A local linear feedback controller (PD-regulator) can be used to stabilize the head horizontally from any initial conditions in the neighborhood of the up-right orientation. The head's tilt angles in sagittal and coronal planes and head's angular velocity are the inputs for the controller:

$$
\begin{aligned}
{}^{\mathbb{H}}\boldsymbol{\tau}_x =& k_p \left(\phi_{x,d} - \arctan \frac{\left[{}_{\mathbb{I}}\mathbf{R}_{\mathbb{H}} \right]_{\{3,2\}}}{\left[{}_{\mathbb{I}}\mathbf{R}_{\mathbb{H}} \right]_{\{3,3\}}} \right) - k_d {}^{\mathbb{H}}_{\mathbb{I}}\boldsymbol{\omega}_{\mathbb{H}x}, , \qquad (4.6) \\
{}^{\mathbb{H}}\boldsymbol{\tau}_y =& k_p \left(\phi_{y,d} - \arctan \frac{\left[{}_{\mathbb{I}}\mathbf{R}_{\mathbb{H}} \right]_{\{3,1\}}}{\left[{}_{\mathbb{I}}\mathbf{R}_{\mathbb{H}} \right]_{\{3,3\}}} \right) - k_d {}^{\mathbb{H}}_{\mathbb{I}}\boldsymbol{\omega}_{\mathbb{H}y}. \qquad (4.7)
\end{aligned}
$$

where k_p, k_d are the control gains; $\phi_{x,d}$ and $\phi_{y,d}$ are desired sagittal and coronal tilts of the head with respect to the inertial frame.

When the head is close to being horizontal, ${}_{\mathbb{I}}\mathbf{R}_{\mathbb{H}} \approx \mathbf{I}_3$, and we can linearize (4.6) and (4.7) around the horizontal orientation of the head and obtain the following control laws:

$$
\begin{aligned}
{}^{\mathbb{H}}\boldsymbol{\tau}_x =& k_{p,x}(\phi_{x,d} - \left[{}_{\mathbb{I}}\mathbf{R}_{\mathbb{H}} \right]_{\{3,2\}}) - k_{d,x} {}^{\mathbb{H}}_{\mathbb{I}}\boldsymbol{\omega}_{\mathbb{H}x}, \qquad (4.8) \\
{}^{\mathbb{H}}\boldsymbol{\tau}_y =& k_{p,y}(\phi_{y,d} - \left[{}_{\mathbb{I}}\mathbf{R}_{\mathbb{H}} \right]_{\{3,1\}}) - k_{d,y} {}^{\mathbb{H}}_{\mathbb{I}}\boldsymbol{\omega}_{\mathbb{H}y}. \qquad (4.9)
\end{aligned}
$$

These linearized control equations stabilize the head to desired angular orientations in the neighborhood of the up-right orientation.

Luenberger observer. In this subsection we design a conventional linear observer [128] for the verticality estimation. For a nonlinear system expressed in the form

$$\dot{\boldsymbol{x}} = f(\boldsymbol{x}, \boldsymbol{u}), \boldsymbol{y} = h(\boldsymbol{x})$$

a Luenberger linear observer will be expressed as follows:

$$\dot{\hat{\boldsymbol{x}}} = A\hat{\boldsymbol{x}} + B\boldsymbol{u} + L(\boldsymbol{y} - C\hat{\boldsymbol{x}}), \qquad (4.10)$$

with $\dot{\hat{\boldsymbol{x}}}$ - the estimated state, L the observer's matrix gain and constant matrices

$$
\begin{aligned}
\mathbf{A} &= \left. \frac{\partial f}{\partial \boldsymbol{x}} \right|_{\substack{\boldsymbol{x} = \boldsymbol{x}_0 \\ {}^{\mathbb{H}}\boldsymbol{a} = 0}} , \\
\mathbf{A} &= \left. \frac{\partial f}{\partial \boldsymbol{x}} \right|_{\substack{\boldsymbol{x} = \boldsymbol{x}_0 \\ {}^{\mathbb{H}}\boldsymbol{a} = 0}} , \\
\mathbf{B} &= \left. \frac{\partial f}{\partial \boldsymbol{u}} \right|_{\substack{\boldsymbol{x} = \boldsymbol{x}_0 \\ {}^{\mathbb{H}}\boldsymbol{a} = 0}} , \\
\mathbf{C} &= \left. \frac{\partial h}{\partial \boldsymbol{x}} \right|_{\substack{\boldsymbol{x} = \boldsymbol{x}_0 \\ {}^{\mathbb{H}}\boldsymbol{a} = 0}}
\end{aligned}
$$

where the state $\boldsymbol{x}_0$ defines the stationary head stabilized in up-right position. For the case of the medial model this state is $\boldsymbol{x}_0 = ((0,0,0), \mathbf{I}, (0,0,0), \mathbf{I})^\top$.

A linear observer was applied to the systems (2.10) and (2.18) and their respected outputs after linearization around the up-right orientation of the non-translated head and pendulums aligned with the gravity vector.

Kalman filter. To evaluate the Luenberger observer's performance when measurements contain noise and there are uncertainties in model information, we compared it to a Kalman filter which is another widely used linear observer [111]. We used classical Kalman filter design equations described in detail in [202].

4.4.3 Simulation results

To test the designed linear observers and controller as well as applicability of the separation principle, simulation of a robotic platform with a liquid-based inclinometer was performed. The model was composed of a tilting platform with a sensor installed on it, as shown in Fig. 5.4 in Chapter 2 of this thesis. We took the parameters as specified by the model of the inclinometer used later in experiments (Model 900, Applied Geomechanics). For a critically-damped sensor with a natural frequency of 10 Hz, we get the following relations between the model parameter values: $\beta/(m_s l_s^2) = 125.6$ N·s/kg·m^2 and $g/l_s = 3943.8$ 1/s^2 with $g = 9.81$ m/s^2. The platform's inertia was taken to be $J_h = 0.0001$ kg·m^2. For simplicity, we present results for only one tilt of the platform (sagittal tilt). In the simulation scenario, the platform was accelerated in the plane with time-dependent linear acceleration ${}^{\mathbb{H}}\boldsymbol{a} = [0,\ 3\sin(10t),\ 0]^\top$. A PD-regulator with control gains $k_p = 1$ N/m/rad and $k_d = 0.1$ N·s/m/rad was used. The platform initial orientation was set to 0.4 radian. Numerical integration of the system equations was performed with a 1 ms time-step.

In Fig. 4.9, two cases of simulation of stabilization control for the nonlinear model are shown: the sensor-based output feedback control and the state-based feedback control. In the first case, direct measurements from the inclinometer and its numerical derivative were fed back to the PD regulator. Two reference tilt angles were given to the controller of the platform's orientation. The value of 1 radian was to simulate the case when the platform was controlled at an angle and the value of 0 radian for the horizontal stabilization. The inclinometer measurements were greatly disturbed by periodic translational disturbance motions of the head. The controller was not able to stabilize the platform's orientation. The platform's orientation was not stable both for the case when the head was not horizontal and for the case when the controller tried to maintain horizontal orientation.

In Fig. 4.9, the panels on the right show the results for the same control task but with the actual platform orientation and angular velocity fed back to the controller. The controller was able to stabilize the platform for both the non-horizontal and horizontal orientations. This means that for efficient stabilization it is necessary to know the actual platform's state, direct tilt measurements are not sufficient.

Next, we checked whether the Luenberger observer or the Kalman filter could lead to platform stabilization and how the orientation influenced the estimation error. The simulation results are shown in Fig. 4.10 when the linearized model of the system and the linearized PD-controller (4.8)-(4.9)

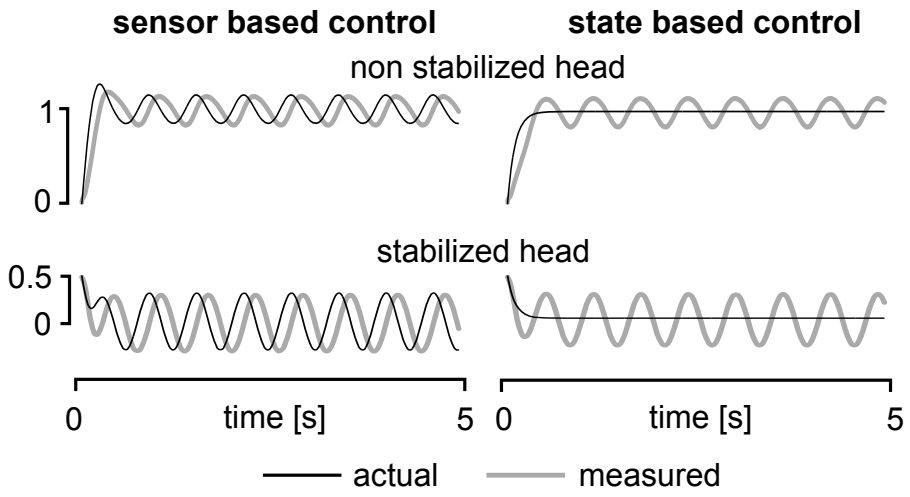

Figure 4.9: Simulation results: head is unstable when direct sensor based control is used (the worst case); head is easily stabilized when state feedback control is used (ideal case).

were used. The platform was linearly accelerated and controlled with a PD-regulator to maintain orientation of 1 radian in the first case; and in the second case, the platform was horizontally stabilized to an orientation of 0 radian. The estimated platform's tilt and angular velocity were fed back to the PD-regulator. The left panels of Fig. 4.10 show the results when the head was not horizontal.

As shown by the angle plots, the actual tilt was more than 1 radian which meant that the PD-regulator was receiving underestimated values of the state. This happened because of the approximation introduced by the linearization of the model around the horizontal orientation for the observer design. The observers were indeed not expected to provide reliable state estimation for significant angular motions. The state was correctly estimated when the PD-regulator maintained a horizontal platform, see the right panels of Fig. 4.10. For the Luenberger observer, the maximum estimation error was about 0.5 radian when the platform was not horizontal and less than 0.05 radian when the platform was horizontally stabilized.

Similar estimation errors were obtained with the Kalman filter. The estimation was significantly better for the case of the stabilized head (platform). As expected, the Kalman filter showed better performance when noise was introduced to the process update and measurements, and when the filter was run with uncertainty in the model's parameters values up to 10%. The controller's performance during platform stabilization was also better when the Kalman filter was used.

In Fig. 4.10, the platform oscillated in the neighborhood of desired tilt when the controller used the estimates from the Luenberger observer, with magnitude ≈ 0.15 radian for non horizontal platform and ≈ 0.03 radian for horizontal platform. There were no oscillations when Kalman filter's estimates were used.

The result hinges on the validity of the separation principle as the controller and observer were designed independently. The latter was valid because the nonlinear system is first linearized and the linearization is minimal, i.e. is both controllable and observable. The separation principle obviously holds for the linearized system, so the linear closed-loop, observer-based control system nat-

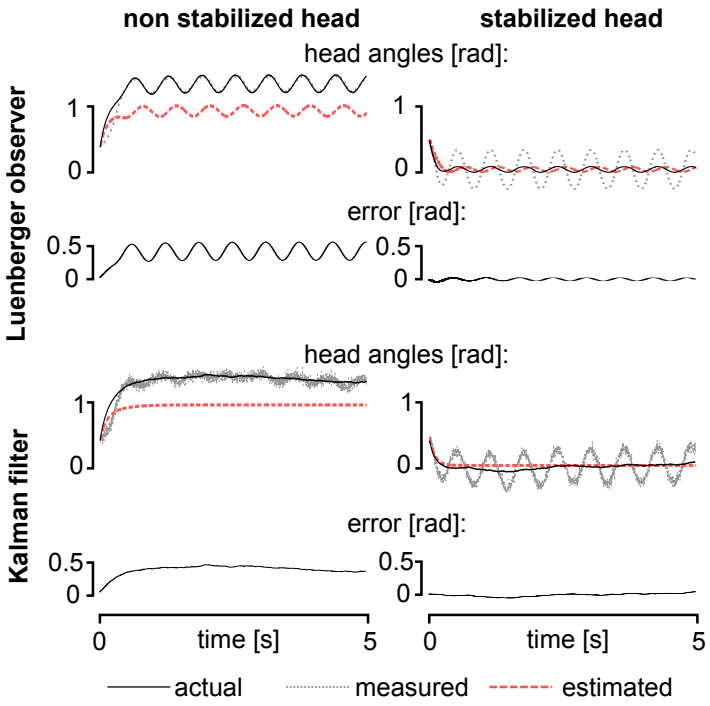

Figure 4.10: Simulation results for Luenberger observer and Kalman filter for the cases of not horizontal and horizontal head stabilization. Linearized model is used

urally possesses some robustness stability margin. As the linear controller and observer were next applied to the nonlinear system, they yielded a closed loop system whose approximation was the closed loop linearized system. Stabilization of the nonlinear closed-loop system then followed, by robustness, the linear approximation. The above observations are at the root of our working hypothesis that seems to hold true in our simulations and experiments, and indeed in the animal world.

4.5 Observation with consideration of ambiguity

4.5.1 Resolving ambiguity during up-right head stabilization

As it was discussed in chapter 3 of the thesis, one of the key problems to be solved by the neural system is the gravito-inertial ambiguity problem in the measurements of otolith organs. In the observer models and simulation scenarios presented above, linear acceleration of the head was considered to be a known input. However, information about linear acceleration of the head cannot be available to the neural system since it is not measured directly by any independent sensory organ. In this section we will consider that the linear acceleration was unknown and had to be estimated based on the otolith measurements.

A control diagram, shown in Fig. 4.11, represents the model of the head. The otolithic organs and their internal model are realized as a linear observer. This diagram represents a general structure of the observer-based head sta-

bilization tested in previous sections. In our vestibular system models (2.10) and (2.18), two inputs were considered: the head's torque control and the linear acceleration of the head. The displacement of otoliths with respect to the gravitational vertical was measured and the head orientation with respect to the gravitational verticality was estimated and used for the head's stabilization control. In further discussion, for simplicity and clarity of explanation, we consider the head rotational and translational motions in the sagittal plane only.

The control diagram in Fig. 4.11 represents the case when linear acceleration of the head was considered to be known for the internal model. Then, the observer could reconstruct the unmeasured vertical head orientation based on the known inputs and available measurements from the otoliths. The estimated head's vertical orientation was used by the controller to stabilize the head. But this 'ideal' case with known linear acceleration input does not represent well the real physical system, because in the vestibular system, like in any other inertial sensors, there is no possibility to obtain a direct linear acceleration measurement.

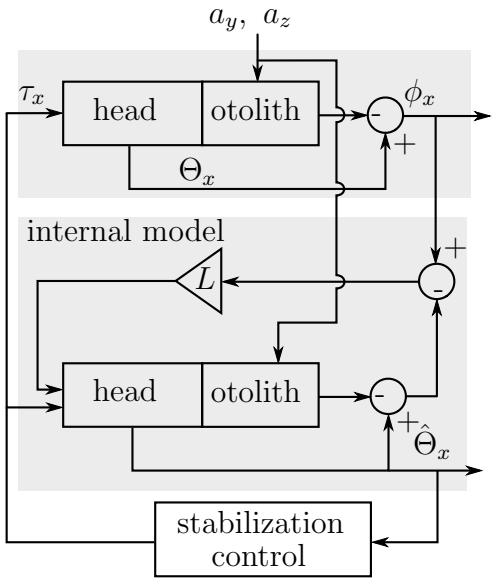

Figure 4.11: Control diagram representing the head-neck-otoliths system and the internal model for verticality estimation for the case when linear acceleration of the head is available to the internal model.

Diagram in Fig. 4.12 represents a more realistic case. In this system, the linear acceleration of the head is not known to the internal model. Instead, it is reconstructed based on the measured angular displacement of otolithic organs and estimated head tilt with respect to the gravitational vertical. The fidelity of the acceleration reconstruction depends on the quality of the estimation for the head's tilt. We consider this control diagram to be more realistic, since it is based on the fundamental principle that otoliths respond to the sum of gravitational and translational accelerations. Actual geometric configuration of the head and the otoliths can be used to resolve the gravitoinertial ambiguity.

In the simulation section below, it will be shown how the head stabilization around the up-right position is important for proper verticality estimation.

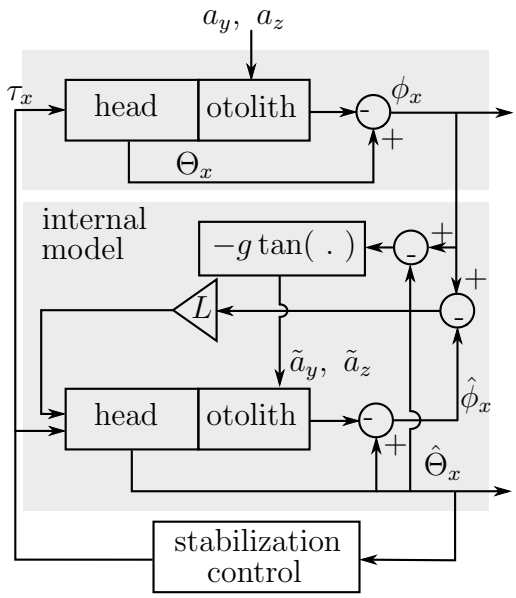

Figure 4.12: Control diagram representing the head-neck-otoliths system and the internal model for verticality estimation for the case when linear acceleration of the head is not available for the internal model. Instead, it is estimated based on the otoliths measurements and assumption of the head up-right stabilization.

4.5.2 Simulation results

The simulation results for the system configurations presented in Fig. 4.11 and Fig. 4.12 are presented in this section. We simulated head stabilization and verticality estimation during normal locomotion in the sagittal plane. The model's parameters were selected such that they represented the critically damped dynamic behavior of otoliths with natural frequency of about 300 Hz [78]; the head's moment of inertia was about 0.0174 kg·m^2 and was taken as an average from human biomechanical studies presented in [211]. The simplest-possible linear Luenberger observer was used in the following tests, which required linearization of the system. The only inputs left, after the medial model linearization around vertical in the sagittal plane are the control torque, τ_x, and the anterior-posterior acceleration, ${}^{\mathbb{H}}\boldsymbol{a}_y$. This linearized system model was used to design the observer and was considered to be the internal model. However, full nonlinear models of the head and the vestibular system (medial model) were used to simulate the real physical process with a full set of control inputs. The initial head tilt was about 5 degrees. In this and subsequent simulations, the head was accelerated in the sagittal plane. The acceleration plots, which were driven by locomotion, are shown in Fig. 4.13. These acceleration patterns were taken from the experimental study on human walking presented in [135].

In Fig. 4.14 the simulation results for head tilt control in the sagittal plane are shown. The head's actual tilt was considered to be unknown. The head's tilting controller received only the estimated angular orientation of the head. The initial condition for the estimation was set to zero for all simulations. Estimation was done based on the known system inputs (head torque and linear acceleration) and otolith measurements. As we can see in Fig. 4.14, the observer converges quickly, independently of the final orientation of the head. In this simulation, linear acceleration was considered to be known. However this information is not normally available, since there is no acceleration sensor

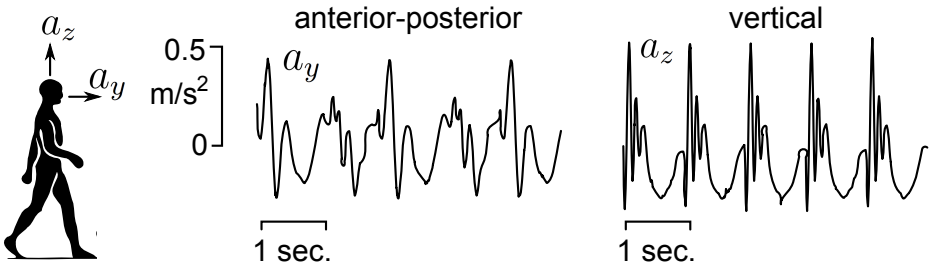

Figure 4.13: Human's head linear acceleration in sagittal plane during locomotion.

that can measure pure translational acceleration.

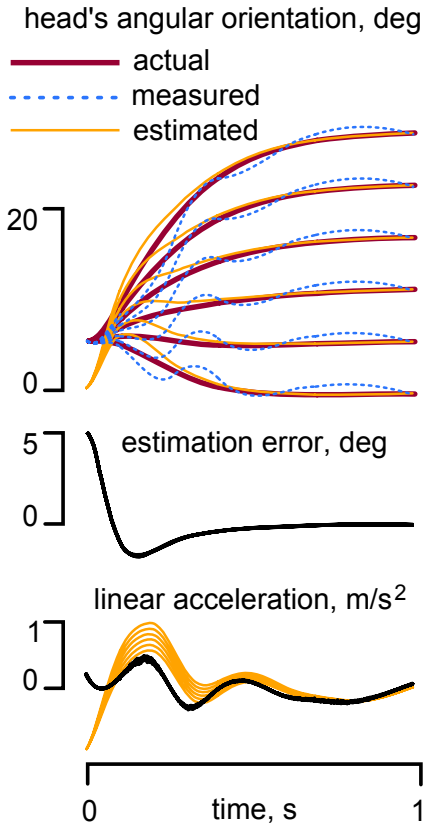

Figure 4.14: Simulation results for the head vertical orientation estimation and control to different desired angular orientations with assumption of known linear acceleration. The observer converges in all cases.

In the next simulation, we considered that the head actual translational acceleration was not known by any means. Therefore, we attempted to use the otolith measurements as a source of information about the head's translations. In Fig. 4.15, the head was tilted to a different non-zero initial tilts in the sagittal plane. The controller's task was to stabilize the head to an up-right orientation based on the head's sagittal tilt estimation and the estimated linear translation of the head.

In the left panel of the Fig. 4.15, the initial tilt of the head was about 12 degrees. The controller managed to stabilize the head horizontally even if the linear acceleration of the head was not measured independently from the gravitational acceleration. The third plot on the left panel of Fig. 4.15 shows

that the estimate of linear acceleration converges to the actual acceleration of the head.

In the central panel of Fig. 4.15, the same simulation scenario was performed for a bigger initial tilt of the head, approx. 25 degrees. In this case, the observer failed to estimate the actual head tilt, and the controller was unable to stabilize the head. Estimation of linear acceleration was wrong and the system generally became unstable.

The right plane of Fig. 4.15 shows the summary of this simulation scenario for different initial orientations of the head. It is easy to see that proper functioning of the observer and the head's controller is possible only for small initial tilts of the head. In other words, it is important for the head to be close to the up-right orientation to provide the internal model with correct angular orientation estimates and to enable proper stabilization control.

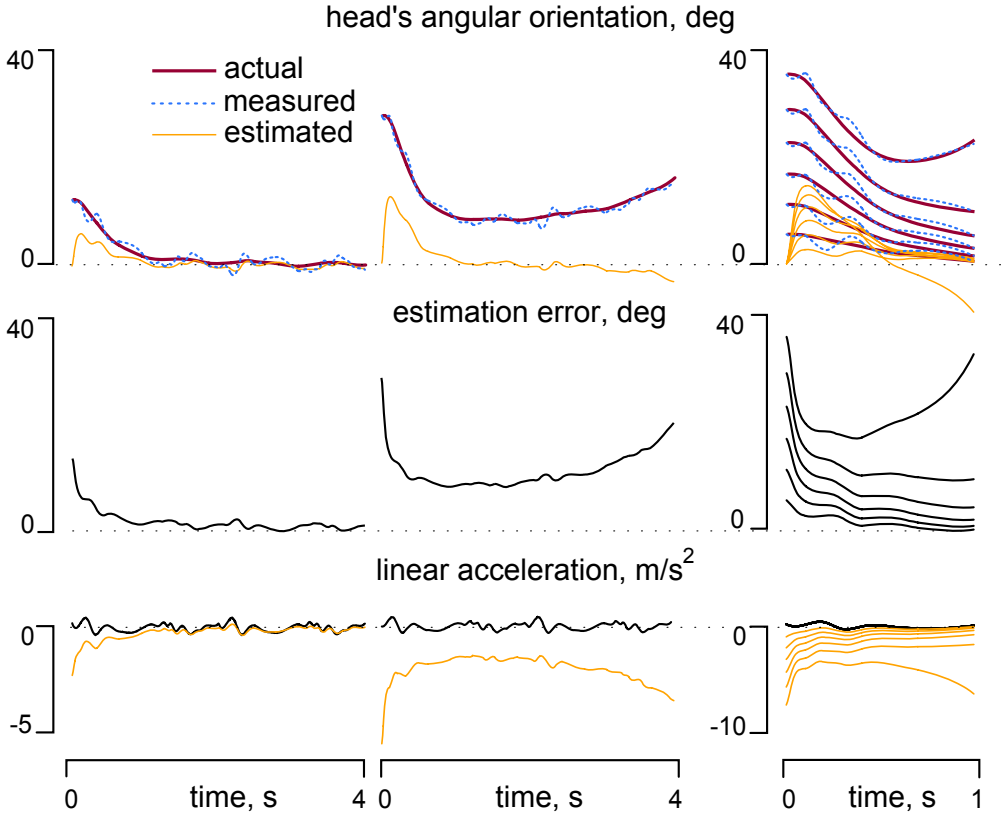

Figure 4.15: Simulation results for the head vertical orientation estimation and the head horizontal stabilization from different initial conditions with estimated linear acceleration.

In Fig. 4.16, the head was initially tilted to a small angle. The head's controller was supposed to orient the head to a desired tilt based on the head's vertical orientation estimate and estimated linear acceleration. As we can see on the left panel of the figure, when the controller stabilized the head to an orientation close to horizontal, both the head's tilt estimate and linear acceleration estimate converged to actual values.

However, The situation was different when the controller was meant to stabilize the head in a non-horizontal orientation, see for instance the central panel of Fig. 4.16. The controller tried to orient the head to a tilt of about 6 degrees. In this case, the observer failed to provide proper estimates, and the controller diverged. The summary for different desired tilts is shown in

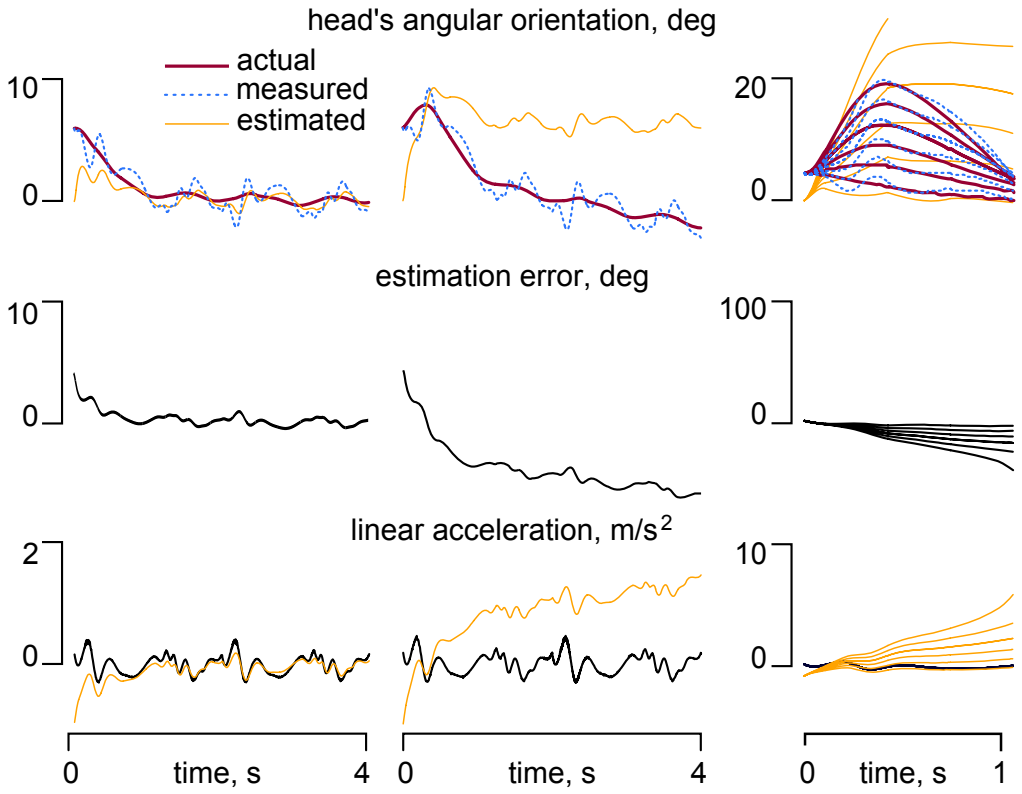

Figure 4.16: Simulation results for the head vertical orientation estimation and control to different desired angular orientations with linear estimated acceleration.

the right panel of Fig. 4.16. In this simulation scenario, the observer and controller worked properly only when the head was stabilized close to the up-right orientation.

4.6 Summary of results

The verticality estimation simulation results presented in this chapter have shown the importance of head stabilization in the up-right position. Here we summarize the benefits that arise from the head stabilization to improve the quality of verticality estimation.

1. Smaller estimation error due to a stationary head. Verticality estimation error was smaller for the stabilized head. Head stabilization slows the overall dynamics of the system, and therefore the system becomes smoother and easier to model within the observer. As a result, the estimation error is generally significantly smaller for a stabilized head.

2. Robustness to internal model uncertainties. Estimators showed better performance for the case of a stabilized head when uncertainty to model parameters was introduced. This happened due to slowed dynamics of the system when the head was stabilized. When the head's velocity was close to zero, uncertainty in the damping and inertia parameters did not greatly influence the quality of the verticality estimation.

3. Simpler system dynamics due to a smaller range of motion. When the head was stabilized around the up-right equilibrium, the model dynamics were quasi-linear. Therefore, a linear controller and linear observer could be used for the estimation-control problem. Following the separation principle, we showed

that independently-designed stable linear controllers and observers were able to properly estimate and stabilize the system, which essentially has nonlinear dynamics. Stability of the overall system was achieved through the up-right stabilization of the head, which enabled the use of a linearized model of the head and the vestibular system.

4. Ambiguity in otolith measurements is resolved. The up-right stabilization of the head provided the observer with a simple way to resolve the tilt/translation ambiguity in otolith measurements. If the neural system assumes that the head is always aligned with gravity, the otolith measurements will provide information on the linear acceleration of the head without the influence of the gravitational field. In this case, otoliths acted as pure accelerometers, and their measurements were used to estimate the immeasurable linear acceleration of the head.

In this thesis, and specifically in this chapter, the vestibular system was considered to be the principal source of information from which verticality could be estimated, while in real biological systems multi modal sources of information are available. In addition to the vestibular cues, other sensory inputs such as retinal-image motion, tactile, proprioception, and motor efference signals provide valuable motion cues which contribute to verticality estimation [44]. Multimodal sensory integration becomes important in these situations [179, 194, 161]. However, the role of the vestibular system in verticality estimation remains dominant, since the vestibular sensory organs, unlike other senses, are governed by the fundamental principles of mechanics, and as a result, vestibular organs provides the central neural system with a global invariant reference, which is gravity.

Chapter 5

Experimental validation

Contents

5.1 Experimental setup

5.1.1 General description

Verticality estimation and head stabilization control were tested with a specially arranged experimental setup. A schematic diagram is presented in Fig. 5.1. The key element of the system is an actuated gimbal-like platform which is driven by two electric motors. The motors control vertical angular orientation of the platform around two horizontal orthogonal axes. Orientation of the platform was measured by a dual-axis liquid based inclinometer which was attached to the center of the platform. The inclinometer's sensing axes were aligned with the platform's spinning axis. As a result, the platform's tilt measurements were decoupled from each other. In addition, a tri-axial accelerometer was attached to the center of the platform, with its sensing axis aligned with the platform's spinning axis. The accelerometer was used to measure the platform's linear acceleration in the body fixed frame. Tilt and acceleration measurements were used by the state observer and the tilting controller which were programmed and implemented in the embedded computer. The state observer included the system's dynamic model and provided the controller with the estimated angular orientation of the platform with respect

to the gravitational vertical, and, as a result, the controller generated the corresponding stabilization signals. These signals were amplified by the electric power drivers which controlled the motors. The goal of the overall system is to maintain the horizontal orientation of the platform independently from the body's linear and translational motion. To do this, the observer has to take into account the gravito-inertial ambiguity in the outputs of the inclinometer and the accelerometer and properly distinguish between tilt and translation.

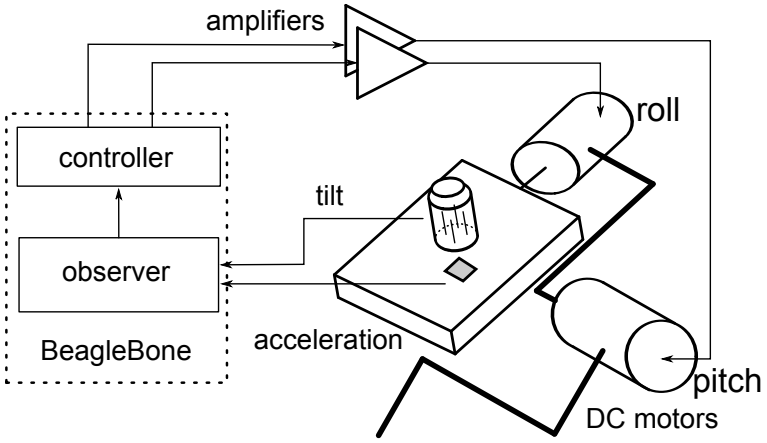

Figure 5.1: Schematic diagram of the experimental setup.

5.1.2 Mechanical design

In this subsection, we describe the mechanical design of the actuated platform. A photo of assembled actuated platform is shown in Fig. 5.2. Dual axis inclinometer was attached on top of the platform. A liquid based inclinometer Model T900 (from Applied Geomechanics) was selected to provide the system with two decoupled orientation measurements based on the degree of immersion of four electrodes in a liquid contained in a vial. This type of inclinometer has several advantages. First of all it has almost linear output characteristic. Second, it has natural physical damping, and that is why the output signal is less noisy. Finally, the sensor mechanical configuration and built-in electronics provides us with decoupled pitch and tilt measurements whose output values do not depend on yaw motion of the sensor. A MEMS-based tri-axis accelerometer (ST Microelectronics, Model LIS344ALH) was attached to the lower surface of the platform for measuring linear acceleration. Location of the sensors was crucial in the design process and we tried to align each inclinometer and accelerometer sensing axis with the spinning axis of the platform.

The platform had two rotational degrees of freedom. Each degree of freedom was actuated with the cable driven transmission. Schematic view of this type of transmission is shown in Fig. 5.3. A driving pinion was rotated by an electric motor in clockwise direction. This pinion was wrapped-around with flexible cable, whose two ends were connected to the platform's left and right sides as shown in the figure. A rigid arc was added to the platform, so that its center coincided with the center of rotation of the platform. The cable fit to the arc's circular surface and the pinion whose surface was threaded in order to have neat rotation of the cable-wrapped pinion. As a result of clockwise rotation of the pinion, the platform was tilted counterclockwise. The advantages of using this type of transmission are the following: low friction, no noise, simple

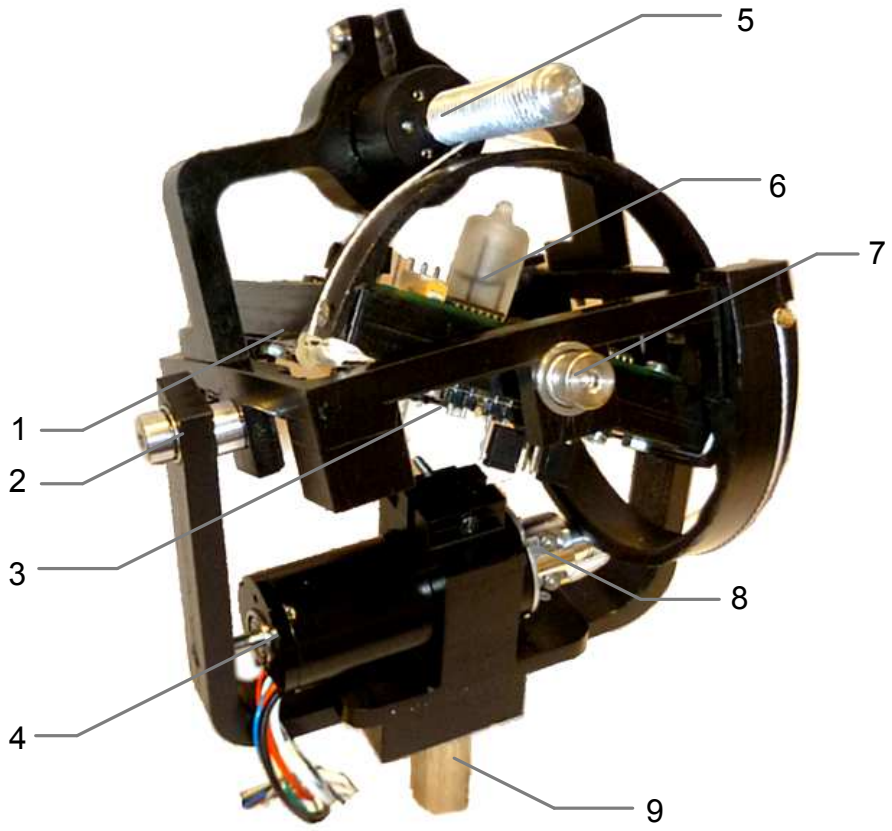

Figure 5.2: Inertial platform stabilization system. 1: gimbal's platform; 2: rotational joint (frontal tilt); 3: MEMS accelerometer; 4: DC motor for frontal tilt; 5: DC motor and cable driven transmission for lateral tilt; 6: liquid based inclinometer; 7: rotational joint (lateral tilt); 8: cable driven transmission for frontal tilt; 9: base link.

implementation, backlash-free motion. The cable-drive transmission was used to control both degrees of freedom of the platform.

In Fig. 5.2, the inclinometer (6) and accelerometer (3) are attached to the platform (1) which is actuated by the motor (5) around the joint (7) through the cable driven mechanism. The motor (5) body frame is rotated together with the corresponding mechanical links around the joint (2). This rotation is performed by the motor (4) through the cable-drive. The body frame of the motor 4 is attached to the body of the robot or any other mechanism through the link (9). As a result, the platform formed the distal link of a gimbal mechanism rotating around a fixed center of rotation where the inclinometer was located. This two degrees-of-freedom actuated gimbal mechanism represents the head-neck system with the liquid based inclinometer used as a robotic model for the otoliths.

5.1.3 Inclinometer model

The inclinometer is an advantageous sensor for measuring the angular orientation of the platform with respect to gravitational verticality. We selected a liquid-based inclinometer [47] as a tilt sensor, because it has several important benefits when compared to the accelerometers that are often used as tilt sensors (Fig. 5.4A). Most importantly, inclinometers provide quasi-linear tilt measurements, while accelerometers necessarily provide measurements that are

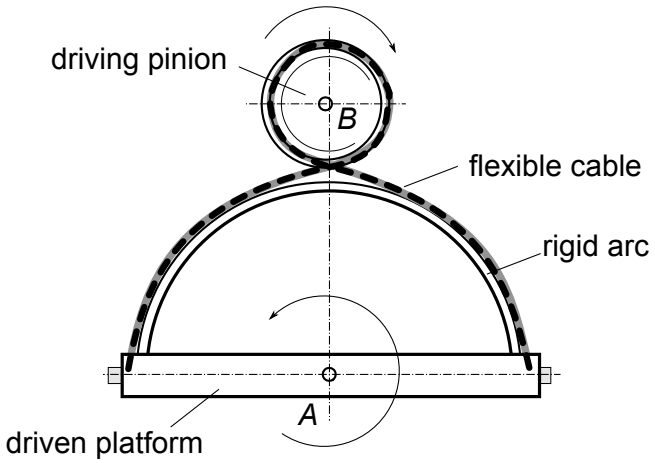

Figure 5.3: Schematic view of the cable driven transmission which was used to actuate each degree of freedom of the platform.

nonlinearly related to the gravitational vertical. The sensing element is a glass vial partially filled with a conductive liquid. In Fig. 5.4B, a simplified three-dimensional view of sensing element is shown. When the sensor is level, the four internal electrodes are immersed in the liquid at equal depths. When the sensor tilts, the depth of immersion of the electrodes changes, altering the electrical resistance between matched pairs of electrodes. In Fig. 5.4C, a planar view of the inclinometer is shown. The figure shows the inclinometer being accelerated to the right, or/and under the influence of an angular movement. A damped pendulum, Fig. 5.4D, can be used as a simplified mechanical model of the sensor.

Another disadvantage of tilt sensors based on accelerometers is their high sensitivity to vibrations, so that they can be used as tilt sensors in the low frequencies only. Finally, due to their mechanical structure liquid-based dual-axis inclinometers provides tilt measurements independent, around two orthogonal axes that can be directly mapped to rotation matrix defining the orientation of the inclinometer with respect to the gravity vector.

We would like to suggest that these three characteristics are in fact shared with natural vestibular systems, which are also linearized, naturally low-passed, and decoupled [73]. In this sense, the liquid-based inclinometer possesses intriguing biomimetic characteristics.

The dynamics of this type of inclinometer in planar case can be expressed as:

$$\dot{\phi} = \omega \tag{5.1}$$

$$\dot{\omega} = -\frac{g}{l}\sin\phi - \frac{b}{ml^2}(\omega - \Omega) + \frac{1}{l}a_x\cos\phi + \frac{1}{l}a_y\sin\phi \tag{5.2}$$

with ϕ angular orientation of the pendulum with respect to gravitational vertical; ω the angular velocity; g the gravitational acceleration; l the length of pendulum; m the concentrated mass of pendulum; Ω the angular velocity of the sensors frame; a_x and a_y the linear accelerations in horizontal and vertical directions of the pendulum's pivot expressed in the world frame, respectively. The measurement of the sensor is expressed directly as

$$y = \phi. \tag{5.3}$$

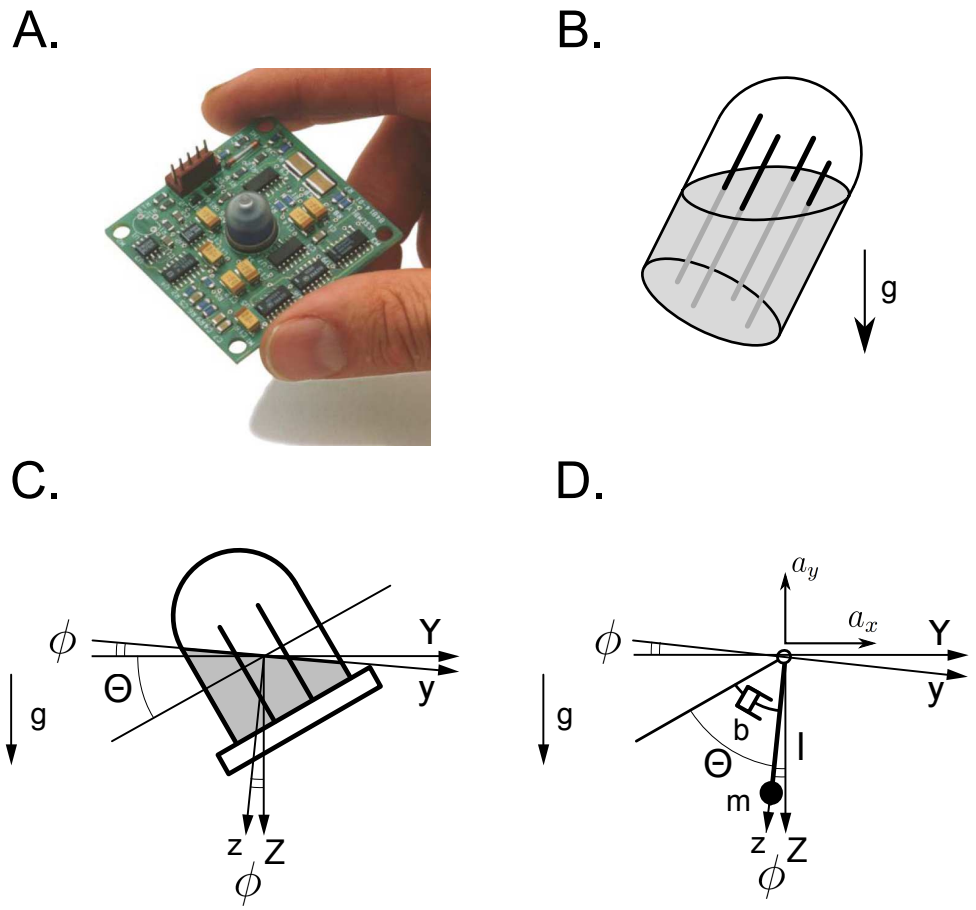

Figure 5.4: Liquid based inclinometer and its model. A. Dual axis inclinometer (Model A900 from Applied Geomechanics). B. Sensing elements are four electrodes and electrically conductive liquid. C. Side view of the liquid half-filled vial. D. Damped pendulum as a model. Its measurements are affected by the 'fictitious forces', if the sensor frame is not inertial.

The sensor dynamics is governed by the gravitational field and damping forces only if the sensor's body is not rotated and not translated. The rotation of the sensor frame influences the measurement through viscous torques via damping component. Linear acceleration of the sensor frame influences the measurement through forces applied to the pivot of the pendulum and the strength of this influence depends on current pendulum orientation. This dynamics expanded to the three dimensional case will be used in the following section to model the otoliths behavior.

5.1.4 System integration and control

Fig. 5.5 presents the overall functional scheme of the experimental setup. The control software which implemented the observer and controller was developed in C-language and compiled under Linux-based computer system. The executable file was then copied to the embedded computer (BeagleBone board) running under real time OS Linux Xenomai. Digital-to-Analogue Converters (DAC) were used to provide the motor amplifiers with the reference control inputs. Both rotational degrees-of-freedom were actuated by DC-motors: Faulhaber Model 024 SR motor (5) for joint (7) and brushless Maxon Model EC-powermax 22 mm motor (4) for joint (2) (See Fig. 5.2 for references). Maxon DC and Maxon 4-Q-EC amplifier DEC 70/10 motor amplifiers were used to provide sufficient driving power for the motors, respectively. The motors acted on the platform and its motion was measured by the inclinometer and the accelerometer. Analog outputs of the sensors were sent back to the embedded system after analog-to-digital conversion (ADC). Additionally, two analog potentiometers (US Digital Model MA3) were attached to the gimbal joints for joint angle monitoring. However, they were not used in the observation and control system design.

The controller and observer algorithms and read/write functions were called in the loop running on a BeagleBone embedded system with a sampling period of 3 ms.

Some additional technical information on mechanical design, system integration and control algorithm implementation is presented in the Appendix.

5.2 Experimental results

We experimentally tested two cases: sensor feedback based stabilization and observer based stabilization. The task of the controller was to stabilize the platform horizontally in spite of any random motions of the mechanism base link. The gimbal platform during the experiment is shown in Fig. 5.6. External forces were manually applied to the base link.

Potentiometers in the rotational joints of the platform measured the angular orientation of the platform with respect to the base link and were used for the results verification. These potentiometers acted as joint encoders, and their measurements provided us with the angular orientation of the base link with respect to the gravitational vertical if the platform was stabilized horizontally. Hence, the encoder measurements represented the robot's trunk angular movements.

As it was discussed in section 4.4, the separation principle can be used if the system can be linearized around the horizontal orientation. This means

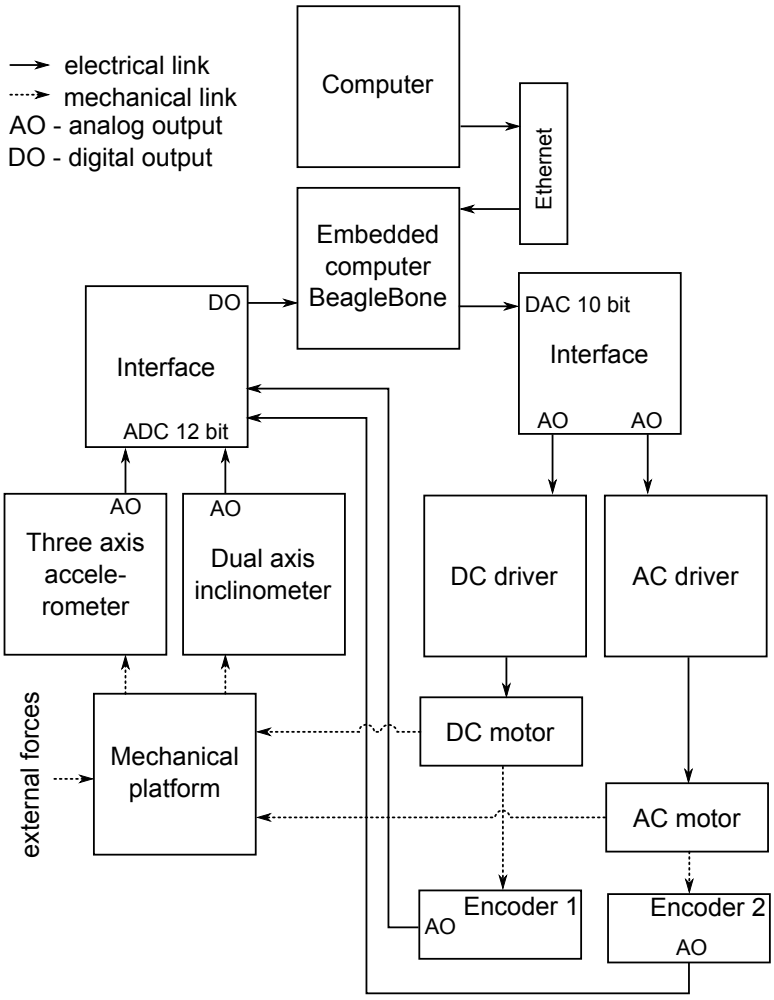

Figure 5.5: Functional diagram of experimental setup.

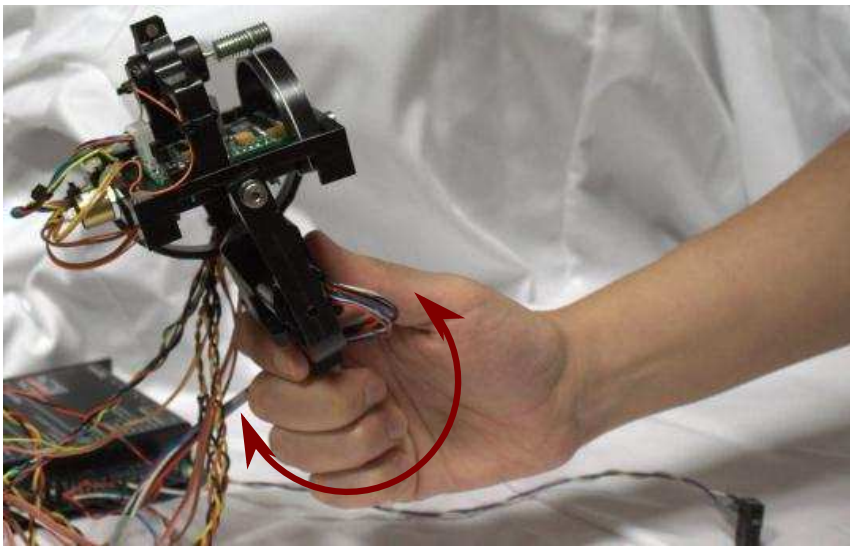

Figure 5.6: Platform stabilization experiment. The base link of the gimbal mechanism was moved manually. The taks of the controller was to stabilize the platform horizontally.

that our nonlinear system can be stabilized by a linear controller and a linear observer which are designed to be stable. The Luenberger observer and PD-controller described in the section 4.2.2 were used in experimental validation. Reference inputs to the motor amplifiers and accelerometer measurements were used as known inputs for the observer. Implementation of linear observer assumes the system model to be known. Therefore, system identification was done. Each of the two degrees of freedom was modeled as first order mass-damper system with an integrator. Pitch and roll rotations were identified independently by providing a set of periodic motor inputs based on step response signals. Angular orientation of the platform was measured as an output with the help of corresponding encoder (potentiometer). The dynamic model parameters were identified with the help of Matlab Identification Toolbox. For the pitch rotation the parameter values are: moment of inertia $J_1 = 0.008$ kg·m^2, damping $b_1 = 1.35$ N·m·s. For the roll rotation the parameters are: moment of inertia $J_2 = 0.0006$ kg·m^2, damping $b_2 = 0.137$ N·m·s. Second order system was used to model the inclinometer dynamics. The following model parameters were obtained after identification: moment of inertia $J_s = 0.0015$ kg·m^2, damping $b_s = 0.3776$ N·m·s, stiffness $k_s = 5.629$ N·m.

We first tested the performance of the head horizontal stabilization when direct tilt measurements were used to control the head with the PD-regulator. The inclinometer measurements of pitch and roll angles of the platform were fed back to PD-controller. Numerical derivatives of the pitch and roll angles were used for computing the derivative component of the control input. Fig. 5.7 presents the results for pitch and roll control of the platform for this case. First row of the figure contains time history of inclinometer measurements for pitch and roll angles with respect to gravitational vertical and encoder measurements of the platform angular orientation with respect to the base link. Inclinometer measurements lagged behind the encoder measurements since the liquid in the capsule had slower dynamic response compared to the dynamics of the PD-regulator. Very quickly the motion of the platform became unstable and the platform's pitch angle was reaching the workspace limits (the encoder measurements were saturated). The last row of the Fig. 5.7 shows the control input plots generated from pitch and roll PD-controllers and were transmitted to motor amplifiers. Magnitudes of pitch and roll control inputs were increasing with the time because of unstable behaviour of the platform which was caused by the slow dynamics of the sensor.

In the second test the observer based stabilization was done. Fig. 5.8, presents the experimental results for the case when the estimated angular orientation of the platform was used to stabilize it. The first row shows the time history of the inclinometer and encoders' measurements, as well as the estimation of the platform's pitch and roll angles. The second row shows the control input generated by the PD-regulators. In this case, when the estimated angular orientation of the platform was used the system was stable. The platform's motion was oscillating around the horizontal orientation with the magnitudes significantly smaller than the magnitudes of the base motion with respect to the platform. The base link was moved with the magnitudes of 40-50° with respect to the platform's orientation. Liquid inside the inclinometer followed the motion of the base link and the platform and the tilt measurements from the inclinometer reached up to 20°.

Additionally we tested the platform stabilization when it was linearly ac-

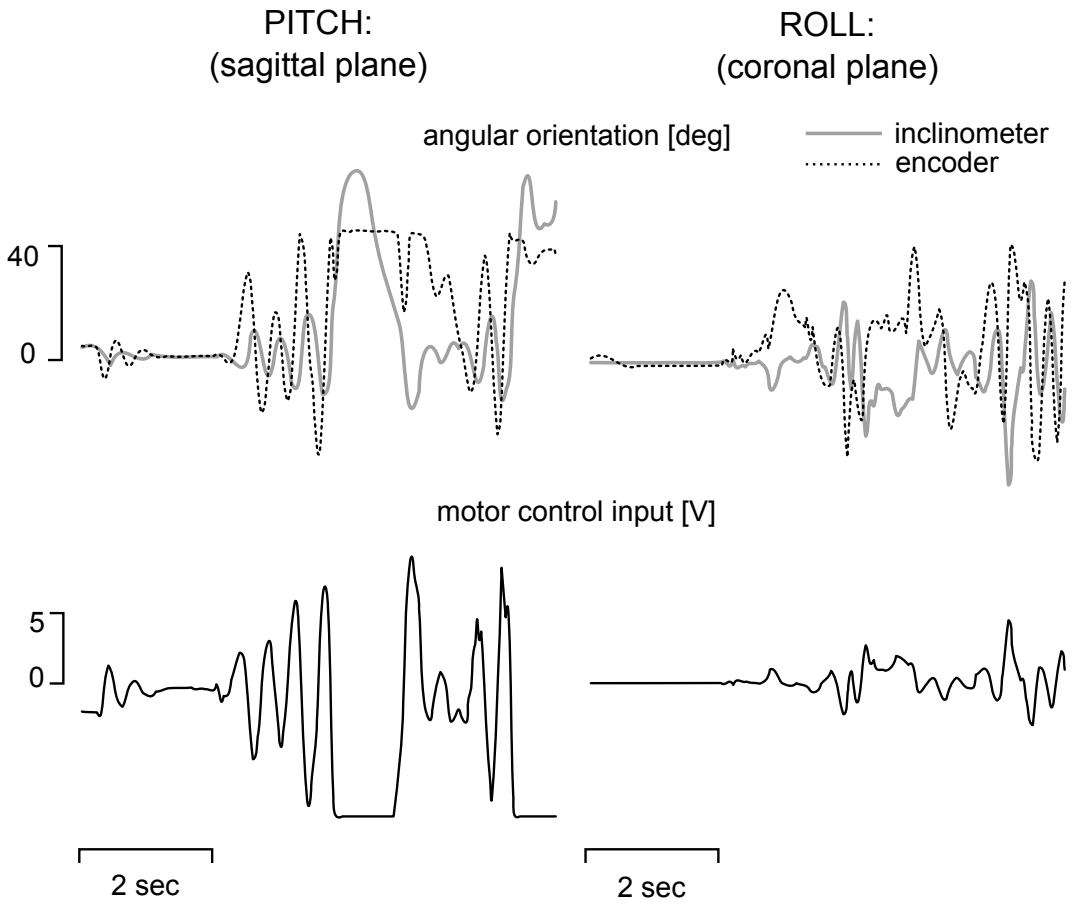

Figure 5.7: Experimental results. The head stabilization was done based on direct roll and pitch measurements from the inclinometer. The system was unstable.

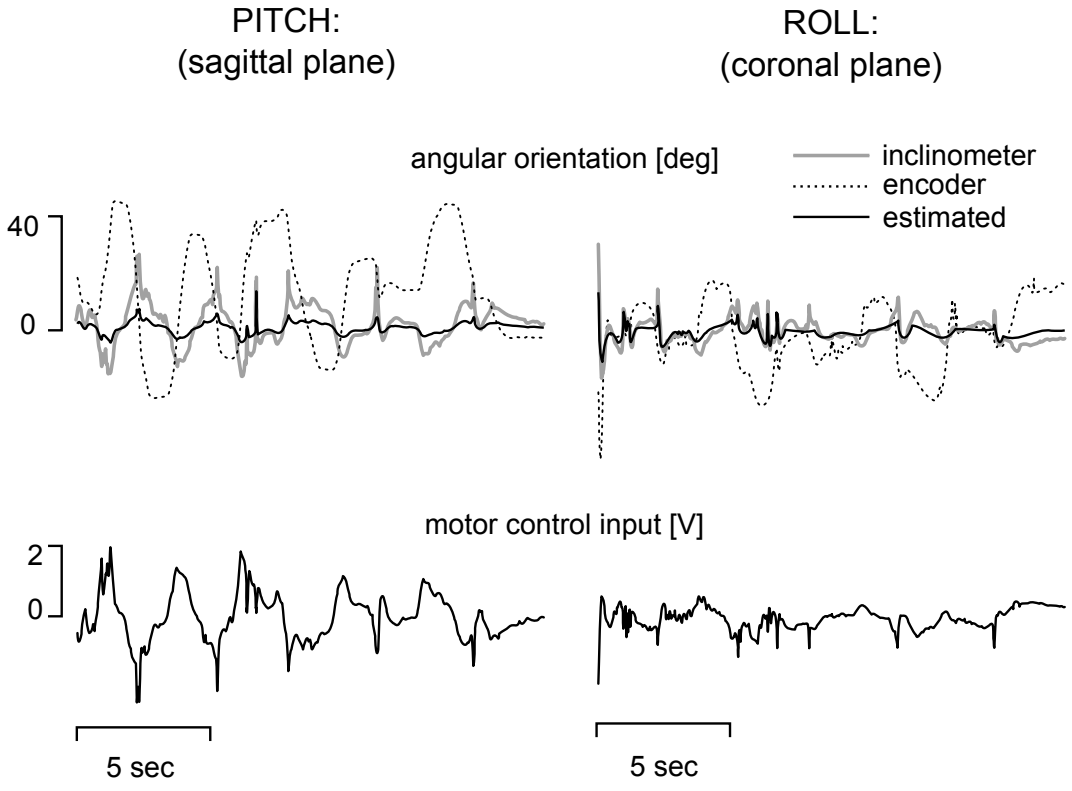

Figure 5.8: Experimental results. The head stabilization was done based on the estimated head's orientation. The system was stable.

celerated with an acceleration up to 2 m/s^2 while the controller tried to maintain the platform horizontally. Results are shown in Fig. 5.9. First, sensor based stabilization was tested when the inclinometer's outputs were fed back to the PD-regulator. The system quickly became unstable due to disturbed inclinometer measurements (Fig. 5.9, left panel). The head oscillated with the magnitude of approximately 0.5 rad. The accelerometer attached to the platform was strongly influenced by its movements and was not providing accurate information about linear translation, as shown in the bottom-left panel of Fig. 5.9.

In the second case, we tested the head stabilization when the controller was provided with the estimated platform orientation and angular velocity. The results are presented in the rightmost panels of Fig. 5.9. Similarly to the previous experiment, the head was linearly accelerated while the PD-regulator forced the platform to remain horizontal. The platform oscillated with a magnitude smaller than 0.1 rad which was significantly smaller compared to the first experiment. The accelerometer measurements were less influenced by the head's actual tilt when head was close to be horizontal orientation, and that is why proper information about the head's linear motion was accessible to the observer. As a result the head remained almost horizontal even though the inclinometer measurements were greatly disturbed by translational motion.

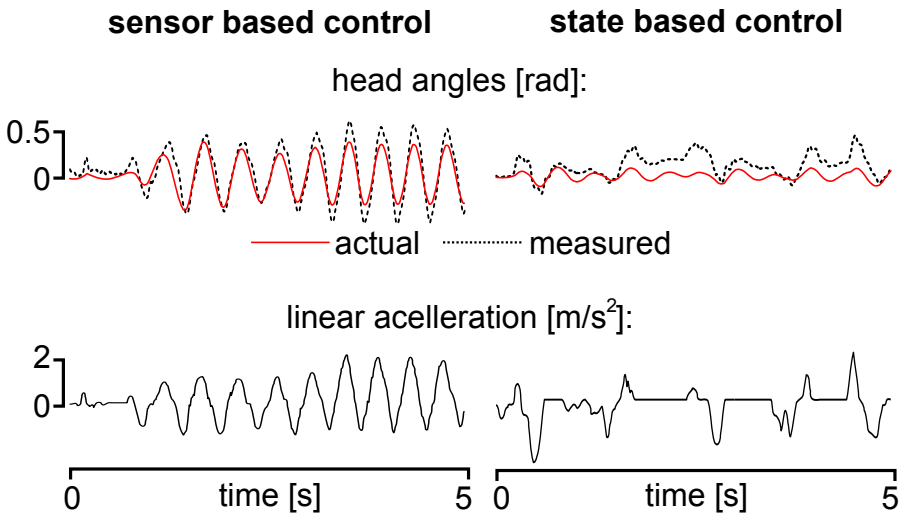

Figure 5.9: Experimental results. The platform was horizontally stabilized while head was translated. Left panels: Control based on direct inclinometer measurements. Right panel: control based on state estimation.

5.3 Discussion

We performed simulations and experiments to study and analyze the stabilization of platforms with a view to provide gravitational verticality estimation based on pure inertial measurements from a non-inertial frame. Such systems are highly nonlinear. When an inertial platform is maintained horizontally by observation and feedback, the measurements respond to translational movements only and angular components are rejected. It is therefore straightforward to estimate its linear acceleration by solving the dynamics equations of

the sensing device. When the platform is not horizontal it is impossible to distinguish between gravitational and body acceleration without additional sensory information such as tilt, angular velocity, etc. The result hinges on the validity of the separation principle as the controller and observer are designed independently. The latter is valid because the nonlinear system is first linearized and the linearization is minimal, i.e. is both controllable and observable. The separation principle obviously holds for the linearized system so the linear closed-loop, observer-based control system naturally possesses some robustness stability margin (just by being exponentially stable). As the linear controller and observer are next applied to the nonlinear system they yield a closed loop whose approximation is the closed loop linearized system. Stabilization of the nonlinear closed loop system then follows by robustness of the linear approximation. The above observations are at the root of our working hypothesis that seems to hold true in our simulations and experiments, and indeed in the animal world.

We set out to design a gravitational verticality estimation system that shares some features with the natural vestibular systems. Chiefly among them is the use of a (liquid) pendulum-type inclinometer that may be compared, in function, to the otolith organs of the natural vestibular systems in the sense that its measurements are naturally low passed. Like all gravitational and inertial sensors, an inclinometer is unable to make a distinction between the four terms of the gravito-inertial forces that can deviate it from its equilibrium. Using an IMU to provide additional acceleration and angular rate measurements, we showed that the gravitational component could be extracted almost exactly under highly dynamic trajectories, up to the accuracy of a nonlinear observer (using Newton iterations to solve the full system dynamics), even with uncertainty in the model parameters and noise in the measurements.

We would like to argue that head stabilization would be of benefit to any robot operating in a non-inertial frame and that such feature should be replicated in their designs.

Chapter 6

Conclusion

A dynamic nonlinear model of verticality estimation in biological systems was developed and analyzed in this thesis. Control theory methods were used to analyze the role of head stabilization for the verticality estimation process. Results have shown that head stabilization is required for accurate estimation of the spatial orientation of the head with respect to gravitational verticality. Linear and nonlinear observers were designed to estimate the spatial orientation of the head. Numerical tests of gravitational verticality estimation showed that the observers had better performance in terms of accuracy and robustness when the head was stabilized. Computational experiments showed that the estimation errors were smaller and the observers were more robust to the internal model uncertainties when the head was stabilized. The difference in the observability properties of the medial and the lateral models of the vestibular system showed the importance of having two sets of vestibular organs, since the spatial orientation of the head was always observable for the lateral model.

It was also shown that the head up-right stabilization and model linearization around this equilibrium enables application of separation principle which yields independent observer and controller design. Independently designed stable linear head controller and linear verticality observer were able to function properly for controlling and estimating the spatial orientation of the head based on the outputs from the vestibular system.

Having a head stabilized in up-right orientation during locomotion facilitates estimation of the verticality by providing the observer with a way to distinguish between otoliths response to tilt and translational motions. In this situation, linear acceleration of the head can be directly expressed based on the otoliths outputs, and then, used by the neural system to solve the tilt/translation ambiguity. Computer simulations of verticality estimation and head stabilization process showed that it is possible to resolve the tilt/translation ambiguity when the head is stabilized in the up-right orientation.

Although the theoretical findings presented in this work are based on modern control theory, the outcome from the observability study and numerical tests can potentially serve as an explanation of the head stabilization phenomenon which was reported in various biological studies.

In terms of application to robotics, the results presented in this thesis suggest locating inertial sensors on horizontally stabilized platforms. Certainly, many machines and engineering systems already do this. Since the invention of the marine compass, stabilized inertial platforms have been widely used in

aerospace and marine navigation systems in order to provide approximations of inertial frames unaffected by the ship's movements. Long ago, it was noticed that guidance was greatly simplified if the inertial sensors where placed on stabilized platforms. In such systems, the application of fundamental mechanical principles and stabilizing control provided engineers with possibilities to establish the gravity referenced Earth's inertial frame without the need of other external references. Similarly, in humanoid robots and other free moving robots, locating the IMU on a stabilized platform would afford key advantages that are well worth the extra complexity, for purposes of postural stabilization and motion planning, without any need for ground or environmental references.

The platform stabilization control problem can be simplified to the linear case with a view to improve verticality estimation quality. Such estimation has many applications in the control of humanoids, rovers and drones. Tests with simple linear observers showed that estimation error was significantly smaller when the head was horizontally stabilized without any external reference. Observation algorithms such as the Kalman filter greatly improved the performance of the head stabilization control, even in the presence of strongly accelerated linear motions. These observations runs counter to the common practice in humanoid robot control to assume that the ground can serve as a reference for gravitational verticality. From this point of view, robot postural control from a stabilized head frame provides opportunities for implementation human-like locomotion not accessible with the current practice of humanoid motion control.

In real biological and robotic systems, sources of information other than inertial measurements may be available (vision, joint kinematics, Earth magnetic field, etc.), which means that these sensory inputs may help to improve the accuracy and convergence rate of the estimation. Inertial information, however, is the only fundamentally absolute measure of the gravitational verticality, which is essential for a variety of tasks. We believe that inertially stabilized platforms could provide the possibility for development of ground-independent locomotion strategies in humanoids and other vehicles. Such robots and vehicles would be free of the assumption of interacting with firm, flat and horizontal grounds. Posture control can then be realized in top-to-down manner, from a stabilized platform down to the robot's appendages and actuators.

Bibliography

[1] D. Aeyels. Generic observability of differentiable Systems. *SIAM Journal on Control and Optimization*, 19(5):595–603, Sept. 1981.

[2] J. Allum, A. Adkin, M. Carpenter, M. Held-Ziolkowska, F. Honegger, and K. Pierchala. Trunk sway measures of postural stability during clinical balance tests: effects of a unilateral vestibular deficit. *Gait & Posture*, 14(3):227–237, Dec. 2001.

[3] J. Allum, F. Honegger, and C. Pfaltz. *Afferent Control of Posture and Locomotion*, volume 80 of *Progress in Brain Research*. Elsevier, 1989.

[4] W. T. Ang, P. K. Khosla, and C. N. Riviere. Nonlinear Regression Model of a Low-g MEMS Accelerometer. *IEEE Sensors Journal*, 7(1):81–88, Jan. 2007.

[5] D. E. Angelaki and K. E. Cullen. Vestibular system: the many facets of a multimodal sense. *Annual Reviews of Neuroscience*, 31:125–150, 2008.

[6] M. Anguelova, G. Cedersund, M. Johansson, C. J. Franzén, and B. Wennberg. Conservation laws and unidentifiability of rate expressions in biochemical models. *IET systems biology*, 1(4):230–7, July 2007.

[7] T. Asfour, P. Azad, N. Vahrenkamp, K. Regenstein, A. Bierbaum, K. Welke, J. Schröder, and R. Dillmann. Toward humanoid manipulation in human-centred environments. *Robotics and Autonomous Systems*, 56(1):54–65, Jan. 2008.

[8] S. Audoly, G. Bellu, L. D'Angiò, M. P. Saccomani, and C. Cobelli. Global identifiability of nonlinear models of biological systems. *IEEE transactions on bio-medical engineering*, 48(1):55–65, Jan. 2001.

[9] A.-J. Baerveldt and R. Klang. A low-cost and low-weight attitude estimation system for an autonomous helicopter. In *Proceedings of IEEE International Conference on Intelligent Engineering Systems*, pages 391–395. IEEE, 1997.

[10] J. Baker, J. Goldberg, and B. Peterson. Spatial and temporal response properties of the vestibulocollic reflex in decerebrate cats. *J Neurophysiol*, 54(3):735–756, Sept. 1985.

[11] G. Baldwin, R. Mahony, and J. Trumpf. A nonlinear observer for 6 DOF pose estimation from inertial and bearing measurements. In *2009 IEEE International Conference on Robotics and Automation*, pages 2237–2242. IEEE, May 2009.

[12] N. Barbour and G. Schmidt. Inertial sensor technology trends. *IEEE Sensors Journal*, 1(4):332–339, 2001.

[13] B. Barshan and H. Durrant-Whyte. Inertial navigation systems for mobile robots. *IEEE Transactions on Robotics and Automation*, 11(3):328–

342, June 1995.

[14] R. Bellman and K. Aström. On structural identifiability. *Mathematical Biosciences*, 7(3-4):329–339, Apr. 1970.

[15] D. Bernardin, H. Kadone, D. Bennequin, T. Sugar, M. Zaoui, and A. Berthoz. Gaze anticipation during human locomotion. *Experimental brain research.*, 223(1):65–78, Nov. 2012.

[16] A. Berthoz. *The Brain's Sense of Movement*. Harvard University Press, 2000.

[17] A. Berthoz, J. Droulez, P. P. Vidal, and K. Yoshida. Neural correlates of horizontal vestibulo-ocular reflex cancellation during rapid eye movements in the cat. *J. Physiol.*, 419(1):717–751, Dec. 1989.

[18] A. Berthoz, M. G. Jones, and A. Begue. Differential visual adaptation of vertical canal-dependent vestibulo-ocular reflexes. *Experimental Brain Research*, 44(1), Sept. 1981.

[19] A. Berthoz, B. Pavard, and L. Young. Perception of linear horizontal self-motion induced by peripheral vision (linear vection) basic characteristics and visual-vestibular interactions. *Experimental Brain Research*, 23(5), Nov. 1975.

[20] A. R. Bisdorff, C. J. Wolsley, D. Anastasopoulos, A. M. Bronstein, and M. A. Gresty. The perception of body verticality (subjective postural vertical) in peripheral and central vestibular disorders. *Brain*, 119(5):1523–1534, Oct. 1996.

[21] A. C. Bittner and J. C. Guignard. Human factors engineering principles for minimizing adverse ship motion effects: theory and practice. *Naval Engineers Journal*, 97(4):205–213, May 1985.

[22] J. Borah, L. R. Young, and R. E. Curry. Optimal estimator model for human spatial orientation. *Annals of the New York Academy of Sciences*, 545(1 Representatio):51–73, Dec. 1988.

[23] D. M. Bramble and D. E. Lieberman. Endurance running and the evolution of Homo. *Nature*, 432(7015):345–52, Nov. 2004.

[24] S. Bras, R. Cunha, J. F. Vasconcelos, C. Silvestre, and P. Oliveira. A nonlinear attitude observer based on active vision and inertial measurements. *IEEE T. on Robotics*, 27(4):664–677, 2011.

[25] M. Brödel. Three unpublished drawings of the anatomy of the human ear. Technical report, W.B. Saunders Co., Philadelphia:, 1946.

[26] A. M. Bronstein. Evidence for a Vestibular Input Contributing to Dynamic Head Stabilization in Man. *Acta oto-laryngologica*, 105(1-2):1–6, July 1998.

[27] R. A. Brooks and C. Breazeal. The Cog project: building a humanoid robot. In *Computation for Metaphors, Analogy, and Agents. Lecture Notes in Computer Science*, volume 1562, pages 52–87. 1999.

[28] J. J. Buchanan and F. B. Horak. Vestibular loss disrupts control of head and trunk on a sinusoidally moving platform. *Journal of vestibular research : equilibrium & orientation*, 11(6):371–89, 2002.

[29] E. Bums, R. Homing, W. Herb, J. Zook, and H. Guckel. Resonant microbeam accelerometers. In *Proceedings of the International Solid-State*

Sensors and Actuators Conference - TRANSDUCERS '95, volume 2, pages 659–662. IEEE, 1995.

[30] T. Buschmann, S. Lohmeier, and H. Ulbrich. Humanoid robot Lola: design and walking control. *Journal of physiology-Paris*, 103(3-5):141–148, 2009.

[31] K. Caluwaerts, M. Staffa, S. N'Guyen, C. Grand, L. Dollé, A. Favre-Félix, B. Girard, and M. Khamassi. A biologically inspired meta-control navigation system for the Psikharpax rat robot. *Bioinspiration & biomimetics*, 7(2):025009, June 2012.

[32] J. P. Carey and C. C. D. Santina. Principles of applied vestibular physiology. In *Cummings Otolaryngology - Head and Neck Surgery*, chapter 163. Mosby, 2005.

[33] Y.-H. Chang, Y. Oh, D. Kim, and S. Hong. Balance control in whole body coordination framework for biped humanoid robot MAHRU-R. In *RO-MAN 2008 - The 17th IEEE International Symposium on Robot and Human Interactive Communication*, pages 401–406. IEEE, Aug. 2008.

[34] W. G. Chase and H. H. Clark. Semantics in the perception of verticality. *British Journal of Psychology*, 62(3):311–326, Aug. 1971.

[35] N. Chaturvedi, F. Bacconi, A. Sanyal, D. Bernstein, and N. McClamroch. Stabilization of a 3D rigid pendulum. In *Proceedings of the 2005, American Control Conference, 2005.*, pages 3030–3035. IEEE, 2005.

[36] N. Chaturvedi, N. McClamroch, and D. Bernstein. Stabilization of a 3D axially symmetric pendulum. *Automatica*, 44(9):2258–2265, Sept. 2008.

[37] N. Chaturvedi, A. Sanyal, and N. McClamroch. Rigid-body attitude control. *IEEE Control Systems*, 31(3):30–51, June 2011.

[38] N. A. Chaturvedi and N. H. McClamroch. Asymptotic stabilization of the hanging equilibrium manifold of the 3D pendulum. *International Journal of Robust and Nonlinear Control*, 17(16):1435–1454, Nov. 2007.

[39] G. Cheng, S.-H. Hyon, J. Morimoto, A. Ude, J. G. Hale, G. Colvin, W. Scroggin, and S. C. Jacobsen. CB: a humanoid research platform for exploring neuroscience. *Advanced Robotics*, 21(10):1097–1114, Jan. 2007.

[40] B. Chiang, G. Y. Fridman, C. Dai, M. A. Rahman, and C. C. Della Santina. Design and performance of a multichannel vestibular prosthesis that restores semicircular canal sensation in rhesus monkey. *IEEE transactions on neural systems and rehabilitation engineering*, 19(5):588–98, Oct. 2011.

[41] G. Ciaravella, C. Laschi, and P. Dario. Biomechanical modeling of semicircular canals for fabricating a biomimetic vestibular system. In *Annual International Conference of the IEEE Engineering in Medicine and Biology Society.*, volume 1, pages 1758–1761, Jan. 2006.

[42] J. L. Crassidis, F. L. Markley, and Y. Cheng. Survey of nonlinear attitude estimation methods. *Journal of Guidance, Control, and Dynamics*, 30(1):12–28, Jan. 2007.

[43] T. W. Cronin, M. R. Kinloch, and G. H. Olsen. Head-bobbing behavior in walking whooping cranes (Grus americana) and sandhill cranes (Grus canadensis). *Journal of Ornithology*, 148(S2):563–569, Aug. 2007.

[44] K. E. Cullen. The neural encoding of self-motion. *Current opinion in neurobiology*, 21(4):587–95, Aug. 2011.

[45] K. E. Cullen. The vestibular system: multimodal integration and encoding of self-motion for motor control. *Trends in neurosciences*, 35(3):185–96, Mar. 2012.

[46] I. S. Curthoys, C. H. Markham, and E. J. Curthoys. Semicircular duct and ampulla dimensions in cat, guinea pig and man. *Journal of morphology*, 151(1):17–34, Jan. 1977.

[47] Datasheet. Inclinometer: model 900 biaxial clinometer, http://www.jewellinstruments.com/ wp-content/uploads/2012/12/ Model_900_Biaxial-Clinometer-Jewell.pdf, 2001.

[48] M. N. Davies and P. R. Green. Head-bobbing during walking, running and flying: relative motion perception in the pigeon. *J. Exp. Biol.*, 138(1):71–91, Sept. 1988.

[49] H. De Vries. The mechanics of the labyrinth otoliths. *Acta otolaryngologica*, 38(3):262–73, June 1951.

[50] J. Di Giovanna, W. Gong, W. Haburcakova, V. Kögler, J. Carpaneto, V. Genovese, D. Merfeld, A. Demosthenous, J. Guyot, K. K.P., Hoffmann, A. Berthoz, M. Morari, and S. Micera. Development of a closed-loop neural prosthesis for vestibular disorders. *Journal of Automatic Control*, 20(1):27–32, 2010.

[51] M. Dieterich and T. Brandt. Vestibulo-ocular reflex. *Current opinion in neurology*, 8(1):83–8, Feb. 1995.

[52] S. Diop and M. Fliess. Nonlinear observability, identifiability, and persistent trajectories. In *Proceedings of the 30th IEEE Conference on Decision and Control*, pages 714–719. IEEE, 1991.

[53] D. C. Dunbar. Stabilization and mobility of the head and trunk in wild monkeys during terrestrial and flat-surface walks and gallops. *Journal of Experimental Biology*, 207(6):1027–1042, Feb. 2004.

[54] D. C. Dunbar, J. M. Macpherson, R. W. Simmons, and A. Zarcades. Stabilization and mobility of the head, neck and trunk in horses during overground locomotion: comparisons with humans and other primates. *The Journal of experimental biology*, 211(Pt 24):3889–907, Dec. 2008.

[55] R. C. Duncan and A. L. F. S. J. Gunnersen. Inertial Guidance, Navigation , and Control Systems. *Journal of Spacecraft and Rockets*, 1(6):577–587, 1964.

[56] M. O. Ernst and H. H. Bülthoff. Merging the senses into a robust percept. *Trends in cognitive sciences*, 8(4):162–9, Apr. 2004.

[57] M. Euston, P. Coote, R. Mahony, and T. Hamel. A complementary filter for attitude estimation of a fixed-wing UAV. In *2008 IEEE/RSJ International Conference on Intelligent Robots and Systems*, pages 340–345. IEEE, Sept. 2008.

[58] K. Ezure, S. Sasaki, Y. Uchino, and V. J. Wilson. Frequency-response analysis of vestibular-induced neck reflex in cat. II. Functional significance of cervical afferents and polysynaptic descending pathways. *J Neurophysiol*, 41(2):459–471, Mar. 1978.

[59] E. Falotico, N. Cauli, K. Hashimoto, P. Kryczka, A. Takanishi, P. Dario,

A. Berthoz, and C. Laschi. Head stabilization based on a feedback error learning in a humanoid robot. In *2012 IEEE RO-MAN: The 21st IEEE International Symposium on Robot and Human Interactive Communication*, pages 449–454. IEEE, Sept. 2012.

[60] I. Farkhatdinov, V. Hayward, and A. Berthoz. On the benefits of head stabilization with a view to control balance and locomotion in humanoids. In *11th IEEE-RAS International Conference on Humanoid Robots 2011*, pages 147–152, Bled, Slovenia, 2011. IEEE.

[61] I. Farkhatdinov, H. Michalska, A. Berthoz, and V. Hayward. Modeling verticality estimation during locomotion. In *Romansy 19, Robot Design, Dynamics and Control*, volume 544 of *CISM International Centre for Mechanical Sciences*, pages 359–366, Paris, France, 2012. Springer.

[62] C. Fernandez and J. M. Goldberg. Physiology of peripheral neurons innervating semicircular canals of the squirrel monkey. II. Response to sinusoidal stimulation and dynamics of peripheral vestibular system. *Journal of neurophysiology*, 34(4):661–75, July 1971.

[63] C. Fernández and J. M. Goldberg. Physiology of peripheral neurons innervating otolith organs of the squirrel monkey. I. Response to static tilts and to long-duration centrifugal force. *Journal of neurophysiology*, 39(5):970–84, Sept. 1976.

[64] C. Fernández and J. M. Goldberg. Physiology of peripheral neurons innervating otolith organs of the squirrel monkey. II. Directional selectivity and force-response relations. *Journal of neurophysiology*, 39(5):985–95, Sept. 1976.

[65] C. Fernández and J. M. Goldberg. Physiology of peripheral neurons innervating otolith organs of the squirrel monkey. III. Response dynamics. *Journal of neurophysiology*, 39(5):996–1008, Sept. 1976.

[66] A. Fialov. Separation principle for nonlinear systems in critical case. In *Proc. of the 10th mediterranean conference on control and automation*, number 2, Lisbon, Portugal, 2002.

[67] M. Fliess, C. Join, and H. Sira-Ramrez. Non-linear estimation is easy. *International Journal of Modelling, Identification and Control*, 5(1):12–27, 2008.

[68] H. Fourati, N. Manamanni, L. Afilal, and Y. Handrich. A nonlinear filtering approach for the attitude and dynamic body acceleration estimation based on inertial and magnetic sensors: bio-logging application. *IEEE Sensors Journal*, 11(1):233–244, Jan. 2011.

[69] M. Fransson and H. Gréen. Comparison of two types of population pharmacokinetic model structures of paclitaxel. *European journal of pharmaceutical sciences : official journal of the European Federation for Pharmaceutical Sciences*, 33(2):128–37, Feb. 2008.

[70] B. J. Frost. The optokinetic basis of head-bobbing in the pigeon. *J. Exp. Biol.*, 74:187–195, 1978.

[71] M. Fujita. Head bobbing and the body movement of little egrets (Egretta garzetta) during walking. *Journal of comparative physiology. A, Neuroethology, sensory, neural, and behavioral physiology*, 189(1):53–8, Jan. 2003.

[72] G. Arechavaleta, J-P. Laumond, H. Hicheur, and A. Berthoz. An optimality principle governing human walking. *IEEE T. on Robotics*, 24(1):5–14, 2008.

[73] G. M. Jones and J. H. Milsum. Frequency response analysis of central vestibular unit activity resulting from rotational stimulation of the semicircular canals. *J. Physiol.*, 219:191–215, 1971.

[74] S. Gay, A. Ijspeert, and J. Santos Victor. Predictive gaze stabilization during periodic locomotion based on adaptive frequency oscillators. In *2012 IEEE International Conference on Robotics and Automation*, pages 271–278. IEEE, May 2012.

[75] D. Gebre-Egziabher, R. Hayward, and J. Powell. A low-cost GPS/inertial attitude heading reference system (AHRS) for general aviation applications. In *IEEE 1998 Position Location and Navigation Symposium (Cat. No.98CH36153)*, pages 518–525. IEEE, 1998.

[76] J. Geen and D. Krakauer. Rate-Sensing Gyroscope. Technical report, ADI Micromachined Products Division, 2003.

[77] J. Goldberg and B. W. Peterson. Reflex and mechanical contributions to head stabilization in alert cats. *J Neurophysiol*, 56(3):857–875, Sept. 1986.

[78] J. M. Goldberg and C. Fernández. Vestibular mechanisms. *Annual review of physiology*, 37:129–62, Jan. 1975.

[79] J. F. Golding, M. I. Finch, and J. R. Stott. Frequency effect of 0.35-1.0 Hz horizontal translational oscillation on motion sickness and the somatogravic illusion. *Aviation, space, and environmental medicine*, 68(5):396–402, May 1997.

[80] J. F. Golding and H. M. Markey. Effect of frequency of horizontal linear oscillation on motion sickness and somatogravic illusion. *Aviation, space, and environmental medicine*, 67(2):121–6, Feb. 1996.

[81] A. Golubev, A. Krishchenko, and S. Tkachev. Separation principle for a class of nonlinear systems. In *Proceedings of the 15th IFAC World Congress, 2002*, volume 15, Barcelona, Spain, 2002.

[82] D. Gouaillier, V. Hugel, P. Blazevic, C. Kilner, J. Monceaux, P. Lafourcade, B. Marnier, J. Serre, and B. Maisonnier. Mechatronic design of NAO humanoid. In *2009 IEEE International Conference on Robotics and Automation*, pages 769–774. IEEE, May 2009.

[83] M. Grassi. Attitude determination and control for a small remote sensing satellite. *Acta Astronautica*, 40(9):675–681, May 1997.

[84] R. Grasso, P. Prévost, Y. P. Ivanenko, and A. Berthoz. Eye-head coordination for the steering of locomotion in humans: an anticipatory synergy. *Neuroscience Letters*, 253(2):115–118, Sept. 1998.

[85] A. M. Green and D. E. Angelaki. Internal models and neural computation in the vestibular system. *Experimental brain research. Experimentelle Hirnforschung. Expérimentation cérébrale*, 200(3-4):197–222, Jan. 2010.

[86] P. R. Green. Head orientation and trajectory of locomotion during jumping and walking in domestic chicks. *Brain, behavior and evolution*, 51(1):48–58, Jan. 1998.

[87] P. Greiff, B. Antkowiak, J. Campbell, and A. Petrovich. Vibrating wheel micromechanical gyro. In *Proceedings of Position, Location and Navigation Symposium - PLANS '96*, pages 31–37. IEEE.

[88] M. Grewal and K. Glover. Identifiability of linear and nonlinear dynamical systems. *IEEE Transactions on Automatic Control*, 21(6):833–837, Dec. 1976.

[89] M. Grewal, V. Henderson, and R. Miyasako. Application of Kalman filtering to the calibration and alignment of inertial navigation systems. *IEEE Transactions on Automatic Control*, 36(1):3–13, 1991.

[90] E. Griffith and K. Kumar. On the observability of nonlinear systems: I. *Journal of Mathematical Analysis and Applications*, 35(1):135–147, July 1971.

[91] J. J. Groen. Cupulometry. *The Laryngoscope*, 67(9):894–905, Sept. 1957.

[92] D. Guitton, R. Kearney, N. Wereley, and B. Peterson. Visual, vestibular and voluntary contributions to human head stabilization. *Experimental Brain Research*, 64(1), Sept. 1986.

[93] T. Hain, T. Ramaswamy, and M. Hilmann. Anatomy and physiology of vestibular system. In *Herdman SJ. Vestibular Rehabilitation*, chapter 1. 2007.

[94] J. Hale and G. Cheng. Full-Body Compliant Human -Humanoid Interaction: Balancing in the Presence of Unknown External Forces. *IEEE Transactions on Robotics*, 23(5):884–898, Oct. 2007.

[95] R. Hermann and A. Krener. Nonlinear controllability and observability. *IEEE Transactions on Automatic Control*, 22(5):728–740, Oct. 1977.

[96] H. Hicheur, S. Vieilledent, and A. Berthoz. Head motion in humans alternating between straight and curved walking path: combination of stabilizing and anticipatory orienting mechanisms. *Neuroscience letters*, 383(1-2):87–92, 2005.

[97] S. M. Highstein and G. R. Holstein. The anatomical and physiological framework for vestibular prostheses. *Anatomical record (Hoboken, N.J. : 2007)*, 295(11):2000–9, Nov. 2012.

[98] J. M. Hillis, M. O. Ernst, M. S. Banks, and M. S. Landy. Combining sensory information: mandatory fusion within, but not between, senses. *Science (New York, N.Y.)*, 298(5598):1627–30, Nov. 2002.

[99] M. Hirose and K. Ogawa. Honda humanoid robots development. *Philosophical transactions. Series A, Mathematical, physical, and engineering sciences*, 365(1850):11–9, Jan. 2007.

[100] R. Hosman and J. V. der Vaart. *Vestibular models and thresholds of motion perception: Results of tests in a flight simulator*. 1978.

[101] J. Hulk and L. B. W. Jongkees. The Turning Test with Small Regulable Stimuli. *The Journal of Laryngology & Otology*, 62(02):70–75, 1948.

[102] M. Igarashi, T. O-Uchi, and B. R. Alford. Volumetric and dimensional measurements of vestibular structures in the squirrel monkey. *Acta otolaryngologica*, 91(5-6):437–44, 1981.

[103] Y. Inouye. On the observability of autonomous nonlinear systems. *Journal of Mathematical Analysis and Applications*, 60(1):236–247, Aug.

1977.

[104] I. Israel, R. Grasso, P. Georges-Francois, T. Tsuzuku, and A. Berthoz. Spatial Memory and Path Integration Studied by Self-Driven Passive Linear Displacement. I.Basic Properties. *J Neurophysiol*, 77(6):3180–3192, June 1997.

[105] I. Israël, S. Rivaud, B. Gaymard, A. Berthoz, and C. Pierrot-Deseilligny. Cortical control of vestibular-guided saccades in man. *Brain*, 118(5):1169–1183, Oct. 1995.

[106] J. E. Jiménez-Hornero, I. M. Santos-Dueñas, and I. Garci A-Garci A. Structural identifiability of a model for the acetic acid fermentation process. *Mathematical biosciences*, 216(2):154–62, Dec. 2008.

[107] Y. Jun, R. Ellenburg, and P. Oh. From concept to realization: designing miniature humanoids for running. *J. on Systemics, Cybernetics and Informatics*, 2010.

[108] H. Kadone, D. Bernardin, D. Bennequin, and A. Berthoz. Gaze anticipation during human locomotion - top-down organization that may invert the concept of locomotion in humanoid robots. *19th International Symposium in Robot and Human Interactive Communication*, pages 552–557, Sept. 2010.

[109] S. Kagami, M. Mochimaru, Y. Ehara, N. Miyata, K. Nishiwaki, T. Kanade, and H. Inoue. Measurement and comparison of humanoid H7 walking with human being. *Robotics and Autonomous Systems*, 48(4):177–187, Oct. 2004.

[110] R. Kalman. On the general theory of control systems. *IRE Transactions on Automatic Control*, 4(3):110–110, Dec. 1959.

[111] R. E. Kalman. A new approach to linear filtering and prediction problems 1. *Transactions of the ASME Journal of Basic Engineering*, 82(Series D):35–45, 1960.

[112] R. E. Kalman. Canonical structure of linear dynamical systems. *Proceedings of the National Academy of Sciences of the United States of America*, 48(4):596–600, Apr. 1962.

[113] G. Katzir, E. Schechtman, N. Carmi, and D. Weihs. Head stabilization in herons. *Journal of Comparative Physiology A: Sensory, Neural, and Behavioral Physiology*, 187(6):423–432, July 2001.

[114] E. A. Keshner, T. C. Hain, and K. J. Chen. Predicting control mechanisms for human head stabilization by altering the passive mechanics. *Journal of vestibular research : equilibrium & orientation*, 9(6):423–34, Jan. 1999.

[115] J.-Y. Kim, I.-W. Park, and J.-H. Oh. Experimental realization of dynamic walking of the biped humanoid robot KHR-2 using zero moment point feedback and inertial measurement. *Advanced Robotics*, 20(6):707–736, Jan. 2006.

[116] A. D. King. Inertial Navigation Forty Years of Evolution. *GEC REVIEW*, 13(3):140–149, 1998.

[117] Y. M. Kostyukovskii. Observability of nonlinear controlled systems. *Automation and Remote Control*, 28:1384–1396, 1968.

[118] P. Kryczka, E. Falotico, K. Hashimoto, H. Lim, A. Takanishi, C. Laschi,

P. Dario, and A. Berthoz. Implementation of a human model for head stabilization on a humanoid platform. In *2012 4th IEEE RAS & EMBS International Conference on Biomedical Robotics and Biomechatronics (BioRob)*, pages 675–680. IEEE, June 2012.

[119] D. Lapadatu, S. Habibi, B. Reppen, G. Salomonsen, and T. Kvisteroy. Dual-axes capacitive inclinometer/low-g accelerometer for automotive applications. In *14th IEEE International Conference on Micro Electro Mechanical Systems*, pages 34–37. IEEE, 2001.

[120] J.-P. Laumond, G. Arechavaleta, T.-V.-A. Truong, H. Hicheur, Q.-C. Pham, and A. Berthoz. The words of the human locomotion. In M. Kaneko and Y. Nakamura, editors, *Robotics Research*, volume 66 of *Springer Tracts in Advanced Robotics*, pages 35–47. Springer Berlin Heidelberg, 2011.

[121] J. Laurens and J. Droulez. Bayesian processing of vestibular information. *Biological cybernetics*, 96(4):389–404, Apr. 2007.

[122] J. Leavitt, A. Sideris, and J. Bobrow. High bandwidth tilt measurement using low-cost sensors. *IEEE/ASME Transactions on Mechatronics*, 11(3):320–327, June 2006.

[123] R. F. Lewis, C. Haburcakova, W. Gong, D. Lee, C. Wall, L. Thompson, and D. M. Merfeld. Vestibular prosthesis tested in rhesus monkeys. *Annual International Conference of the IEEE Engineering in Medicine and Biology Society.*, 2011:2277–9, Jan. 2011.

[124] C.-H. Lin and S.-M. Kuo. High-performance inclinometer with wide-angle measurement capability without damping effect. In *2007 IEEE 20th International Conference on Micro Electro Mechanical Systems (MEMS)*, pages 585–588. IEEE, 2007.

[125] Y.-Y. Liu, J.-J. Slotine, and A.-L. Barabási. Observability of complex systems. *Proceedings of the National Academy of Sciences of the United States of America*, 110(7):2460–5, Feb. 2013.

[126] S. Lohmeier, T. Buschmann, and H. Ulbrich. System design and control of anthropomorphic walking robot LOLA. *IEEE/ASME Transactions on Mechatronics*, 14(6):658–666, Dec. 2009.

[127] M. Lopes, A. Bernardino, J. Santos-Victor, K. Rosander, and C. von Hofsten. Biomimetic Eye-Neck Coordination. In *2009 IEEE 8th International Conference on Development and Learning*. IEEE, 2009.

[128] D. G. Luenberger. Observing the state of a linear system. *IEEE Transactions on Military Electronics*, 8(2):74–80, 1964.

[129] P. R. MacNeilage, N. Ganesan, and D. E. Angelaki. Computational approaches to spatial orientation: from transfer functions to dynamic Bayesian inference. *Journal of neurophysiology*, 100(6):2981–96, Dec. 2008.

[130] A. B. A. Manaf, K. Nakamura, J. Onishi, and Y. Matsumoto. One-side-electrode-type fluid-based inclinometer combined with CMOS circuitry. In *2007 IEEE Sensors*, pages 844–847. IEEE, 2007.

[131] D. Manchester, M. Woollacott, N. Zederbauer-Hylton, and O. Marin. Visual, vestibular and somatosensory contributions to balance control in the older adult. *Journal of Gerontology*, 44(4):M118–M127, July 1989.

[132] R. Mayne. The functions and operating principles of the otolith organs. Part II The mechanics of the otolith organs. Technical report, Goodyear Aerospace Corp. Arizona Div., rept. GERA-1112 (NASA Contract NAS 9-4460), 1966.

[133] J. L. Meiry. The vestibular dynamic system and human dynamics space orientation. Technical Report October, National aeronautics ans space administration, Washington D.C., 1966.

[134] G. Melvill Jones, A. Berthoz, and B. Segal. Adaptive modification of the vestibulo-ocular reflex by mental effort in darkness. *Experimental Brain Research*, 56(1), Aug. 1984.

[135] H. B. Menz, S. R. Lord, and R. C. Fitzpatrick. Acceleration patterns of the head and pelvis when walking on level and irregular surfaces. *Gait & Posture*, 18(1):35–46, Aug. 2003.

[136] D. Merfeld. Modeling the vestibulo-ocular reflex of the squirrel monkey during eccentric rotation and roll tilt. *Experimental Brain Research*, 106(1), Sept. 1995.

[137] D. Merfeld and L. Young. A multidimensional model of the effect of gravity on the spatial orientation of the monkey. *Journal of vestibular research: equilibrium & orientation*, 1993.

[138] D. M. Merfeld and R. F. Lewis. Replacing semicircular canal function with a vestibular implant. *Current opinion in otolaryngology & head and neck surgery*, 20(5):386–92, Oct. 2012.

[139] D. M. Merfeld, L. Zupan, and R. J. Peterka. Humans use internal models to estimate gravity and linear acceleration. *Nature*, 398(6728):615–8, Apr. 1999.

[140] D. M. Merfeld and L. H. Zupan. Neural Processing of Gravitoinertial Cues in Humans. III. Modeling Tilt and Translation Responses. *J Neurophysiol*, 87(2):819–833, Feb. 2002.

[141] D. M. Merfeld, L. H. Zupan, and C. A. Gifford. Neural Processing of Gravito-Inertial Cues in Humans. II. Influence of the Semicircular Canals During Eccentric Rotation. *J Neurophysiol*, 85(4):1648–1660, Apr. 2001.

[142] U. Mescheder and S. Majer. Micromechanical inclinometer. *Sensors and Actuators A: Physical*, 60(1-3):134–138, May 1997.

[143] N. Metni, J.-M. Pflimlin, T. Hamel, and P. Souères. Attitude and gyro bias estimation for a VTOL UAV. *Control Engineering Practice*, 14(12):1511–1520, Dec. 2006.

[144] J.-A. Meyer, A. Guillot, B. Girard, M. Khamassi, P. Pirim, and A. Berthoz. The Psikharpax project: towards building an artificial rat. *Robotics and Autonomous Systems*, 50(4):211–223, Mar. 2005.

[145] P. Moraal and J. Grizzle. Observer design for nonlinear systems with discrete-time measurements. *IEEE Transactions on Automatic Control*, 40(3):395–404, Mar. 1995.

[146] P. Mottier and P. Pouteau. Solid state optical gyrometer integrated on silicon. *Electronics Letters*, 33(23), Nov. 1997.

[147] R. Necker. Head-bobbing of walking birds. *Journal of comparative physiology. A, Neuroethology, sensory, neural, and behavioral physiology*, 193(12):1177–83, Dec. 2007.

[148] H. Nijmeijer. Observability of autonomous discrete time non-linear systems: a geometric approach. *International Journal of Control*, 36(5):867–874, Nov. 1982.

[149] J. Niven and W. Hixson. Frequency response of the human semicircular canals: I. Steady-State Ocular Nystagmus Response to High-level Sinusoidal Angular Rotations. Technical report, NASA Naval School of Aviation Medicine., 1961.

[150] M. J. Novack. *Design and fabrication of a thin film micromachined accelerometer*. PhD thesis, Massachusetts Institute of Technology, 1992.

[151] C. Oman, B. Lichtenberg, K. Money, and R. McCoy. M.I.T./Canadian vestibular experiments on the Spacelab-1 mission: 4. Space motion sickness: symptoms, stimuli, and predictability. *Experimental Brain Research*, 64(2), Oct. 1986.

[152] F. Paian, C. Laschi, H. Miwa, E. Guglielmelli, P. Dario, and A. Takanishi. Design and development of a biologically-inspired artificial vestibular system for robot heads. In *2004 IEEE/RSJ International Conference on Intelligent Robots and Systems (IROS)*, volume 2, pages 1317–1322. IEEE, 2004.

[153] F. Panerai, G. Metta, and G. Sandini. Learning visual stabilization reflexes in robots with moving eyes. *Neurocomputing*, 48(1-4):323–337, Oct. 2002.

[154] A. Paramiggiani, M. Maggiali, L. Natale, F. Nori, A. Schmitz, N. Tsagarakis, J. S. Victor, F. Becchi, G. Sandini, and G. Metta. The design of the iCub humanoid robot. *International Journal of Humanoid Robotics*, page 1250027, Nov. 2012.

[155] C.-w. Park and S. Lee. Local separation principle for a special class of nonlinear systems. *International Mathematical Forum*, 1(40):1983–1995, 2007.

[156] I.-W. Park, J.-Y. Kim, J. Lee, and J.-H. Oh. Mechanical design of humanoid robot platform KHR-3 (KAIST humanoid robot - 3: HUBO). In *5th IEEE-RAS International Conference on Humanoid Robots, 2005.*, pages 321–326. IEEE, 2005.

[157] H. Pohjanpalo. System identifiability based on the power series expansion of the solution. *Mathematical Biosciences*, 41(1-2):21–33, Sept. 1978.

[158] T. Pozzo, A. Berthoz, and L. Lefort. Head stabilisation during various locomotor tasks in humans. *Experimental Brain Research*, 82(1):97–106, 1990.

[159] T. Pozzo, Y. Levik, and A. Berthoz. Head and trunk movements in the frontal plane during complex dynamic equilibrium tasks in humans. *Experimental Brain Research*, 106(2):327–338, 1995.

[160] P. Prévost, I. Yuri, G. Renato, and B. Alain. Spatial invariance in anticipatory orienting behaviour during human navigation. *Neuroscience Letters*, 339(3):243–247, Mar. 2003.

[161] M. Prsa, S. Gale, and O. Blanke. Self-motion leads to mandatory cue fusion across sensory modalities. *Journal of neurophysiology*, 108(8):2282–91, Oct. 2012.

[162] R. Puers and S. Reyntjens. Design and processing experiments of a new

miniaturized capacitive triaxial accelerometer. *Sensors and Actuators A: Physical*, 68(1-3):324–328, June 1998.

[163] J. Qian, B. Fang, W. Yang, X. Luan, and H. Nan. Accurate Tilt Sensing with Linear Model. *IEEE Sensors Journal*, 11(10):2301–2309, Oct. 2011.

[164] A. Raksanyi, Y. Lecourtier, E. Walter, and A. Venot. Identifiability and distinguishability testing via computer algebra. *Mathematical Biosciences*, 77(1-2):245–266, Dec. 1985.

[165] H. Rehbinder and X. Hu. Drift-free attitude estimation for accelerated rigid bodies. In *Proceedings 2001 ICRA. IEEE International Conference on Robotics and Automation (Cat. No.01CH37164)*, volume 4, pages 4244–4249. IEEE, 2001.

[166] H. Rehbinder and X. Hu. Drift-free attitude estimation for accelerated rigid bodies. *Automatica*, 40(4):653–659, Apr. 2004.

[167] H. Reisine, J. I. Simpson, and V. Henn. A geometric analysis of semicircular canals and induced activity in their peripheral afferents in the rhesus monkey. *Annals of the New York Academy of Sciences*, 545:10–20, Jan. 1988.

[168] G. E. Riccio and T. A. Stoffregen. An ecological Theory of Motion Sickness and Postural Instability. *Ecological Psychology*, 3(3):195–240, Sept. 1991.

[169] Y. Sakagami, R. Watanabe, C. Aoyama, S. Matsunaga, N. Higaki, and K. Fujimura. The intelligent ASIMO: system overview and integration. In *IEEE/RSJ International Conference on Intelligent Robots and System*, volume 3, pages 2478–2483. IEEE, 2002.

[170] A. Sanyal, N. Chaturvedi, D. Bernstein, and H. McClamroch. Dynamics and control of a 3D pendulum. In *2004 43rd IEEE Conference on Decision and Control (CDC) (IEEE Cat. No.04CH37601)*, volume 1, pages 323–328 Vol.1. IEEE, 2004.

[171] A. Sedoglavic. A probabilistic algorithm to test local algebraic observability in polynomial time. In *Proceedings of the 2001 international symposium on Symbolic and algebraic computation - ISSAC '01*, pages 309–317, New York, New York, USA, July 2001. ACM Press.

[172] A. Sedoglavic. A probabilistic algorithm to test local algebraic observability in polynomial time. In B. Mourrain, editor, *Proceedings of the 2001 International Symposium on Symbolic and Algebraic Computation*, pages 309–316, London, Ontario, Canada, 2001. ACM, ACM press.

[173] P. Selva and C. M. Oman. Relationships between observer and Kalman Filter models for human dynamic spatial orientation. *Journal of vestibular research : equilibrium & orientation*, 22(2):69–80, Jan. 2012.

[174] N. T. Shepard, S. A. Telian, M. Smith-Wheelock, and A. Raj. Vestibular and balance rehabilitation therapy. *The Annals of otology, rhinology, and laryngology*, 102(3 Pt 1):198–205, Mar. 1993.

[175] T. Shibata and S. Schaal. Biomimetic gaze stabilization based on feedback-error-learning with nonparametric regression networks. *Neural Networks*, 14(2):201–216, Mar. 2001.

[176] T. Shibata and S. Vijayakumar. Humanoid Oculomotor Control Based on Concepts of Computational Neuroscience. In *IEEE-RAS Int. Conf.*

on Humanoid robots, Japan, 2001.

[177] M. N. Sreenivasa, P. Soueres, J.-P. Laumond, and A. Berthoz. Steering a humanoid robot by its head. In *2009 IEEE/RSJ International Conference on Intelligent Robots and Systems*, pages 4451–4456. IEEE, Oct. 2009.

[178] B. J. Stephens and C. G. Atkeson. Dynamic balance force control for compliant humanoid robots. In *2010 IEEE/RSJ International Conference on Intelligent Robots and Systems*, pages 1248–1255. IEEE, Oct. 2010.

[179] T. A. Stoffregen and G. E. Riccio. An ecological theory of orientation and the vestibular system. *Psychological review*, 95(1):3–14, Jan. 1988.

[180] N. Sugimoto, J. Morimoto, S.-H. Hyon, and M. Kawato. The eMOSAIC model for humanoid robot control. *Neural networks : the official journal of the International Neural Network Society*, 29-30(null):8–19, May 2012.

[181] M. S. Svendsen, J. Helbo, M. R. Hansen, D. B. Popovic, J. Stoustrup, and M. M. Pedersen. AAU-BOT1: a platform for studying dynamic, life-like walking. *Applied Bionics and Biomechanics*, 6(3-4):285–299, Dec. 2009.

[182] T. Pozzo, A. Berthoz, L. Lefort, and E. Vitte. Head stabilization during various locomotory tasks in humans II. Patients with bilateral vestibular deficits. *Exp. Brain Res.*, 85:208–217, 1991.

[183] K. A. Tahboub. Biologically-inspired postural and reaching control of a multi-segment humanoid robot. *International Journal of Biomechatronics and Biomedical Robotics*, 1(3):175–190, 2011.

[184] S. Trimpe and R. D'Andrea. Accelerometer-based tilt estimation of a rigid body with only rotational degrees of freedom. In *2010 IEEE International Conference on Robotics and Automation*, pages 2630–2636. IEEE, May 2010.

[185] N. Troje and B. Frost. Head-bobbing in pigeons: how stable is the hold phase? *J. Exp. Biol.*, 203(5):935–940, Mar. 2000.

[186] N. G. Tsagarakis, G. Metta, G. Sandini, D. Vernon, R. Beira, F. Becchi, L. Righetti, J. Santos-Victor, A. J. Ijspeert, M. C. Carrozza, and D. G. Caldwell. iCub: the design and realization of an open humanoid platform for cognitive and neuroscience research. *Advanced Robotics*, 21(10):1151–1175, Jan. 2007.

[187] J. Vaganay, M. Aldon, and A. Fournier. Mobile robot attitude estimation by fusion of inertial data. In *Proceedings IEEE International Conference on Robotics and Automation*, pages 277–282. IEEE Comput. Soc. Press, 1993.

[188] W. C. Van Buskirk, R. G. Watts, and Y. K. Liu. The fluid mechanics of the semicircular canals. *Journal of Fluid Mechanics*, 78(01):87–98, 1976.

[189] A. A. J. Van Egmond, J. J. Groen, and L. B. W. Jongkees. The mechanics of the semicircular canal. *The Journal of physiology*, 110(1-2):1–17, Dec. 1949.

[190] J. Vasconcelos, R. Cunha, C. Silvestre, and P. Oliveira. A nonlinear position and attitude observer on SE(3) using landmark measurements. *Systems & Control Letters*, 59(3-4):155–166, Mar. 2010.

[191] P. H. Veltink, H. J. Luinge, B. J. Kooi, C. T. M. Baten, and P. Slycke. The artificial vestibular system - design of a tri-axial inertial sensor system and its application in the study of human movement. In *Proceedings of the International Society for Postural and Gait Research ISPG*, number figure 1, 2001.

[192] D. R. Vera, K. A. Krohn, P. O. Scheibe, and R. C. Stadalnik. Identifiability analysis of an in vivo receptor-binding radiopharmacokinetic system. *IEEE transactions on bio-medical engineering*, 32(5):312–22, May 1985.

[193] P. P. Vidal, W. Graf, and A. Berthoz. Skeletal geometry underlying head movements. *Annals of the New York Academy of Sciences*, 545(1 Representatio):228–238, Dec. 1988.

[194] R. A. A. Vingerhoets, M. De Vrijer, J. A. M. Van Gisbergen, and W. P. Medendorp. Fusion of visual and vestibular tilt cues in the perception of visual vertical. *Journal of neurophysiology*, 101(3):1321–33, Mar. 2009.

[195] M. Vukobratovic and B. Borovac. Zero-moment point - thirty five years of its life. *International Journal of Humanoid Robotics*, 01(01):157–173, Mar. 2004.

[196] M. Vukobratovic and D. Juricic. Contribution to the synthesis of biped gait. *IEEE Transactions on Biomedical Engineering*, BME-16(1):1–6, Jan. 1969.

[197] C. Wall, D. M. Merfeld, S. D. Rauch, and F. O. Black. Vestibular prostheses: the engineering and biomedical issues. *Journal of vestibular research : equilibrium & orientation*, 12(2-3):95–113, 2003.

[198] E. Walter. *Identifiability of state space models, with applications to transformation systems*. Springer, 1982.

[199] E. Walter and Y. Lecourtier. Global approaches to identifiability testing for linear and nonlinear state space models. *Mathematics and Computers in Simulation*, 24(6):472–482, Dec. 1982.

[200] E. Walter and L. Pronzato. On the identifiability and distinguishability of nonlinear parametric models. *Mathematics and Computers in Simulation*, 42(2-3):125–134, Oct. 1996.

[201] D. Watt and L. Lefebvre. Vestibular suppression during space flight. *Journal of Vestibular Research*, 13(4):363–376, 2003.

[202] G. Welch, G. Bishop, and C. Hill. An Introduction to the Kalman Filter. Technical report, 1995.

[203] G. Welch and E. Foxlin. Motion tracking: no silver bullet, but a respectable arsenal. *IEEE Computer Graphics and Applications*, 22(6):24–38, Nov. 2002.

[204] C. R. Wilpizeski, L. D. Lowry, M. E. Raheb, U. Eyyunni, R. B. Contrucci, and W. S. Goldman. Experimental motion sickness induced in squirrel monkeys by continuous off-axis horizontal rotation. *American Journal of Otolaryngology*, 6(1):1–22, Jan. 1985.

[205] D. Winter. Human balance and posture control during standing and walking. *Gait & Posture*, 3(4):193–214, Dec. 1995.

[206] D. A. Winter, A. E. Patla, F. Prince, M. Ishac, and K. Gielo-Perczak. Stiffness Control of Balance in Quiet Standing. *J Neurophysiol*, 80(3):1211–1221, Sept. 1998.

[207] H. Wongsuwarn and D. Laowattana. Experimental Study for a FIBO Humanoid Robot. In *IEEE Conference on Robotics, Automation and Mechatronics*, 2006.

[208] S. J. Wood. Human otolithocular reflexes during off-vertical axis rotation: effect of frequency on tilttranslation ambiguity and motion sickness. *Neuroscience Letters*, 323(1):41–44, Apr. 2002.

[209] Y. Xiang, S. B. Yakushin, M. Kunin, T. Raphan, and B. Cohen. Head stabilization by vestibulocollic reflexes during quadrupedal locomotion in monkey. *Journal of neurophysiology*, 100(2):763–80, Aug. 2008.

[210] A. P. Yelnik. Perception of verticality after recent cerebral hemispheric-stroke. *Stroke*, 33(9):2247–2253, Sept. 2002.

[211] N. Yoganandan, F. A. Pintar, J. Zhang, and J. L. Baisden. Physical properties of the human head: mass, center of gravity and moment of inertia. *Journal of biomechanics*, 42(9):1177–92, June 2009.

[212] R. Yotter, R. Baxter, S. Ohno, S. Hawley, and D. Wilson. On a micromachined fluidic inclinometer. In *TRANSDUCERS '03. 12th International Conference on Solid-State Sensors, Actuators and Microsystems.*, volume 2, pages 1279–1282. IEEE, 2003.

[213] L. R. Young. The current status of vestibular system models. *Automatica*, 5(3):369–383, May 1969.

[214] L. R. Young. Optimal estimator models for spatial orientation and vestibular nystagmus. *Experimental brain research.*, 210(3-4):465–76, May 2011.

[215] L. H. Zupan, R. J. Peterka, and D. M. Merfeld. Neural processing of gravito-inertial cues in humans. I. influence of the semicircular canals following post-rotatory tilt. *J Neurophysiol*, 84(4):2001–2015, Oct. 2000.

Appendix

Appendix contains some technical materials which describe the experimental setup. Mechanical design of the setup was done in Solidworks. Most of mechanical parts are manufactured from plastic with the help of CNC milling machine. Electrical part of the setup is based on the BeagleBone emebedded computer. Additional voltage custom designed interfacing board was used for leveling the voltage level from then analog sensor outputs to analog inputs of the BeagleBone computer.

Mechanical drawings

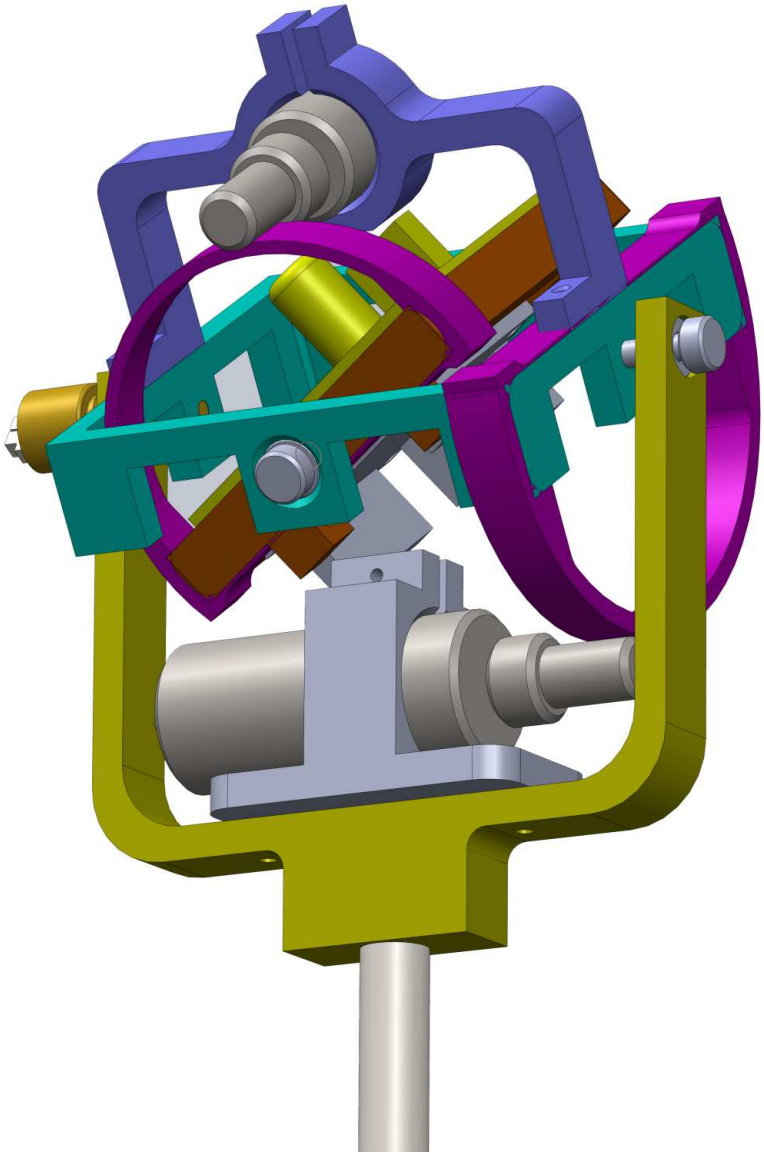

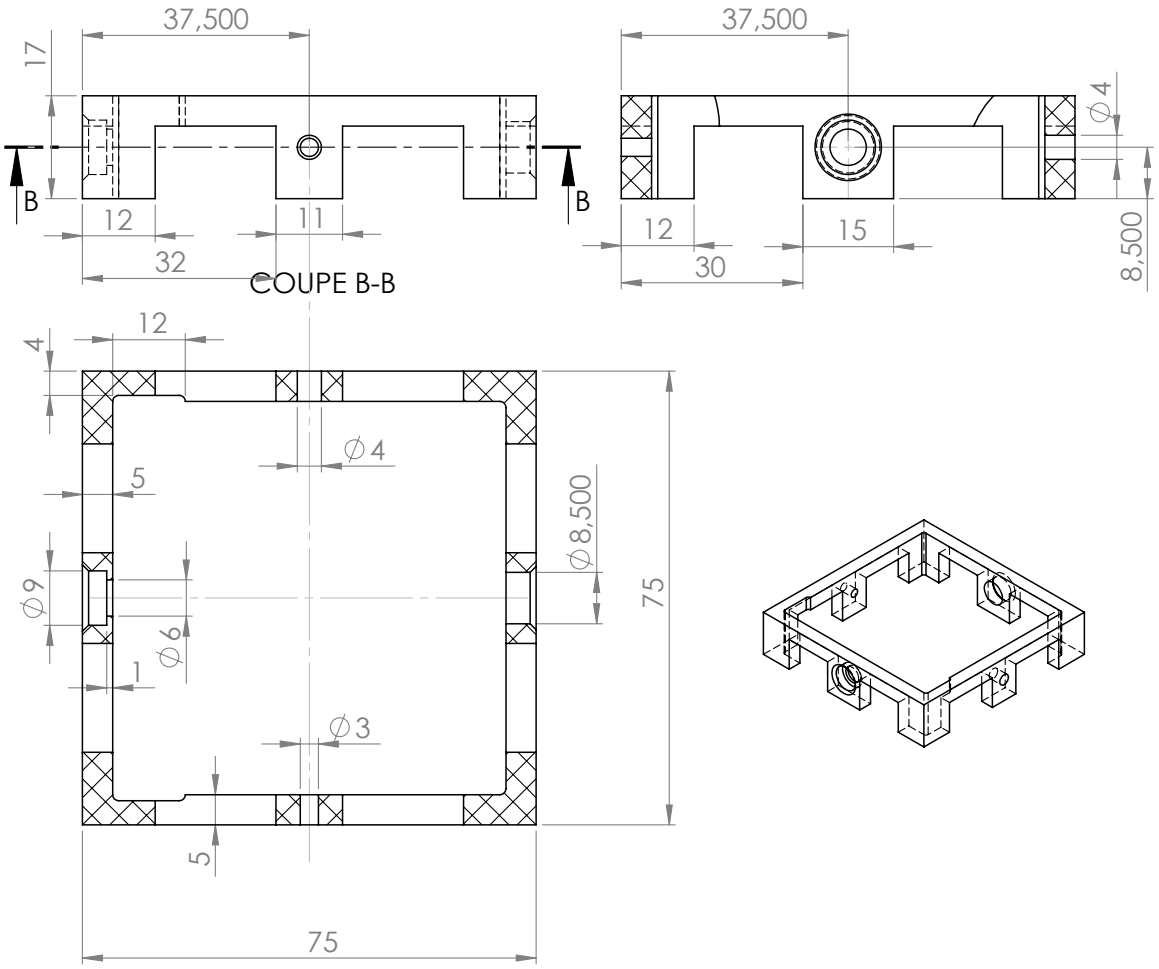

UNLESS OTHERWISE SPECIFIED: DIMENSIONS ARE IN MILLIMETERS SURFACE FINISH: TOLERANCES: LINEAR: ANGULAR:	FINISH:		DEBUR AND BREAK SHARP EDGES			DO NOT SCALE DRAWING	REVISION
	NAME	SIGNATURE	DATE			TITLE:	
DRAWN	Ildar Farkhatdinov						
CHK'D							
APPV'D							
MFG							
Q.A				MATERIAL:		DWG NO. body	A4
				WEIGHT:		SCALE:1:1	SHEET 1 OF 1

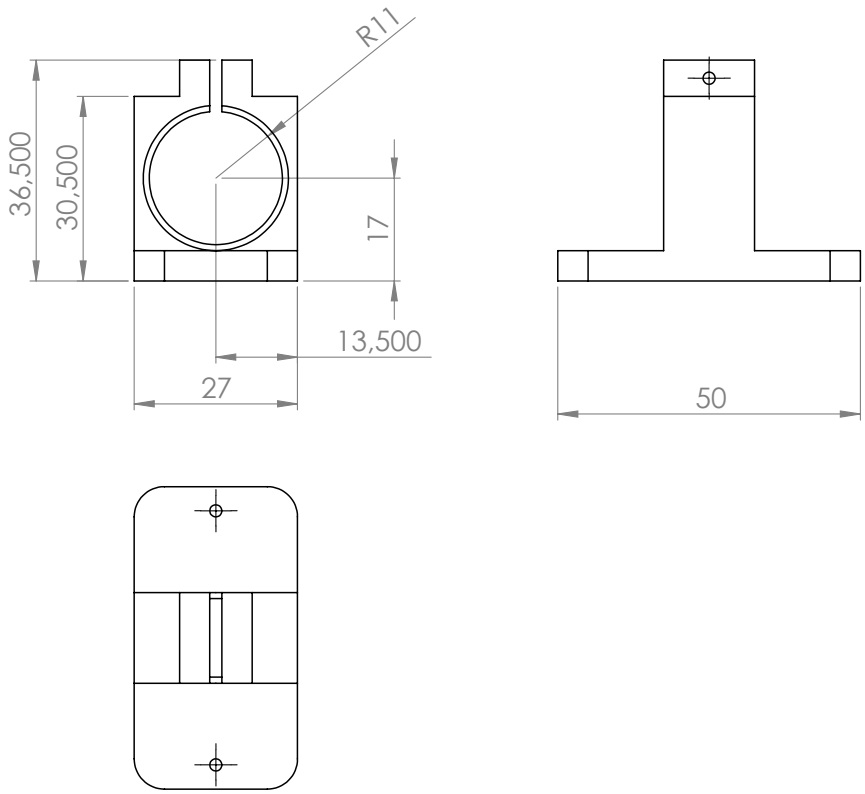

SAUF INDICATION CONTRAIRE: LES COTES SONT EN MILLIMETRES ETAT DE SURFACE: TOLERANCES: LINEAIRES: ANGULAIRES:		FINITION:			CASSER LES ANGLES VIFS	NE PAS CHANGER L'ECHELLE	REVISION
	NOM	SIGNATURE	DATE				
AUTEUR	Ildar Farkhatdinov					TITRE:	
VERIF.							
APPR.							
FAB.							
QUAL.				MATERIAU:		No. DE PLAN	A4
						down_motor_support	
				MASSE:		ECHELLE:1:1	FEUILLE 1 SUR 1

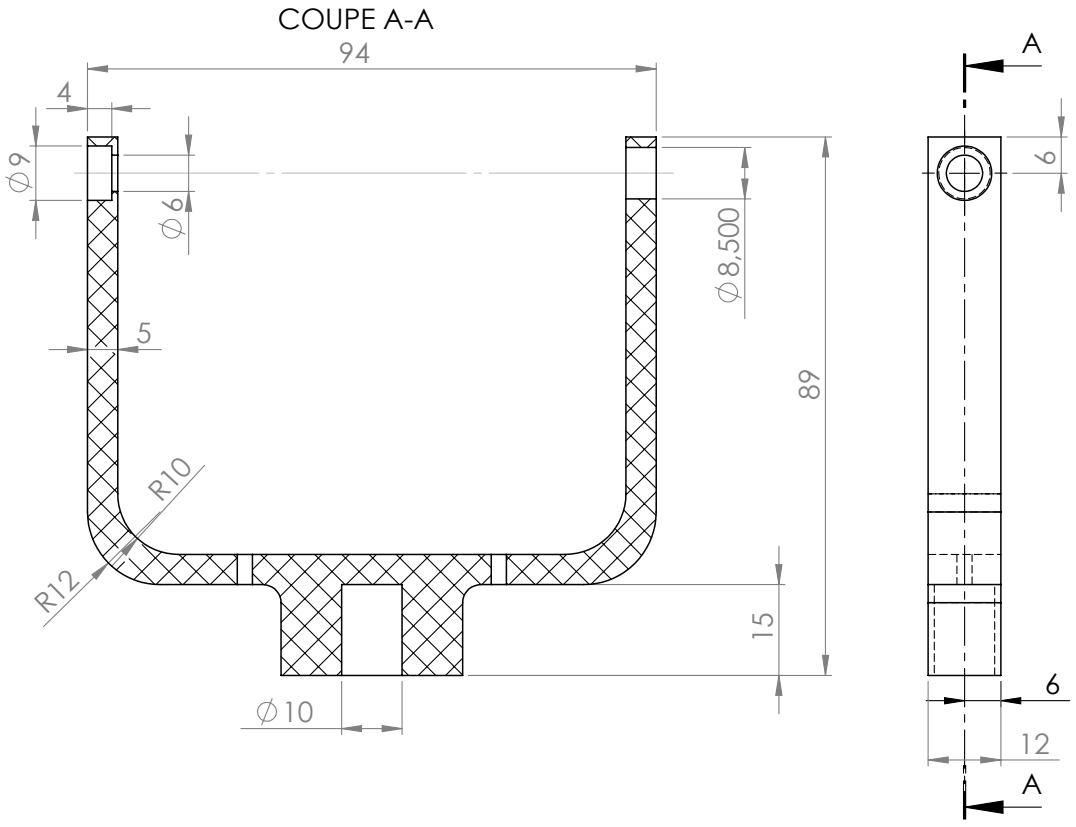

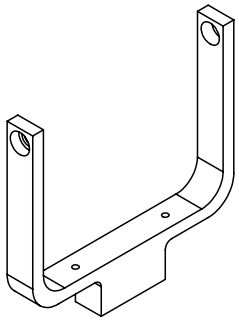

SAUF INDICATION CONTRAIRE: LES COTES SONT EN MILLIMETRES ETAT DE SURFACE: TOLERANCES: LINEAIRES: ANGULAIRES:	FINITION:				CASSER LES ANGLES VIFS	NE PAS CHANGER L'ECHELLE	REVISION
	NOM	SIGNATURE	DATE			TITRE:	
AUTEUR	Ildar Farkhatdinov						
VERIF.							
APPR.							
FAB.							
QUAL.				MATERIAU:		No. DE PLAN	A4
						out_link	
				MASSE:		ECHELLE:1:1	FEUILLE 1 SUR 1

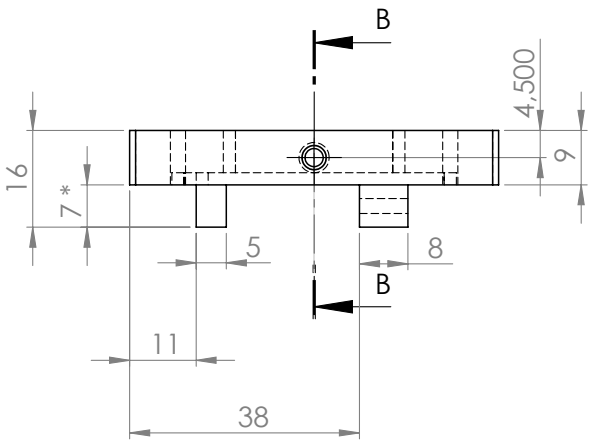

COUPE B-B
ECHELLE 1 : 1

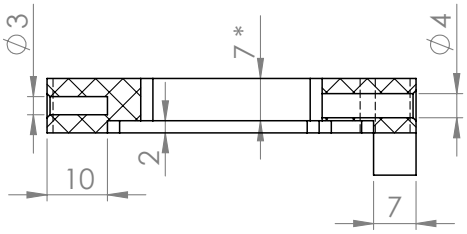

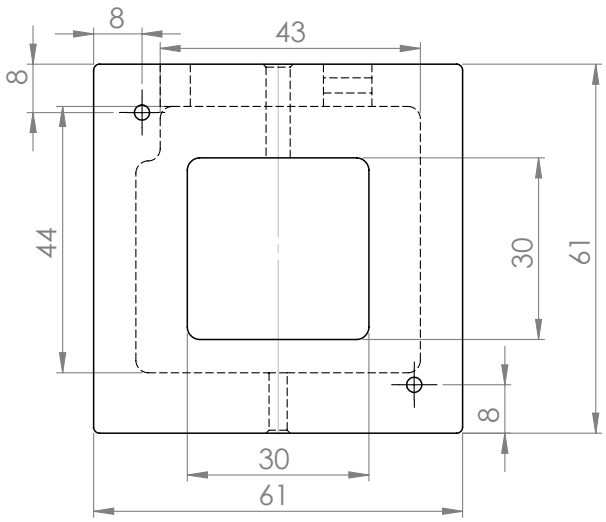

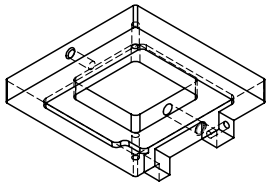

SAUF INDICATION CONTRAIRE: LES COTES SONT EN MILLIMETRES ETAT DE SURFACE: TOLERANCES: LINEAIRES: ANGULAIRES:		FINITION:		CASSER LES ANGLES VIFS		NE PAS CHANGER L'ECHELLE	REVISION
	NOM	SIGNATURE	DATE			TITRE:	
AUTEUR	Ildar Farkhatdinov						
VERIF.							
APPR.							
FAB.							
QUAL.				MATERIAU:		No. DE PLAN	A4
						plate_drawing	
				MASSE:		ECHELLE:1:2	FEUILLE 1 SUR 1

Electrical schematics

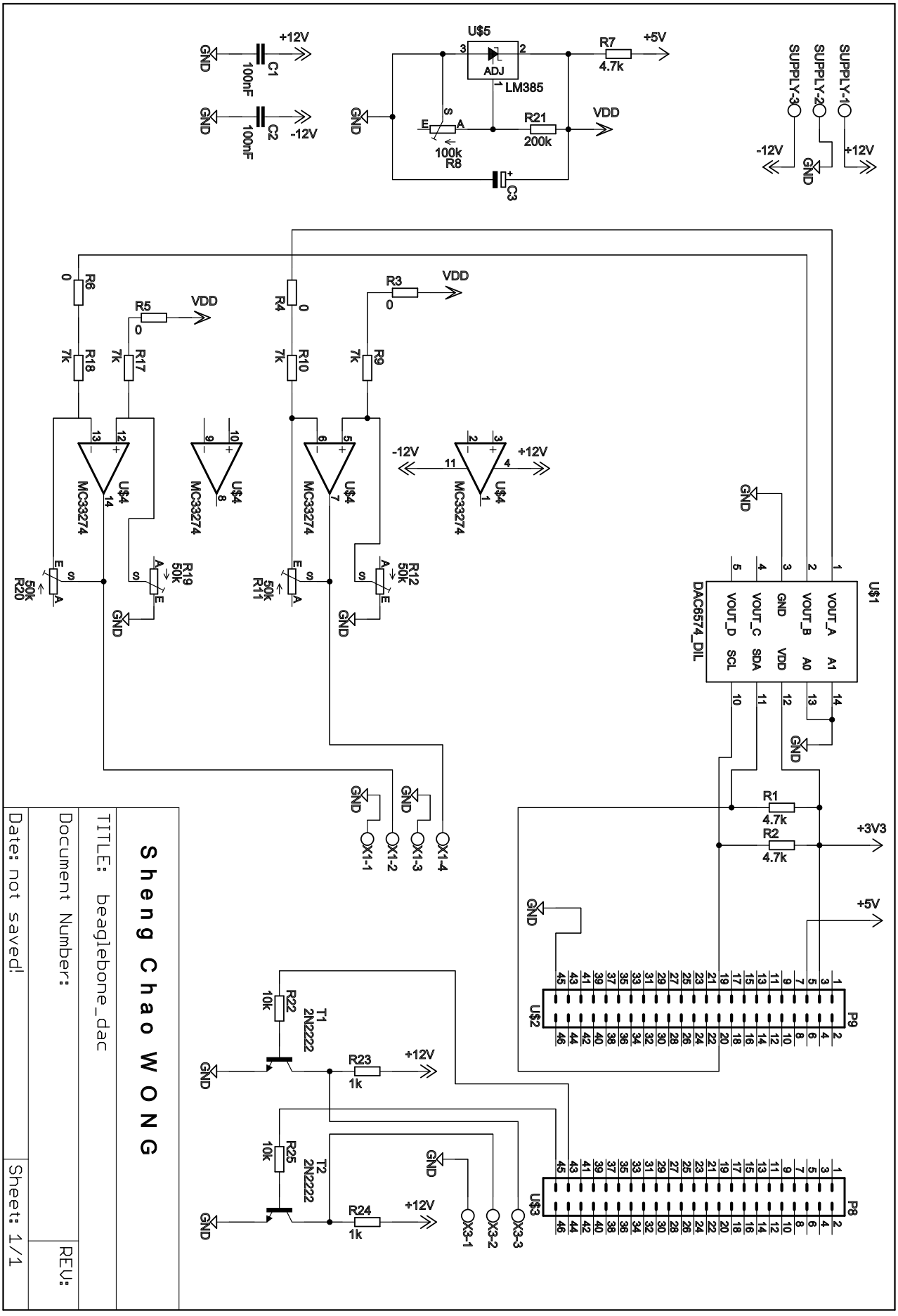

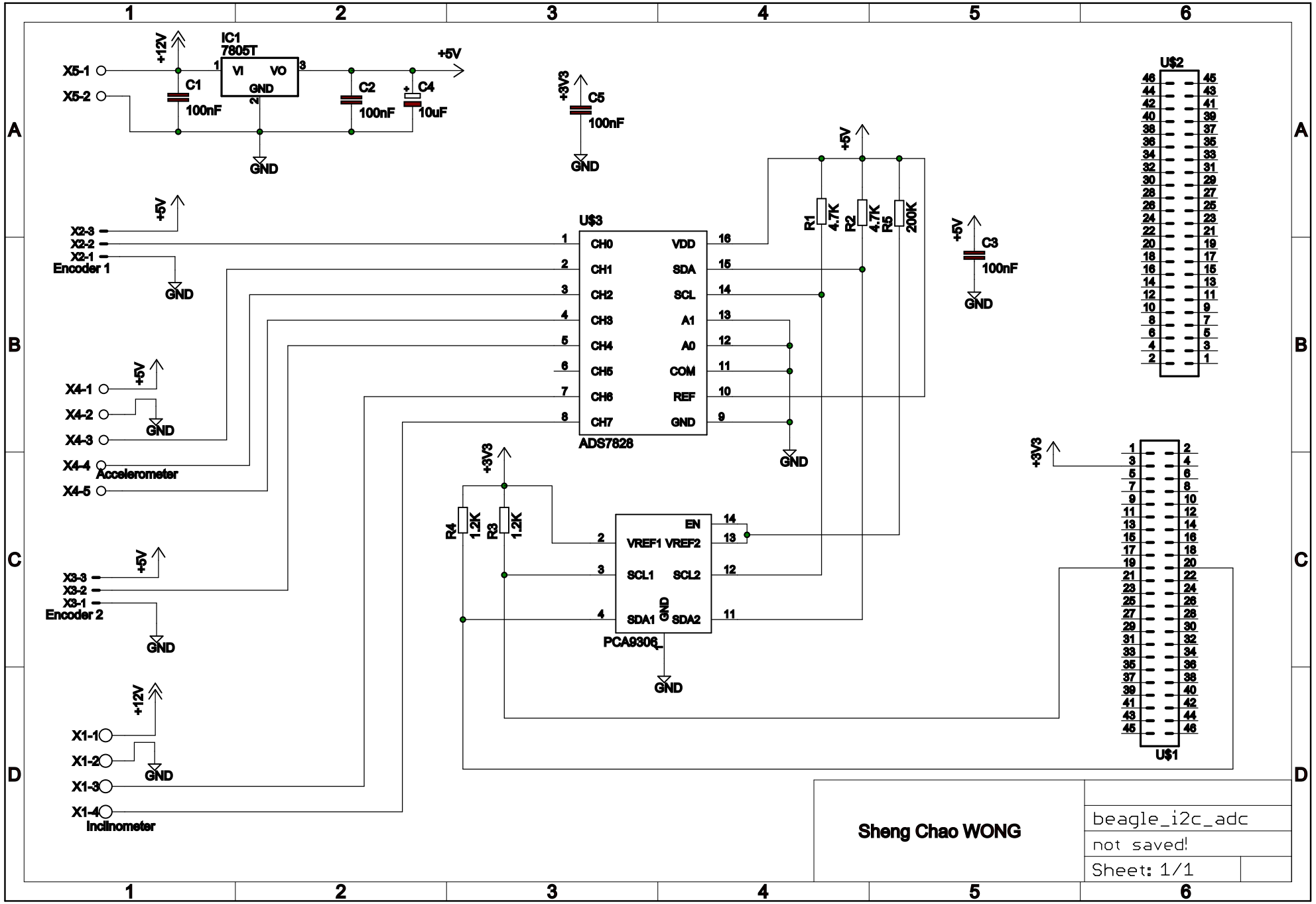
IC1
7805T
VI
VO
GND
+12V
+5V
+3V3
C1
100nF
C2
100nF
C4
10uF
C5
100nF
C3
100nF
X5-1
X5-2
U$3
CH0
CH1
CH2
CH3
CH4
CH5
CH6
CH7
VDD
SDA
SCL
A1
A0
COM
REF
GND
ADS7828
R1
4.7K
R2
4.7K
R5
200K
X2-3
X2-2
X2-1
Encoder 1
X4-1
X4-2
X4-3
X4-4
Accelerometer
X4-5
X3-3
X3-2
X3-1
Encoder 2
X1-1
X1-2
X1-3
X1-4
Inclinometer
R4
1.2K
R3
1.2K
EN
VREF1
VREF2
SCL1
SCL2
SDA1
SDA2
PCA9306
U$2
U$1
Sheng Chao WONG
beagle_i2c_adc
not saved!
Sheet: 1/1